

**CHAPTER 3  
TABLE OF CONTENTS**

<b>3. THERMAL EVALUATION</b> .....	<b>3.1-1</b>
3.1 Discussion .....	3.1-1
3.1.1 Design Features .....	3.1-1
3.1.2 Thermal Criteria .....	3.1-1
3.1.3 Summary of Evaluation .....	3.1-1
3.2 Summary of Thermal Properties of Materials .....	3.2-1
3.3 Technical Specifications of Components .....	3.3-1
3.4 Thermal Evaluation for Normal Conditions of Transport .....	3.4-1
3.4.1 Thermal Models .....	3.4-1
3.4.2 Maximum Temperatures .....	3.4-7
3.4.3 Minimum Temperatures .....	3.4-12
3.4.4 Maximum Internal Pressures .....	3.4-12
3.4.5 Maximum Thermal Stresses .....	3.4-12
3.4.6 Evaluation of Package Performance for Normal Conditions of Transport .....	3.4-12
3.5 Hypothetical Accident Thermal Evaluation .....	3.5-1
3.5.1 Thermal Models .....	3.5-1
3.5.1.1 TAC2D Models .....	3.5-1
3.5.1.2 ANSYS Model .....	3.5-4
3.5.2 Package Conditions and Environment .....	3.5-4
3.5.3 Package Temperatures .....	3.5-7
3.5.4 Maximum Internal Pressures .....	3.5-7
3.5.5 Maximum Thermal Stresses .....	3.5-10
3.5.6 Evaluation of Package Performance for Hypothetical Accident Thermal Conditions .....	3.5-10
3.6 Appendix .....	3.6-1
3.6.1 Effective Thermal Properties .....	3.6-1
3.6.1.1 ANSYS Model, Sec. 3.4 .....	3.6-1
3.6.1.2 TAC2D Model, Sec. 3.4 .....	3.6-3
3.6.1.3 TAC2D Model, Sec. 3.5 .....	3.6-4
3.6.1.4 ANSYS Model, Sec. 3.5 .....	3.6-7
3.6.2 Heat Transfer Correlations .....	3.6-7
3.6.2.1 Normal Conditions, TAC2D Model .....	3.6-7
3.6.2.2 Accident Conditions, All Models .....	3.6-9
3.6.3 Air Flow inside Personnel Barrier, TAC2D Model .....	3.6-11
3.6.4 Effective Ambient Temperature for ANSYS Model, Sec. 3.4 .....	3.6-11
3.6.5 Solar Radiation .....	3.6-14
3.6.6 Maximum Internal Pressure Calculation .....	3.6-15
3.6.6.1 Assumptions and Bases .....	3.6-15
3.6.6.2 MNOP Analysis .....	3.6-16
3.6.6.3 Accident Analysis .....	3.6-18
3.6.7 Neutron Shield Test .....	3.6-18
3.6.7.1 Set-up and Description .....	3.6-18
3.6.7.2 Results .....	3.6-20
3.6.7.3 Conclusions .....	3.6-23

3.6.8	Thermal Evaluation with Hotter Fuel	3.6-26
3.6.8.1	Summary	3.6-26
3.6.8.2	Analysis Method	3.6-26
3.6.8.3	Base Case	3.6-27
3.6.8.4	Other Cases	3.6-27
3.6.8.5	Effect of Empty Fuel Cavities	3.6-34
3.6.8.6	Hypothetical Accident Conditions	3.6-38
3.6.9	Other Thermal Considerations	3.6-38
3.6.9.1	Welded Fuel Support Structure (FSS)	3.6-38
3.6.9.2	Sensitivity to Tube/Skin Contact	3.6-40
3.6.9.3	Aluminum vs. Copper on Outer Skin	3.6-42
3.6.9.4	Melting of Impact Limiters	3.6-42
3.6.9.5	Verification of Fuel Assembly Temperature Method	3.6-43
3.6.10	References for Sections 3.2 through 3.6	3.6-45

## FIGURES

3.3-1	Seal life at various temperatures for ethylene propylene	3.3-2
3.4-1	3-D finite-element model for normal conditions	3.4-2
3.4-2	TAC2D model for normal conditions	3.4-4
3.4-3	Isotherms for 3-D model (hot normal conditions)	3.4-8
3.4-4	Temperatures for TAC2D model (hot normal conditions)	3.4-9
3.4-5	Axial temperature profiles (hot normal conditions)	3.4-10
3.4-6	Temperatures for normal transient (hot conditions)	3.4-11
3.4-7	Temperatures for normal transient (cold conditions)	3.4-14
3.5-1	TAC2D model for hypothetical accident conditions	3.5-2
3.5-2	3-D finite-element model for hypothetical accident conditions	3.5-5
3.5-3	Modeling of closure area exposed by puncture	3.5-6
3.5-4	TAC2D model temperatures for hypothetical accident conditions	3.5-8
3.6-1	Results of effective ambient temperature model	3.6-13
3.6-2	Neutron shield test article with thermocouple locations	3.6-19
3.6-3	Neutron shield test furnace	3.6-21
3.6-4	Average environment temperature	3.6-22
3.6-5	Front side thermocouple response	3.6-24
3.6-6	Back side thermocouple response	3.6-25
3.6-7	TAC2D model for hotter fuel cases	3.6-28
3.6-8	Base case results	3.6-29
3.6-9	Decay heat configurations for hotter fuel cases	3.6-30
3.6-10	Case 2 results	3.6-31
3.6-11	Case 3 results	3.6-32
3.6-12	Case 4 results	3.6-33
3.6-13	Temperature difference between FSS/liner and DU	3.6-39
3.6-14	Temperature distribution in FSS and liner	3.6-41

TABLES

3.2-1 MATERIAL PROPERTIES ..... 3.2-2  
3.2-2 THERMAL RADIATION PROPERTIES ..... 3.2-3  
3.4-1 PWR DECAY HEAT AXIAL PROFILE ..... 3.4-5  
3.4-2 AXIAL CONDUCTION EFFECT ON PEAK TEMPERATURES ..... 3.4-7  
3.4-3 SUMMARY OF TEMPERATURES FOR NORMAL CONDITIONS,  
STEADY STATE (°F) ..... 3.4-13  
3.5-1 MAXIMUM TEMPERATURES FOR THERMAL ACCIDENT CONDITIONS ..... 3.5-9  
3.6-1 CONSTANTS FOR IMPACT LIMITER SUPPORT STRUCTURE (ILSS)  
THERMAL PROPERTIES, TAC2D MODEL ..... 3.6-6  
3.6-2 THERMAL PROPERTIES FOR ILSS, ANSYS MODEL ..... 3.6-6  
3.6-3 TEMPERATURES FOR NORMAL CONDITIONS, CASE 2 (°F) ..... 3.6-35  
3.6-4 TEMPERATURES FOR NORMAL CONDITIONS, CASE 3 (°F) ..... 3.6-36  
3.6-5 TEMPERATURES FOR NORMAL CONDITIONS, CASE 4 (°F) ..... 3.6-37

THIS PAGE LEFT BLANK INTENTIONALLY

### 3. THERMAL EVALUATION

#### 3.1 Discussion

The thermal evaluation of the GA-4 cask design considers normal and hypothetical accident conditions of transport as specified in 10 CFR Part 71. We have carried out extensive analytical modeling and testing to perform this evaluation. This section addresses the thermal design features of the cask, discusses thermal criteria, and summarizes the results of the thermal evaluation.

##### 3.1.1 Design Features

Several aspects of the cask design and operation provide significant thermal advantages. The first of these is the mass of steel and depleted uranium (DU) used in the cask body, closure end, and gamma shielding. These materials provide a large heat sink for hypothetical accident conditions and help minimize peak temperatures, particularly for the containment seals. The neutron shielding material, although assumed to be partially consumed in the thermal accident, will not itself provide significant heat input and will actually serve as an insulator. For normal conditions, the use of helium rather than nitrogen as an inerting gas reduces internal component temperatures by about 60°F. Although the fuel support structure (FSS) primarily performs a mechanical function, it also serves as a set of internal fins to help dissipate heat. The neutron shield support structure, an array of aluminum tubes, provides the main heat conduction path between the cask body and the outer skin. A vented personnel barrier permits external air flow to the outer skin.

##### 3.1.2 Thermal Criteria

Under normal conditions of transport, the maximum fuel cladding temperature must remain below 380°C (716°F), and the accessible package surface temperature with no solar radiation must not exceed 82°C (180°F), as specified in 10 CFR Part 71.43. The neutron shield material must remain below its softening point for normal conditions and must not provide a significant source of heat input during hypothetical accident conditions. The temperature history of the seals must indicate that the seals will continue to function and maintain containment integrity.

For other components the only criteria are that the temperatures must not exceed values which would compromise any required structural integrity.

##### 3.1.3 Summary of Evaluation

We utilized ANSYS 4.4, PATRAN Plus 2.4, and TAC2D (Versions 1.0 and 0002) for the thermal evaluation. ANSYS is a general-purpose finite-element computer program that solves engineering problems in statics, dynamics, heat transfer, and fluid flow. PATRAN Plus (PATRAN) is a software package that provides solid geometry construction, finite-element modeling, and enhanced graphics. Our analysis used PATRAN to construct the finite-element meshes for the thermal models and ANSYS to perform the actual heat transfer calculations.

We employed the translator program PATANS 2.2 to interface between PATRAN and ANSYS. TAC2D is a general-purpose, finite-difference, two-dimensional heat transfer computer program. Models may be quickly set up, and output results are easily interpreted. The geometry of the model must conform to a rectangular, cylindrical, or circular coordinate system.

Altogether, we used four models in the thermal evaluation. We considered two models for normal conditions of transport:

1. A three-dimensional (3-D) ANSYS model of the GA-4 cask, representing half a cross section approximately midway along the axis.
2. A TAC2D model of the whole cask, using cylindrical geometry (also used for the post-accident analysis).

For the hypothetical accident thermal condition we used two models:

3. A TAC2D model of the closure end, with crushed end impact limiter, and a punch directly above the closure seal.
4. A 3-D ANSYS model of the closure end, with the end impact limiter crushed and punched through the center.

We used all four models to predict temperatures for the thermal evaluation. In addition, we used model 4 to provide a temperature distribution for the thermal stress analysis of the structural evaluation (see Section 2.7.3). The thermal stress analysis also provided an evaluation of the seal interface distortion for the containment analysis.

Results for the GA-4 cask design indicate that it will meet all criteria for normal conditions of transport. The maximum fuel cladding temperature is 373°F, while the allowable is 716°F. We determined a maximum personnel barrier surface temperature of 136°F (with solar radiation) and this is within the criterion of 180°F in the shade set by 10 CFR Part 71.43 for accessible package surfaces. For the polypropylene neutron shield, the analysis predicts a maximum temperature of 213°F, well below the softening point of 302°F for this material. The maximum temperature of the seals is 143°F for the closure and 155°F for the drain. The selected seal material, ethylene propylene, can function at 300°F for 1000 hr, according to manufacturer's data. GA tested the seal and found it to be leaktight at -42°F, ambient (~75°F), and 250°F. The maximum temperature of the impact limiters is 145°F, while the aluminum honeycomb material has been qualified at 200°F.

For hypothetical accident conditions the analysis shows that the maximum primary seal temperature is 365°F, with a total time of about 1 hour above 350°F. This includes the closure seal and the seal for the gas sample and drain ports. Manufacturer's data indicate the seal material can withstand a temperature of 350°F for 50 hr and 400°F for several hours. We have tested the seal at 380°F, after heating for 1.5 hr above 350°F, and determined it to be leaktight. Therefore, the seal will function during the hypothetical accident thermal event.

For the post-accident steady-state condition the seal attains a maximum temperature of 155°F.

The accident analysis assumed that the impact limiters were in place, since they are designed to remain attached following the drop and puncture events. Conservatively, we assumed that the end of the impact limiter was crushed and punched directly above the seal, and that the outer skin and the neutron shield underneath it were completely gone during the thermal event. The post-accident analysis assumed partial damage of the neutron shield and its support tubes to maximize steady-state temperatures.

We assessed the performance of the neutron shield material during the hypothetical accident condition with a testing program. The testing showed that the selected material, KOBESH PP-R01 made by Kobe Steel, Ltd., will not produce significant heat input in the cask.

The reference decay heat used in the analysis was 617 W per assembly, and we applied an axial power profile that resulted in a peaking factor of 1.22. We considered other decay heat configurations to permit the shipment of hotter fuel assemblies. The following table shows the per-assembly and total decay heat limits for the GA-4 cask.

No. Assemblies	Max. Allowed Decay Heat per Assembly (W)	Max. Allowed Total Decay Heat (W)
2-4	617	2468
	740	2220
	845	2078
1-2 <sup>(a)</sup>	1234	2468
<sup>(a)</sup> Special configuration with inserts in diagonal cavities.		

THIS PAGE LEFT BLANK INTENTIONALLY

### 3.2 Summary of Thermal Properties of Materials

Table 3.2-1 provides a compilation of the thermal conductivity, density, and specific heat of the cask materials, while Table 3.2-2 gives the thermal radiation properties (emissivity and absorptivity). The emissivity of any material is a strong function of its surface characteristics and may be subject to considerable uncertainty. For the spent fuel assemblies (SFAs) a rod emissivity of 0.7 was used, and the emissivity of the cavity liner interior (shroud) was assumed to be 0.2. A review of other analytical as well as experimental work in SFA heat transfer (Refs. 3.2-11 through 3.2-15) shows that these are conservatively low values. Fuel rod emissivity values cited varied from 0.42 to 0.93, with the majority ranging from 0.7 to 0.9. Shroud emissivities were between 0.2 and 0.8, with the majority varying from 0.2 to 0.4.

For those cases in which a value of emissivity could not be readily determined or justified, the analysis assumed a conservatively low value of 0.2 for normal conditions of transport, in which heat flows out of the cask, and 0.8 for hypothetical accident conditions, in which heat flows into the cask.

Frequently the thermal properties were not used directly as input to the thermal models but were used to calculate effective or composite thermal properties, which were then input. Section 3.6.1 gives these effective properties.

TABLE 3.2-1  
MATERIAL PROPERTIES

Material	k (Btu/hr-in.-°R)	$\rho$ (lb <sub>m</sub> /in. <sup>3</sup> )	$c_p$ (Btu/lb <sub>m</sub> -°R)	Reference (3.2- ...)
Uranium oxide (UO <sub>2</sub> )	0.417	--	0.065	1
Zircaloy-4	0.750	--	0.071	2(k); 1(c <sub>p</sub> )
304 stainless steel	0.833	0.284	0.11	3
XM-19 stainless steel	0.667 <sup>(a)</sup>	0.285	0.11 – 0.15 <sup>(b)</sup>	4(k,c <sub>p</sub> ); 5(ρ)
Depleted uranium (DU)	1.23	0.697	0.0315	6
Neutron shielding polypropylene	0.007	0.034	0.46	7
Boron carbide (B <sub>4</sub> C)	1.25	0.091	0.29	8
Aluminum alloy 5052	6.67	0.097	0.22	4, 9
Air	(c)	~0	0.24	3
Helium	(d)	~0	--	10
Aluminum alloy 6061	8.25	0.098	0.22	4, 9
Copper	18.8	0.323	0.092	9

<sup>(a)</sup>At 300°F. For those areas where a wide range of temperatures was possible, the equation

$$k = 0.30 + 4.43 \times 10^{-4} T \text{ was used, based on a linear fit to the data of Ref. 3.2-4. } T \text{ is } ^\circ\text{R.}$$

<sup>(b)</sup>Determined from thermal diffusivity data of Ref. 3.2-4.

<sup>(c)</sup> $k = 4.532 \times 10^{-4} + 1.51 \times 10^{-6} T$ , based on a fit to the data of Ref. 3.2-3.

<sup>(d)</sup>0.00651 @ 460°R

0.01009 @ 860°R

0.01319 @ 1260°R

$$k = 0.002746 + 8.35 \times 10^{-6} T \text{ linear fit}$$

**TABLE 3.2-2  
THERMAL RADIATION PROPERTIES**

Surface	$\epsilon$	$\alpha$ (Solar)	Reference (3.2- ...)
Fuel rod	0.7	--	See text
Interior of cavity liner (Fuel assembly shroud)	0.2	--	See text
B <sub>4</sub> C	0.8	--	7
Depleted uranium	0.8	--	6
Outer skin (electropolished) (normal conditions only)	0.15	--	3
Personnel barrier (normal conditions only)	0.8	0.8	16 ( $\epsilon$ ). Dark surface (conservative) assumed for $\alpha$ .
All other surfaces			
Normal conditions	0.2	--	Conservatively low value
Accident conditions	0.8	--	Conservatively high value
Surfaces exposed to thermal accident environment	0.8	--	10 CFR Part 71.73

THIS PAGE LEFT BLANK INTENTIONALLY

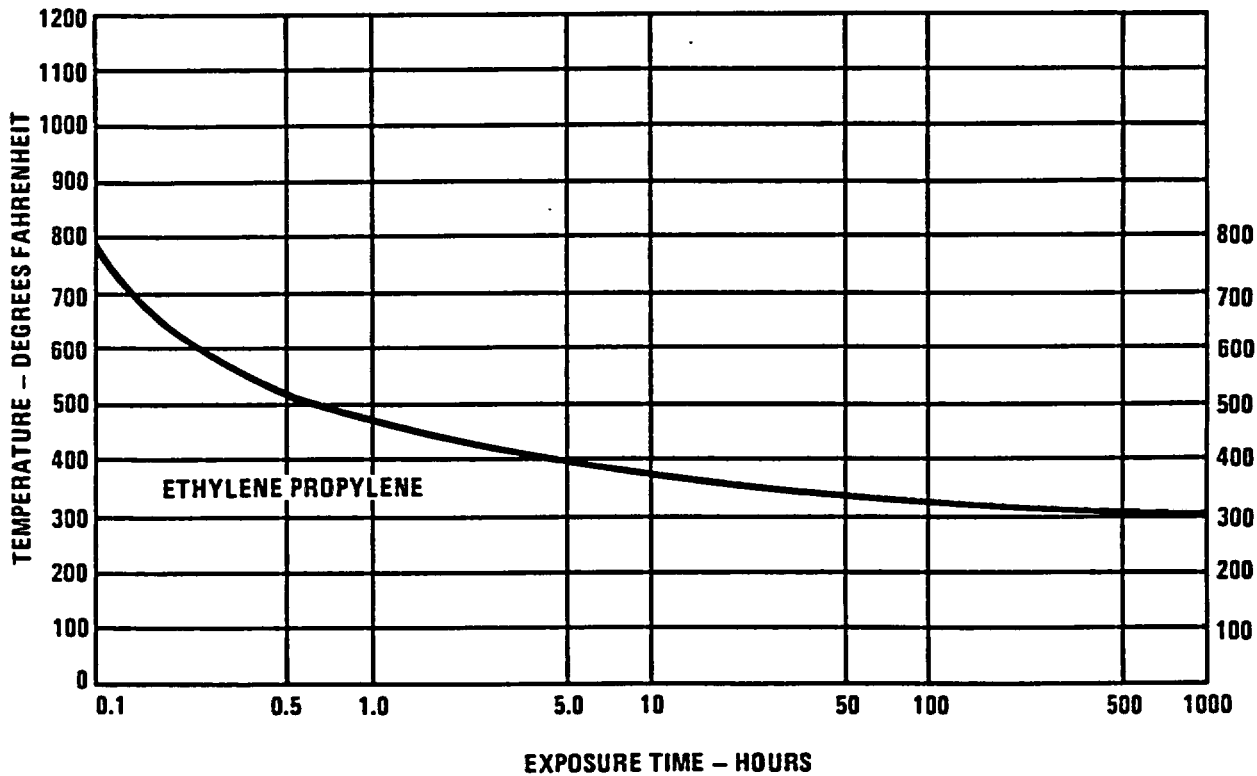
### 3.3 Technical Specifications of Components

The package components which are of concern from a thermal standpoint are the spent fuel assembly, the primary seals (which form part of the containment boundary), the neutron shielding material, and the impact limiters. Three seals constitute part of the containment boundary: the inner closure seal and gas sample port seal in the closure lid, and the drain seal at the bottom end.

During normal conditions of transport the fuel cladding temperature must not exceed 380°C (716°F). Temperature criteria for the seals are taken from Ref. 3.3-2. All seals are Parker E740-75 O-rings and use an ethylene propylene compound. This material has a lower temperature limit of -65°F. For elevated temperatures, Fig. 3.3-1 gives the life-at-temperature curve (Ref. 3.3-1). Section 4.5.1 discusses full-scale testing of the closure seals.

The neutron shielding is a modified polypropylene with 1% boron and a nominal density of 0.94 g/cm<sup>3</sup>. At the maximum normal predicted temperature, the material must retain a compressive strength sufficient to withstand normal condition structural loads (as discussed in Section 2.6). The softening point must be at least 20°F higher than the maximum normal predicted temperature. For the hypothetical accident condition. The neutron shielding must not provide a source of thermal input to the cask sufficient to degrade containment integrity.

The honeycomb impact limiters are made from aluminum alloy 5052 and use adhesives which have been tested under normal condition structural loads at -20°F and 200°F (Section 2.10.3.5). The adhesive bond is not required to survive a hypothetical thermal accident.



K-215(38)  
6-16-93

Fig. 3.3-1. Seal life at various temperatures for ethylene propylene

### 3.4 Thermal Evaluation for Normal Conditions of Transport

Regulations in 10 CFR Part 71 specify that the package shall be evaluated for normal conditions of transport under both hot and cold ambient temperatures. The hot ambient temperature is 100°F, and for this case solar radiation and maximum decay heat must also be considered. The solar radiation is specified by 10 CFR Part 71.71 to be the following for a 12-hr period:

- 800 cal/cm<sup>2</sup> (2950 Btu/ft<sup>2</sup>) for horizontal surfaces.
- 200 cal/cm<sup>2</sup> (737 Btu/ft<sup>2</sup>) for flat surfaces not horizontal.
- 400 cal/cm<sup>2</sup> (1475 Btu/ft<sup>2</sup>) for curved surfaces.

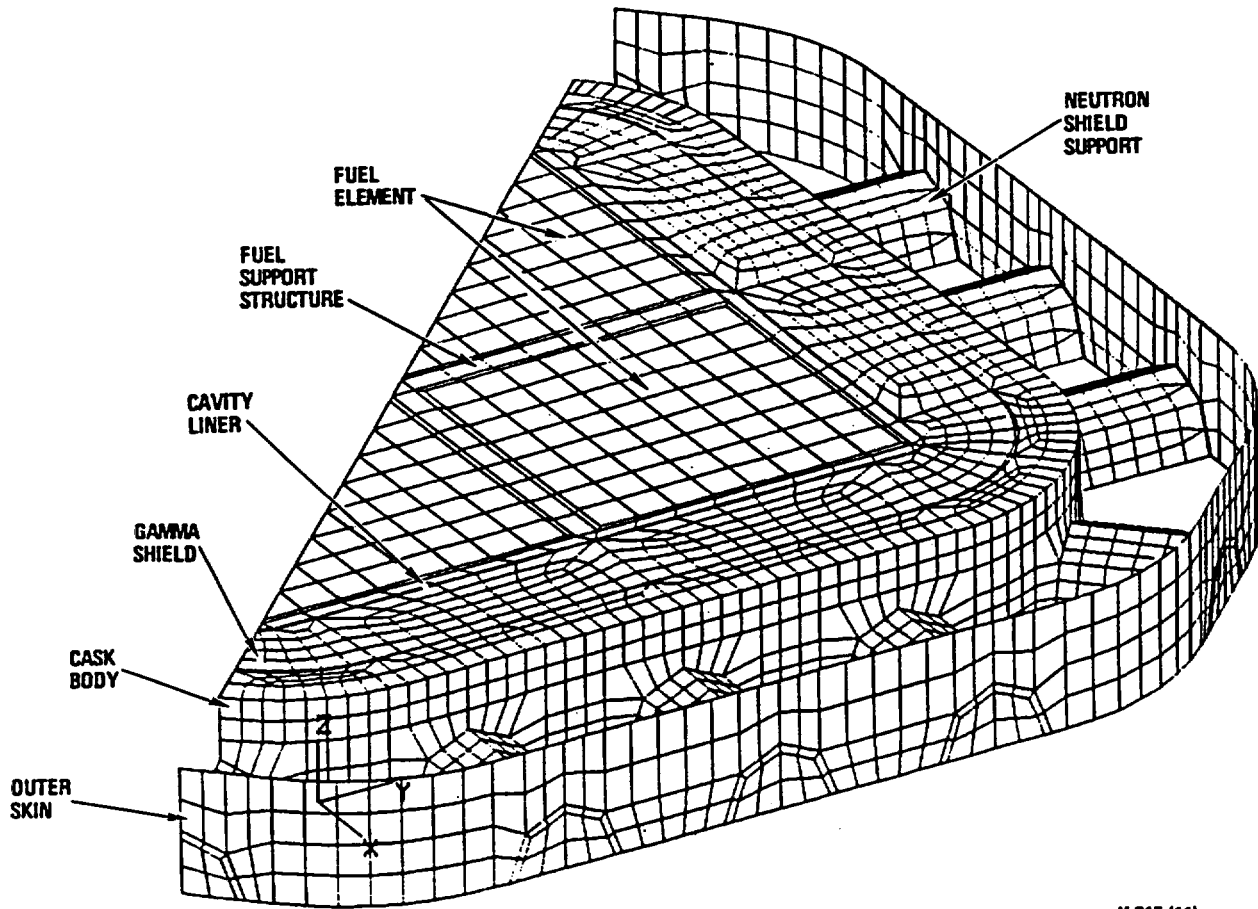
The cold ambient temperature is -40°F with no solar radiation. Both maximum decay heat and zero decay heat must be considered. (Note that for zero decay heat, all temperatures will attain steady-state values of -40°F.)

#### 3.4.1 Thermal Models

The thermal evaluation used several computer programs: ANSYS Version 4.4 (Ref. 3.4-1), PATRAN Plus (Ref. 3.4-2), and TAC2D Version 1.0 (Ref. 3.4-3). ANSYS is a general-purpose finite-element program for structural and thermal problems. PATRAN Plus (PATRAN) provides solid geometry construction, finite element modeling, and enhanced graphics. We used PATRAN to prepare the meshes for ANSYS (the preprocessing phase) and to display many of the temperature distributions in the form of isotherm plots (the postprocessing phase). To interface between the two programs, the analysis employed the PATANS translator program, Version 2.2 (Ref. 3.4-4). TAC2D is a finite-difference, two-dimensional heat transfer computer program. It solves steady-state and transient problems in rectangular, cylindrical, or circular coordinates.

For normal conditions, we developed two analytical models:

1. A 3-D PATRAN/ANSYS finite-element model of the cask representing a cross section along the axis between the impact limiters (Fig. 3.4-1). A half-section of the cask was considered in order to permit non-uniform gaps and boundary conditions. The thickness of the model in the axial direction is 3.114 in., which is half the pitch between the neutron shield supports. The neutron shield itself is conservatively omitted since its thermal conductivity is very low. This model provides a very detailed temperature distribution of major cask components and accurately treats the neutron shield support structure.



K-215 (11)  
93-91

Fig. 3.4-1. 3-D finite-element model for normal conditions

2. A TAC2D model of the whole GA-4 cask (Fig. 3.4-2). A cylindrical (r-z) coordinate system is assumed for the model. The radial gridlines were computed to give a circumference equal to that of the actual "square/round" geometry. Since no circumferential variation is permitted, we used nominal gap sizes and average solar radiation. The fuel elements and fuel support structure (FSS) are combined into a single material with composite properties. The purpose of this model is to complement model 1 by providing axial profile gradients along the cask and temperatures at the closure and bottom ends.

The following sections discuss other general aspects of the thermal models:

1. **Effective Thermal Properties.** A detailed, explicit representation of all cask components was not feasible. Therefore it was necessary to use composite or effective thermal properties in the models. The calculation of effective thermal properties followed two general procedures. One was to combine two modes of heat transfer (typically conduction and thermal radiation) into a single effective thermal conductivity. An example of this is the spent fuel assembly (SFA), which was modeled as a homogeneous, heat-generating mass. Another procedure was to treat two or more materials as a single composite material (for example, the boron carbide pellets in the FSS and the steel with which the FSS is constructed). Section 3.6.1 gives effective thermal properties for normal and hypothetical accident conditions.
2. **Decay Heat.** For the reference case, we used a PWR decay heat of 617 W per assembly. This is based on use of the ORIGEN-S computer code, as discussed in Section 5.2, and assumes 35 GWd/MTU burnup, 10-yr cooling, and a conservative enrichment of 3 percent. In addition, we imposed an axial power profile (Table 3.4-1) on the decay heat. The axial power profile gives a peaking factor of 1.22. We input the entire decay heat profile in the TAC2D model and used the average decay heat with peaking factor in the ANSYS model to give temperatures at the hottest section of the cask.

Both models assume that all the decay heat is generated in the fuel. Since the heat arises largely from gamma energy, a significant portion will be produced in other components outside the fuel, mostly in the DU gamma shielding. The calculation of spent fuel assembly and cavity temperatures is therefore conservative.

Other decay heat configurations were also considered, to permit the shipment of hotter fuel assemblies. Section 3.6.8 provides the details of this part of the thermal evaluation.

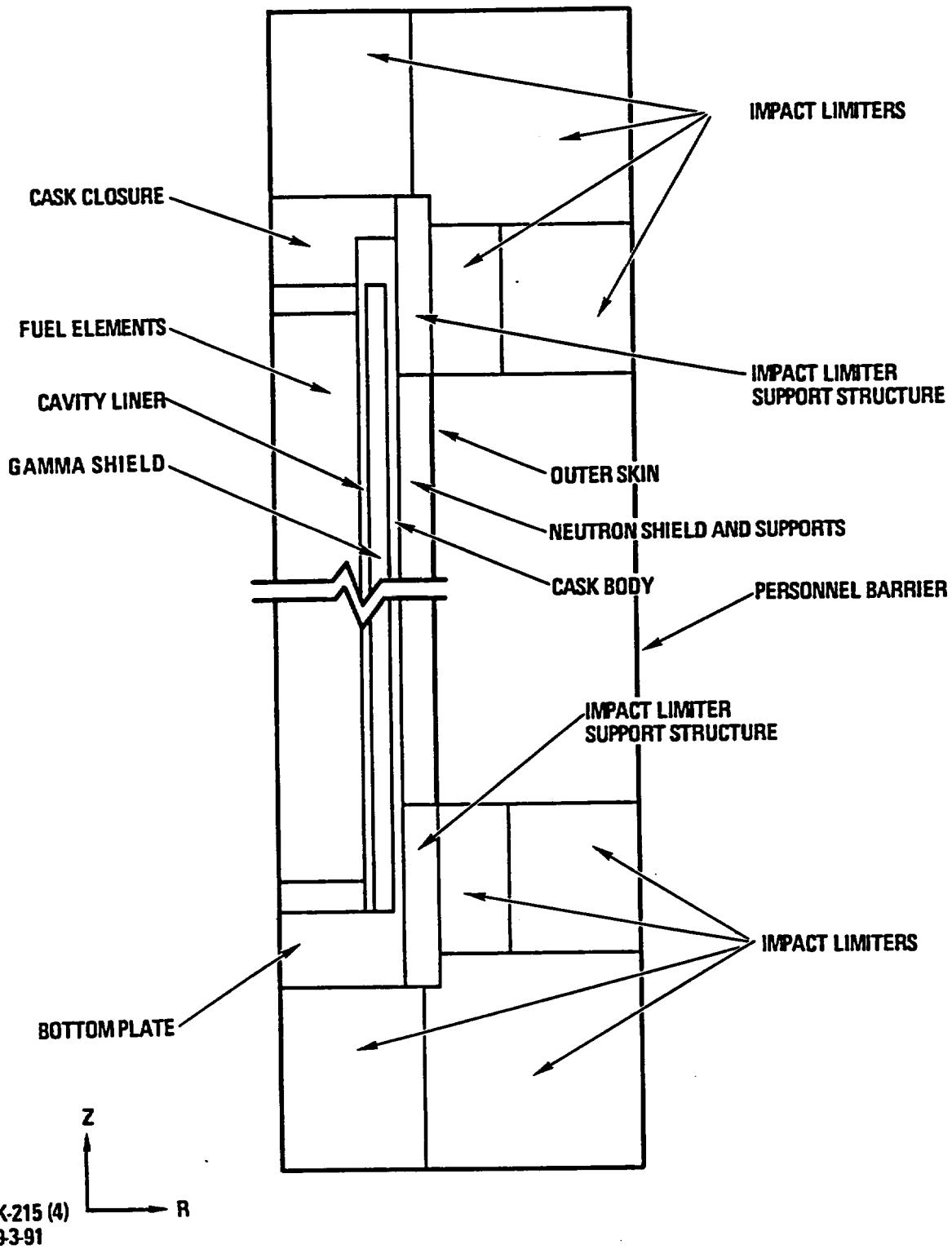


Fig. 3.4-2. TAC2D model for normal conditions

TABLE 3.4-1  
PWR DECAY HEAT AXIAL PROFILE

Distance from Bottom of Fuel (in.)	Decay Heat (Watts/in.)	Relative Power <sup>(a)</sup>
2.0	1.85	0.432
6.0	2.70	0.630
11.0	3.63	0.847
16.0	4.13	0.964
22.0	4.66	1.09
35.0	5.23	1.22
56.0	5.23	1.22
95.0	4.66	1.09
112.0	4.13	0.964
122.0	3.63	0.847
132.0	2.70	0.630
139.0	1.85	0.432
144.0	1.08	0.252

<sup>(a)</sup>Average Power =  $617/144 = 4.285$  W/in.

3. **Boundary Conditions.** During transport, heat transfer from the external surface (personnel barrier) to ambient assumes combined natural convection and thermal radiation. For an ambient temperature of 100°F and a representative surface temperature of 130°F, a typical combined coefficient is 1.5 Btu/hr-ft<sup>2</sup>-°F. Thermal radiation contributes about two-thirds of this. Correlations for natural convection and thermal radiation are given in Section 3.6.2
4. **Air Space inside Personnel Barrier.** For the space between the personnel barrier and the outer skin, we developed equations to calculate the air flow. Ambient air enters at the bottom of the trailer through the gap between the splash pan and frame, and exits at the top through a vent in the personnel barrier. The flow is determined by balancing the pressure drop with the driving head caused by the temperature (density) difference. The resulting equations are given in Section 3.6.3. The TAC2D model uses these equations to calculate the air temperature rise and also treats the radiation interchange between the outer skin and personnel barrier.

The ANSYS model does not explicitly include the personnel barrier but terminates with the outer skin. However, the personnel barrier is fully accounted for by use of an effective ambient temperature calculated to yield the same heat transfer from the outer skin as if the personnel barrier were in place. The calculation of this effective ambient temperature is documented in Section 3.6.4.

5. **Solar Radiation.** Using the data of 10 CFR Part 71.71, we computed incident solar radiation values to be applied to the outer surfaces of the TAC2D model. For the axial ends, the value is equal to the vertical surface value; for the outer cylindrical surface of the model we computed an average value based on a combination of a curved and a vertical surface, representing the true shape of the personnel barrier. The solar radiation values are given in Section 3.6.5.

For the ANSYS model, which does not include the personnel barrier, the effective ambient temperature discussed in the preceding section accounts for the solar radiation.

6. **Neutron Shield Support Tubes.** As shown in Fig. 3.4-1, the neutron shield support tubes are explicitly treated in the ANSYS model. Heat flow relies on mechanical contact between the tube flange and the outer skin. When the connector is welded to the skin, weld shrinkage will tend to clamp the tube flange tightly against the skin. Section 3.6.9.2 discusses the sensitivity of the cask temperatures to this contact. For the TAC2D model the neutron shield and support tubes are lumped together with an effective thermal conductivity, based on the results of the ANSYS model.

### 3.4.2 Maximum Temperatures

Figure 3.4-3 shows steady-state isotherms produced by the ANSYS model with non-uniform gaps under conditions of 100°F ambient, decay heat with peaking factor, and solar radiation. Non-uniform gap results are shown because these are more realistic during transportation of the cask. However, the difference between the results for uniform and non-uniform gaps is not great, the largest effect being in the cavity liner, whose maximum temperature is about 7°F higher with non-uniform gaps.

More significant is the effect of axial heat conduction. The ANSYS model, being essentially a cross section through the cask, assumes adiabatic ends and therefore no axial conduction. However, using the TAC2D model with and without axial conductivities allows an assessment of this effect. Results from this study indicate that axial conduction is particularly significant for the temperatures near the center, i.e., the spent fuel and cavity liner. Table 3.4-2 summarizes the axial conduction effect. These temperature differentials can then be applied to the results of Fig. 3.4-3 to obtain a more realistic picture of the temperature distribution at the cask center.

Location	Temperature Decrease (°F)
Fuel/FSS	18
Cavity liner	15
Gamma shield	15
Cask body	14
Neutron shield	12
Outer skin	9

Figure 3.4-4 provides a steady-state temperature map of the whole cask, using the TAC2D model under conditions of 100°F ambient, decay heat with axial power profile, and solar radiation. Fig. 3.4-5 plots axial temperature profiles along the length of the fuel cavity. Superimposed on these profiles are circumferential temperature variations as taken from the ANSYS results of Fig. 3.4-3.

Figure 3.4-6 gives a temperature history of the cask components for a transient situation in which the cask goes from a uniform loading temperature of 100°F to hot normal transport conditions. Note that the cask achieves steady-state conditions in about 100 hours. We produced these results with the same TAC2D model as used for steady-state.

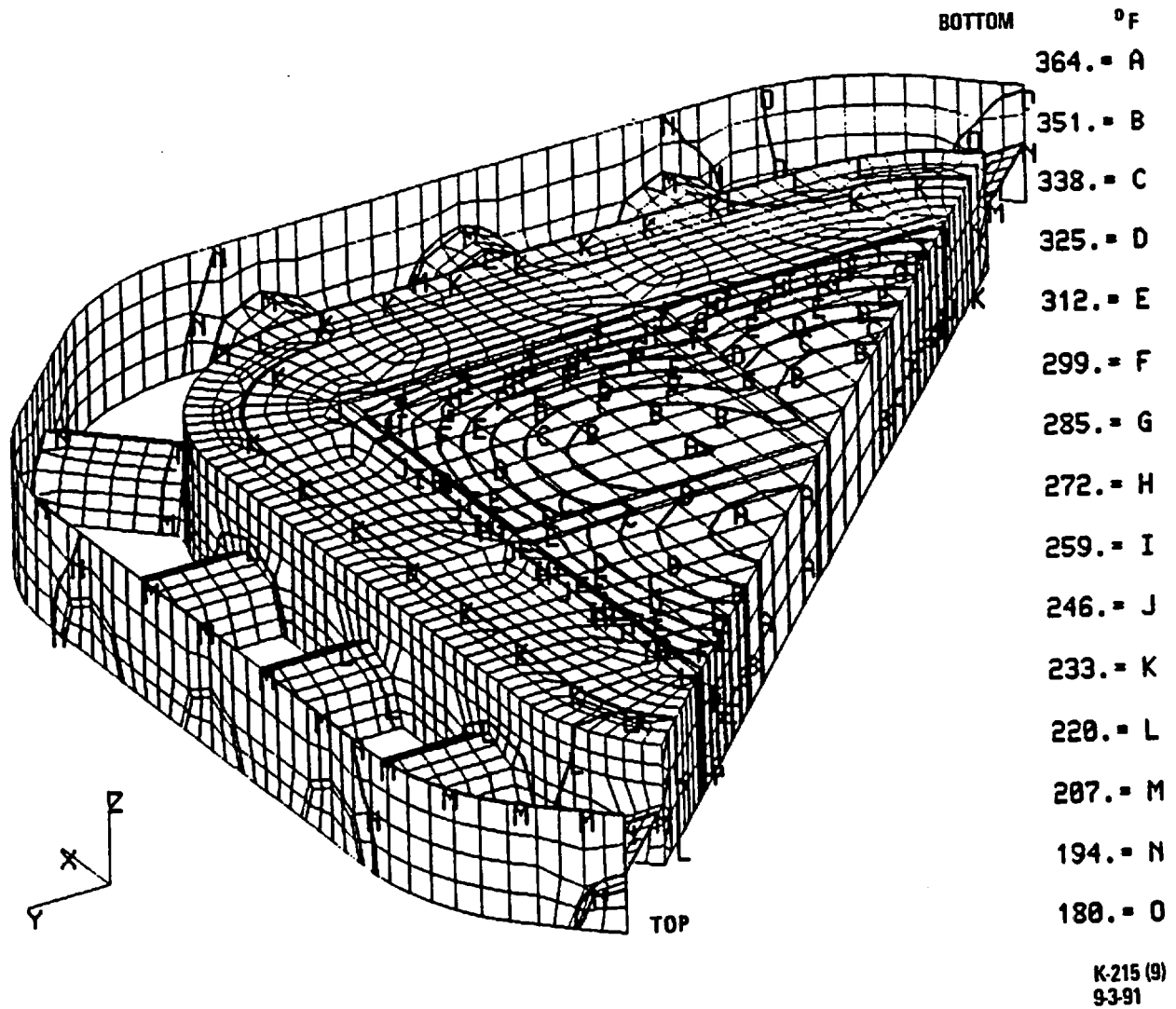


Fig. 3.4-3. Isotherms for 3-D model (hot normal conditions)



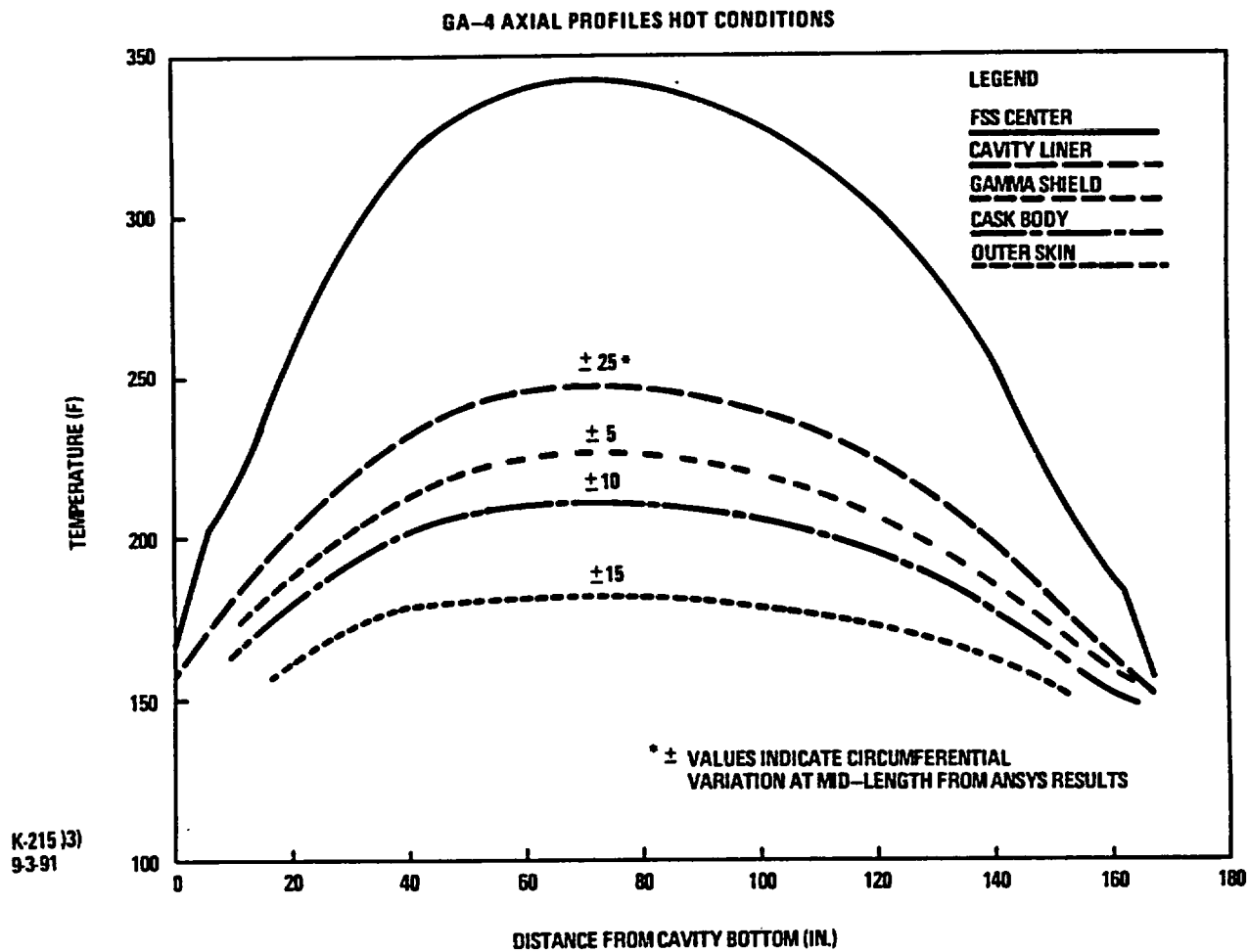


Fig. 3.4-5. Axial temperature profiles (hot normal conditions)

GA-4 NORMAL TRANSIENT (HOT)

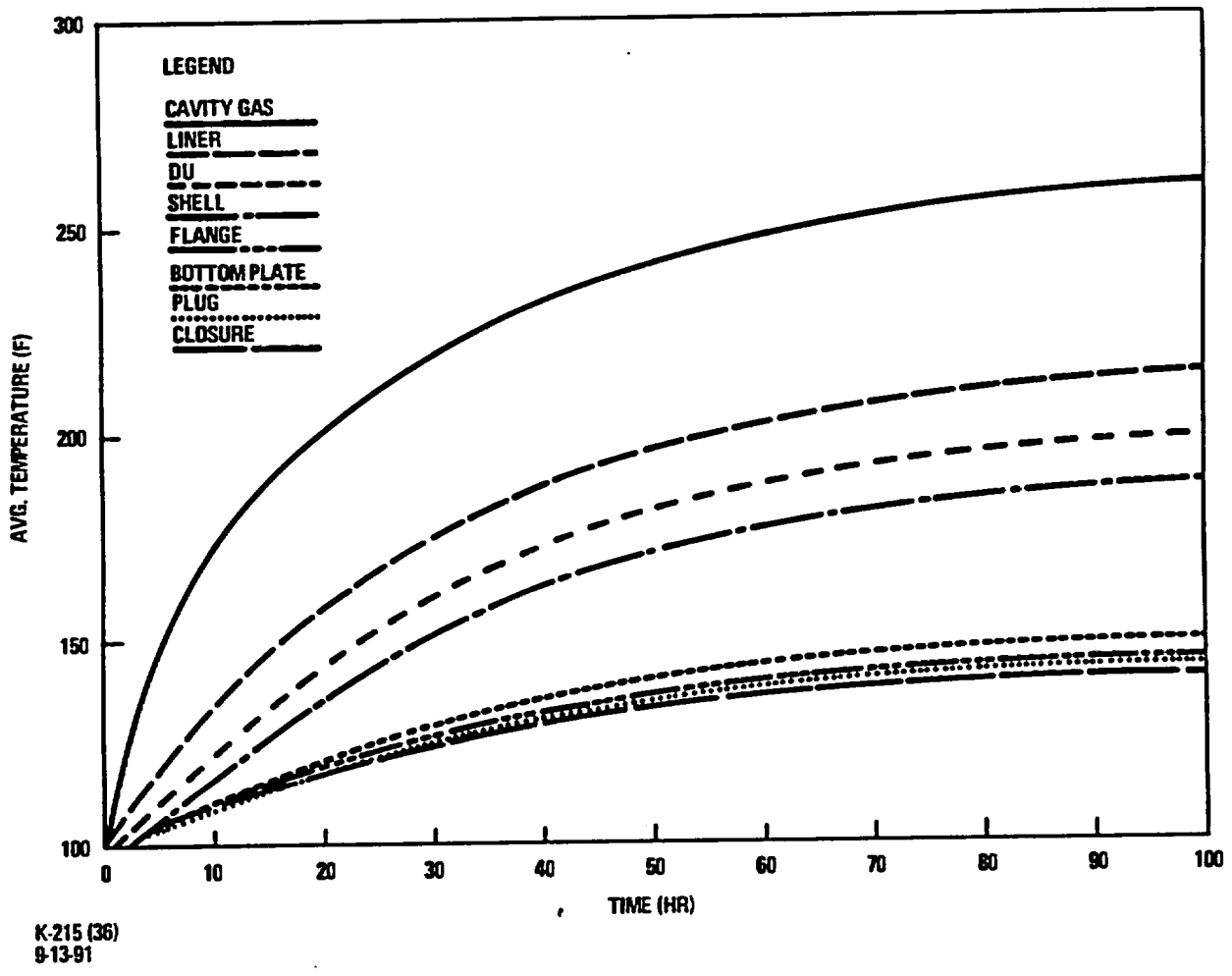


Fig. 3.4-6. Temperatures for normal transient (hot conditions)

Combining all steady-state results, Table 3.4-3 summarizes maximum and average component temperatures. These temperatures are used to compare with allowables and to calculate thermal growth and stresses in Section 2.6.1. The results for configurations with hotter fuel assemblies are presented in Section 3.6.8, and the temperatures are lower than or equal to those of Table 3.4-3.

### 3.4.3 Minimum Temperatures

Figure 3.4-7 gives a temperature history of the cask components for a transient situation in which the cask goes from a uniform loading temperature of 100°F to transport conditions at -40°F ambient with maximum decay heat. However, the minimum cask temperatures occur with no decay heat and will eventually all attain -40°F.

### 3.4.4 Maximum Internal Pressures

The maximum normal operating pressure (MNOP) for the GA-4 cask results from three sources: (1) cavity temperature increase, and under the assumed condition of 100% rod cladding failure, (2) release of initial fill pressure, and (3) release of gas fission products.

We analyzed the worst-case fuel elements to envelop all the spent fuel elements identified in Section 1.2.3, Contents of Packaging. The B&W 15 x 15 Mark B fuel element gives the highest MNOP of 36.9 psig for the GA-4 cask. Calculations are given in Section 3.6.6.

### 3.4.5 Maximum Thermal Stresses

The calculation of thermal stresses is given in Section 2.6.1 and uses the information of Table 3.4-3. Temperature gradients through the cavity liner and cask body walls are very small ( $< 2^\circ\text{F}$ ).

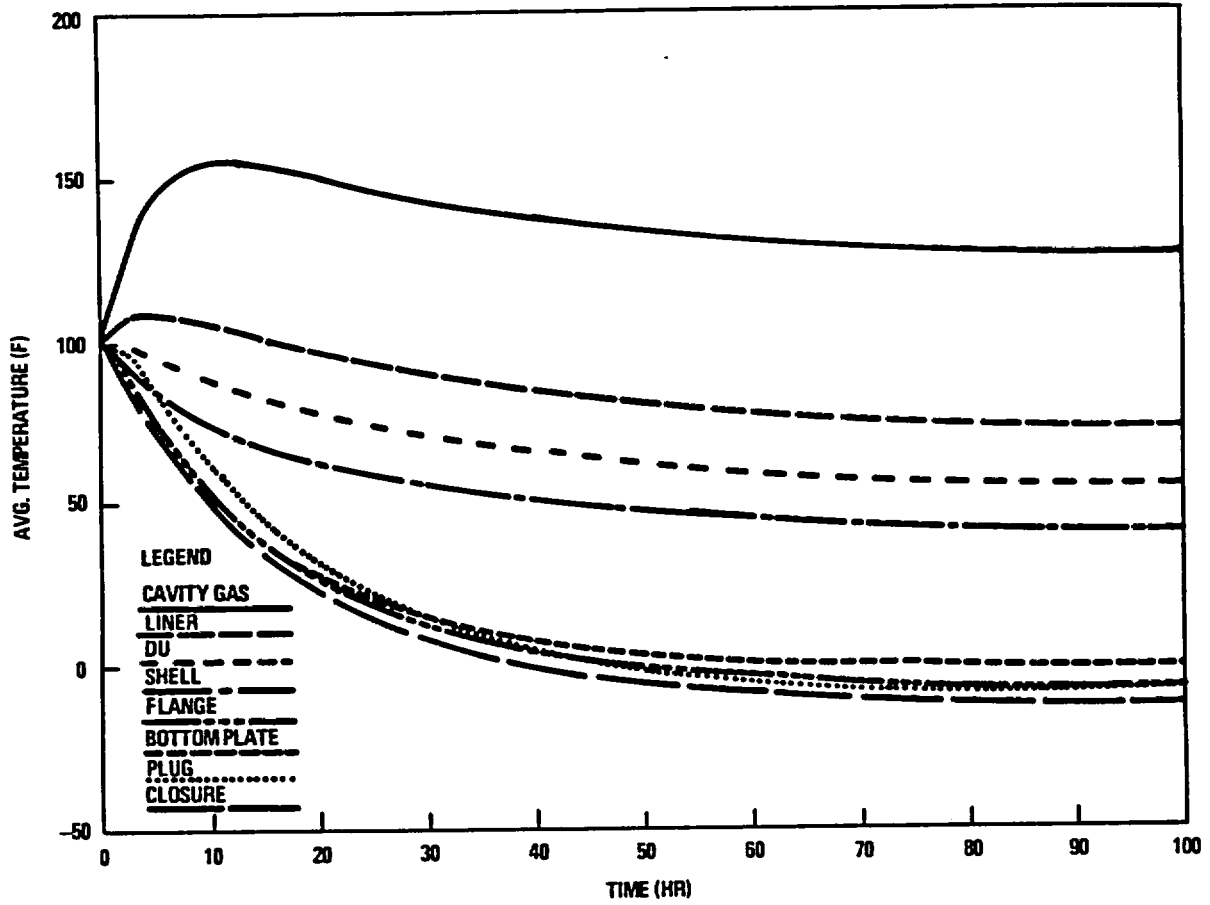
### 3.4.6 Evaluation of Package Performance for Normal Conditions of Transport

Table 3.4-3 shows that all component temperatures for the case of 100°F ambient are within design limits. The maximum cladding temperature of 373°F is well below the allowable of 716°F. No accessible surface of the package exceeds 136°F even with full solar radiation, so the criterion of 180°F maximum in the shade set by 10 CFR 71.43 is satisfied. The neutron shield (polypropylene) has a softening temperature of 302°F (Ref. 3.4-5). Since the highest calculated neutron shield temperature is 213°F, the margin exceeds the 20°F criterion specified in Section 3.3. At 250°F, the compressive strength (1% strain) of the neutron shield is 239 psi (Ref. 3.4-5), which is more than adequate to withstand normal-condition structural loads. The maximum temperature of the closure and gas sample port seals, 143°F, is well within the limit of 300°F at which the ethylene propylene can function for 1000 hr. The same is true for the drain seal at 155°F. At the opposite end the minimum seal temperature of -40°F is above the low-temperature limit of -65°F. Performance of the seals at normal-condition temperatures was verified by testing at temperatures of -42°F, ambient (~75°F), and 250°F (Section 4.5.1). For the impact limiters, the maximum temperature of 145°F is below the 200°F at which the impact limiters were tested.

**TABLE 3.4-3  
SUMMARY OF TEMPERATURES FOR NORMAL CONDITIONS, STEADY STATE (°F)**

Component	Maximum		Cross-section Average		Axial Average
	Midlength	End <sup>(a)</sup>	Midlength	End	
FSS	343	235 <sup>(b)</sup>	314	228	286
Cavity liner	273	214	248	189	216
Gamma shield (DU)	232	185	227	180	201
Cask wall	221	180	211	170	190
Neutron shield	213	180 <sup>(c)</sup>	197	164	183
Outer skin	197	173	182	158	175

Fuel cladding	348 max. <sup>(d)</sup>	<sup>(a)</sup> 15 in. from cavity bottom. <sup>(b)</sup> 173 at true FSS end. <sup>(c)</sup> Conservatively assumed same as cask wall. <sup>(d)</sup> 373 for hotter fuel (Section 3.6.8). <sup>(e)</sup> Cask wall temperature 30 in. from cavity bottom.
Cavity gas	262 avg.	
Closure seal	143	
Drain seal	155	
Closure (plug)	147	
Impact limiters	145 max.	
Trunnions	190 <sup>(e)</sup>	
Personnel barrier	136 max.	



K-215 (35)  
9-13-91

Fig. 3.4-7. Temperatures for normal transient (cold conditions)

### 3.5 Hypothetical Accident Thermal Evaluation

For hypothetical accident conditions, 10 CFR Part 71.73 states that the package must be exposed for at least 30 min to a radiation environment whose temperature is 800°C (1475°F). The environment emissivity must be 0.9 and the surface absorptivity of the package 0.8. No artificial cooling is to be applied to the package after the 30 min of exposure. The effects of solar radiation may be neglected before, during, and after the accident. Initial conditions must be based on 100°F ambient with maximum decay heat or -20°F ambient with no decay heat, whichever is worse.

#### 3.5.1 Thermal Models

Using the TAC2D and ANSYS codes, we employed three analytical models to analyze the cask under accident and post-accident conditions. Section 3.6.1 gives effective thermal properties for these models.

##### 3.5.1.1 TAC2D Models.

**3.5.1.1.1 Accident Transient.** Figure 3.5-1 shows the TAC2D model for calculating the transient primary closure seal and average cavity gas temperatures during the accident. For this situation we considered only the portion of the cask from the axial midpoint to the closure. Restricting the scope of the model allowed a much finer grid spacing to adequately handle the expected thermal gradients without using an excessive number of gridlines.

The model assumes the absence of the personnel barrier, outer skin, neutron shielding, and support tubes. These components may at least be severely damaged in the 30-ft drop and puncture events (which must precede the thermal accident in the regulatory sequence) and are not designed for accident condition loads. In addition, the neutron shielding and its support tubes may partially melt during the thermal accident. (See Section 3.6.7 for an assessment of the thermal performance of the neutron shielding.) It is therefore conservative to omit these components altogether. We did take credit for the structural integrity of the impact limiters because they are designed to remain attached. However, as a result of the drop and puncture events, we assumed the end impact limiter at the closure end to be crushed to 30% of its original thickness (based on results in Section 2.10.3), and we allowed for a 6-in.-diameter hole completely through this impact limiter directly over the closure seals. The end impact limiter is therefore crushed to a thickness of  $0.30 \times 23 = 6.9$  in., and we assumed the corner impact limiter to be crushed by the same amount ( $23 - 6.9 = 16.1$  in.) in the same direction. We simulated damage from an end (rather than a corner or side) drop because this would provide the most direct thermal path from the accident environment (1475°F) to the closure seals.

An inherent conservatism in this approach lies in the fact that, because of the axisymmetric model, the 6-in.-diameter hole is actually a 6-in.-wide "ring." (See inset, Fig. 3.5-1.) As a result, the closure surface area exposed to the accident is about 18 times greater than a 6-in.-diameter hole.

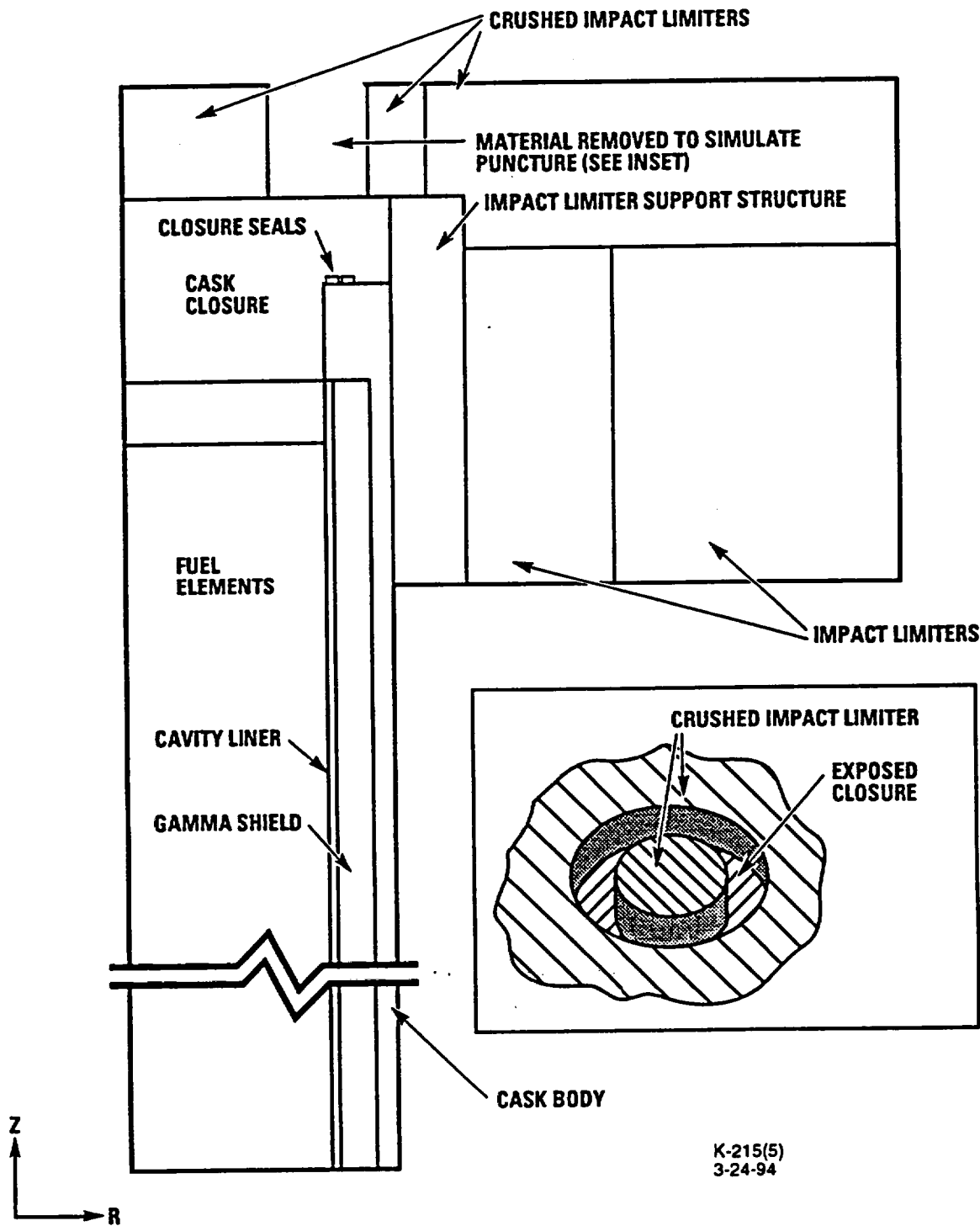


Fig. 3.5-1. TAC2D model for hypothetical accident conditions

We used initial conditions for a hot (100°F) ambient with maximum decay heat. To generate an initial temperature distribution, we ran a steady-state case using a slight modification in the accident model. (Temperatures determined by the normal-condition TAC2D model cannot be imposed as initial temperatures on the accident model because the nodes for the two models are not in the same locations.) Prior to the accident there is no damage to the cask, and for the initial-condition case we thus replaced the "hole" with impact limiter material. We kept the impact limiter thickness at 30% but altered the thermal conductivity so that the conductance reflected an initial uncrushed state. Rather than changing the model to include the personnel barrier, outer skin, and neutron shielding just for initial conditions, we took temperature results from the normal-condition model (Fig. 3.4-4) and calculated interpolated boundary conditions for the corresponding locations in the accident model. We therefore produced initial steady-state conditions that closely match the actual temperature distribution for an undamaged cask.

We determined the external heat transfer coefficient during the accident and cooldown on the basis of convection and radiation. During the 30-min exposure we used a forced convection coefficient of 2.0 Btu/hr-ft<sup>2</sup>-°F, which is based on an external velocity of 20 ft/s. We calculated the radiation portion to be between 13 and 36 Btu/hr-ft<sup>2</sup>-°F, depending on the surface temperature. Correlations are given in Section 3.6.2.

**3.5.1.1.2 Post-Accident Steady-State.** The previous model accounted for cask damage that would produce the highest peak temperatures during the hypothetical thermal event. After the thermal event the cask will achieve a steady-state condition whose temperatures are dependent on the damage. However, the damage assumed for peak temperatures will not necessarily produce the greatest post-accident steady-state temperatures. If the neutron shield and aluminum support tubes only partially melt, the cask will not dissipate heat as efficiently as if they are completely absent, as assumed in the previous model.

To calculate post-accident maximum temperatures, we used the model for normal conditions of transport (Fig. 3.4-1) with some modifications. Several damaged states were considered for the neutron shield and its support tubes:

- The neutron shield and tubes partially melt, leaving an 0.5-in. air gap between them and the intact outer skin. Heat transfer across the gap occurs by conduction and thermal radiation.
- As above, with a 1-in. air gap.
- The neutron shield and tubes are completely absent. Heat transfer across the air space occurs by natural convection and thermal radiation.

In all cases contact between the tubes and the skin is broken, eliminating the main heat flow path. We also assumed partial melting of the impact limiters, and a 1-in. air gap was introduced between the impact limiters and their steel outer skin. Finally, the personnel barrier was assumed absent since the tarpaulin would not survive a thermal event sufficient to melt the neutron shield and aluminum tubes. The heat transfer from the cask surfaces to

ambient was based on natural convection (see Section 3.6.2.1) and thermal radiation with a post-accident surface emissivity of 0.8.

As with normal conditions of transport, the analysis used the reference decay heat of 4 PWR with 617 W per assembly, solar radiation, and an ambient temperature of 100°F.

**3.5.1.2 ANSYS Model.** Figure 3.5-2 shows the finite-element mesh for the ANSYS model. This model was constructed specifically to provide temperatures for the corresponding thermal stress analysis in Section 2.7.3. The model is a 1/8 section of the cask and extends axially from a point 18 in. below the impact limiter support structure to the closure end. The distance of 18 in. was judged to be sufficiently long to handle any thermal effects the cask body might exert on the closure end. Components included in the model are the cask body, gamma shield, cavity liner, flange, closure, impact limiters, and impact limiter support structure. We did not consider the spent fuel assemblies and fuel support structure. The cavity's inner surface is therefore an adiabatic boundary during the thermal accident. We also omitted the personnel barrier, outer skin, and neutron shield, as in the TAC2D model.

As with the TAC2D model, we assumed the end impact limiter to be crushed to 30% of its original thickness. For the puncture damage, thermal stresses in the closure will increase with the size of the hole in the impact limiter. The largest possible area that can be created by a 6-in. bar is a diagonal gash across the cask closure. Since only a 1/8 section of the cask is modeled, the total closure area exposed by the gash was calculated and converted to an equivalent-area square hole centered on the closure. See Fig. 3.5-3.

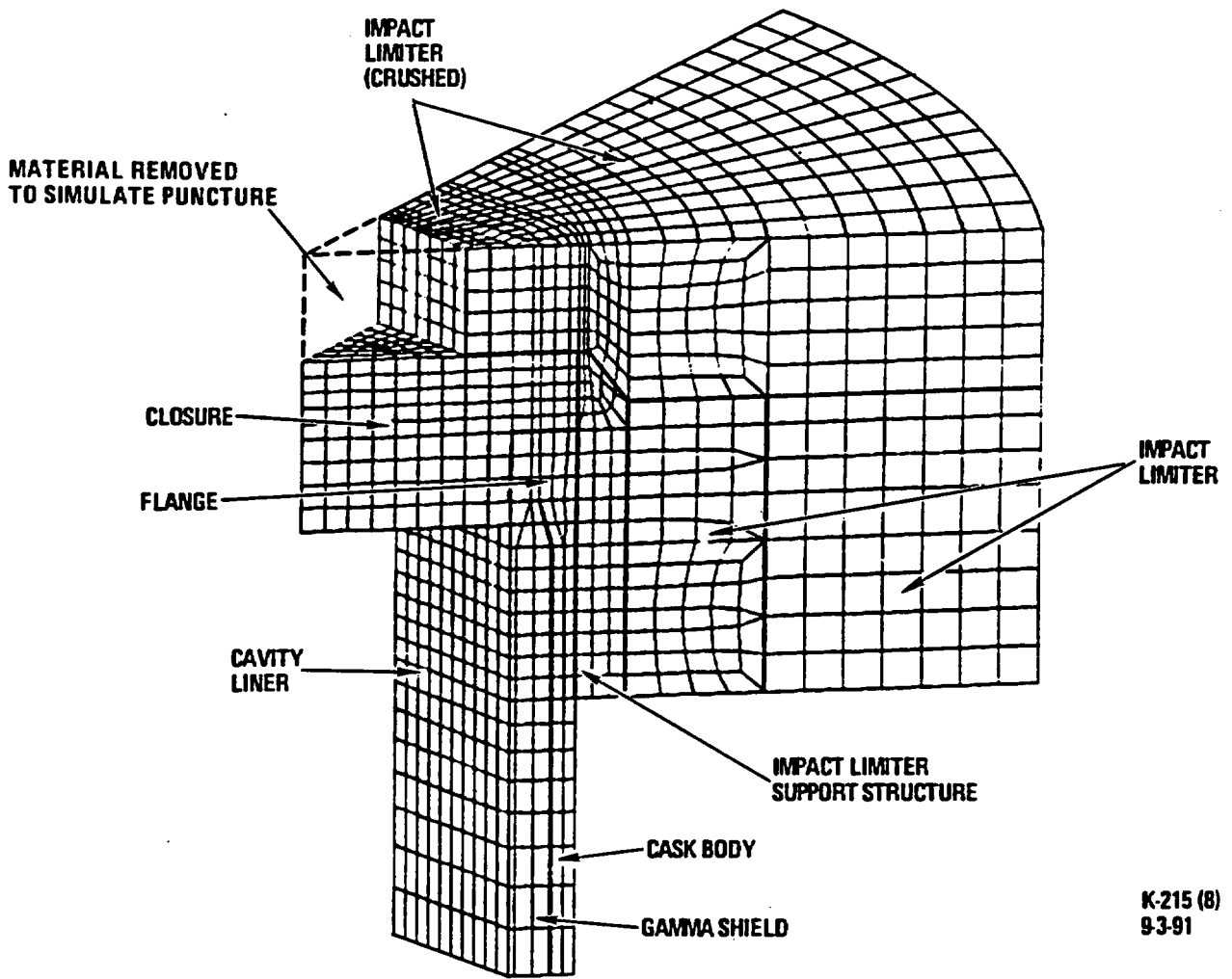
We used the ANSYS model with both hot and cold (-20°F) initial conditions to find the worst case for the thermal stresses. Initial temperatures for the hot condition were produced in a manner similar to that for the TAC2D model: the end impact limiter was modeled without the puncture, but its thickness remained at 30%. Boundary conditions from the TAC2D analysis of Section 3.4 were imposed at the appropriate locations on the model. These boundary conditions consisted of heat fluxes for the interior surfaces (plug, cavity liner) and surface temperatures for the exterior (cask body, impact limiters).

For a cold initial condition there is no decay heat. The initial temperature distribution for the accident model is therefore a uniform -20°F, which can be specified directly in the ANSYS input.

Heat transfer coefficients during the hypothetical accident were calculated with the same correlations used for the TAC2D model.

### **3.5.2 Package Conditions and Environment**

Damage to the package is discussed in the previous section.



K-215 (8)  
9-3-91

Fig. 3.5-2. 3-D finite-element model for hypothetical accident conditions

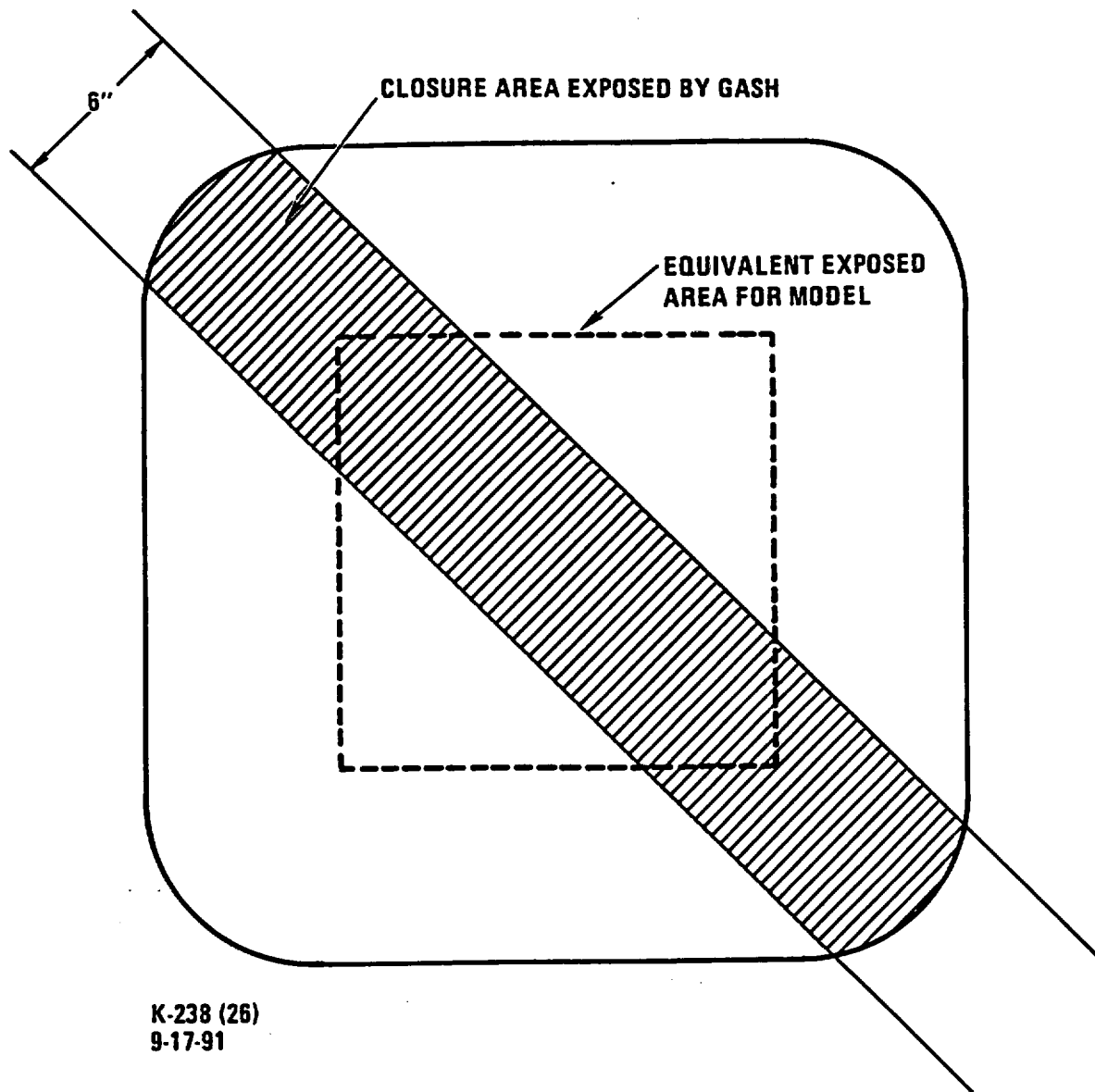


Fig. 3.5-3. Modeling of closure area exposed by puncture

### 3.5.3 Package Temperatures

Figure 3.5-4 presents transient temperature plots for the primary closure seal and the average cavity gas as produced with the TAC2D model. Since the model considers the impact limiter puncture directly over the seal and begins with hot initial conditions, the peak temperatures in these plots represent the maximums encountered in the thermal accident. The gas sample port seal is located at a depth further into the closure, in both the radial and axial directions, than the primary closure seal. It will therefore see a maximum temperature lower than will the primary closure seal. The primary drain seal is located in the bottom plate. Although the bottom end is not included in the TAC2D model, this seal is situated in approximately the same radial position as the primary closure seal and at an axial depth about 1 in. further into the bottom plate than the primary closure seal is into the closure. Thus the primary drain seal will also see a peak temperature lower than will the closure seal.

Table 3.5-1 gives maximum temperatures for the seals, average cavity gas, and containment boundary. The containment boundary temperatures are taken from the ANSYS model results with hot initial conditions and are used in Section 2.7.3 in the evaluation of allowable stresses due to pressure.

Melting of the aluminum honeycomb impact limiters is not considered in these results. Although the thermal models predict that temperatures of these components may exceed their melting point (~ 1100°F), the assumption that the impact limiters remain intact and solid has been shown to be conservative. (See Sec. 3.6.9.4)

The post-accident steady state analysis shows that for the reference decay heat (2468 W) the maximum closure seal temperature, considering all the damaged states described in Section 3.5.1.1.2, is 155°F and the maximum cavity gas temperature is 305°F. From Section 3.6.8, the reference decay heat is the maximum total allowed and therefore these temperatures are also the maximum for all the hotter fuel cases.

### 3.5.4 Maximum Internal Pressures

The maximum internal pressure during hypothetical accident conditions results from an increase in cavity temperature. Using the maximum average cavity temperature of 393°F, we calculated a maximum internal pressure of 46.3 psig (61.0 psia). This was obtained by multiplying the MNOP of 36.9 psig (51.6 psia) given in Section 3.4.4 by the ratio of the absolute temperatures (853/722).

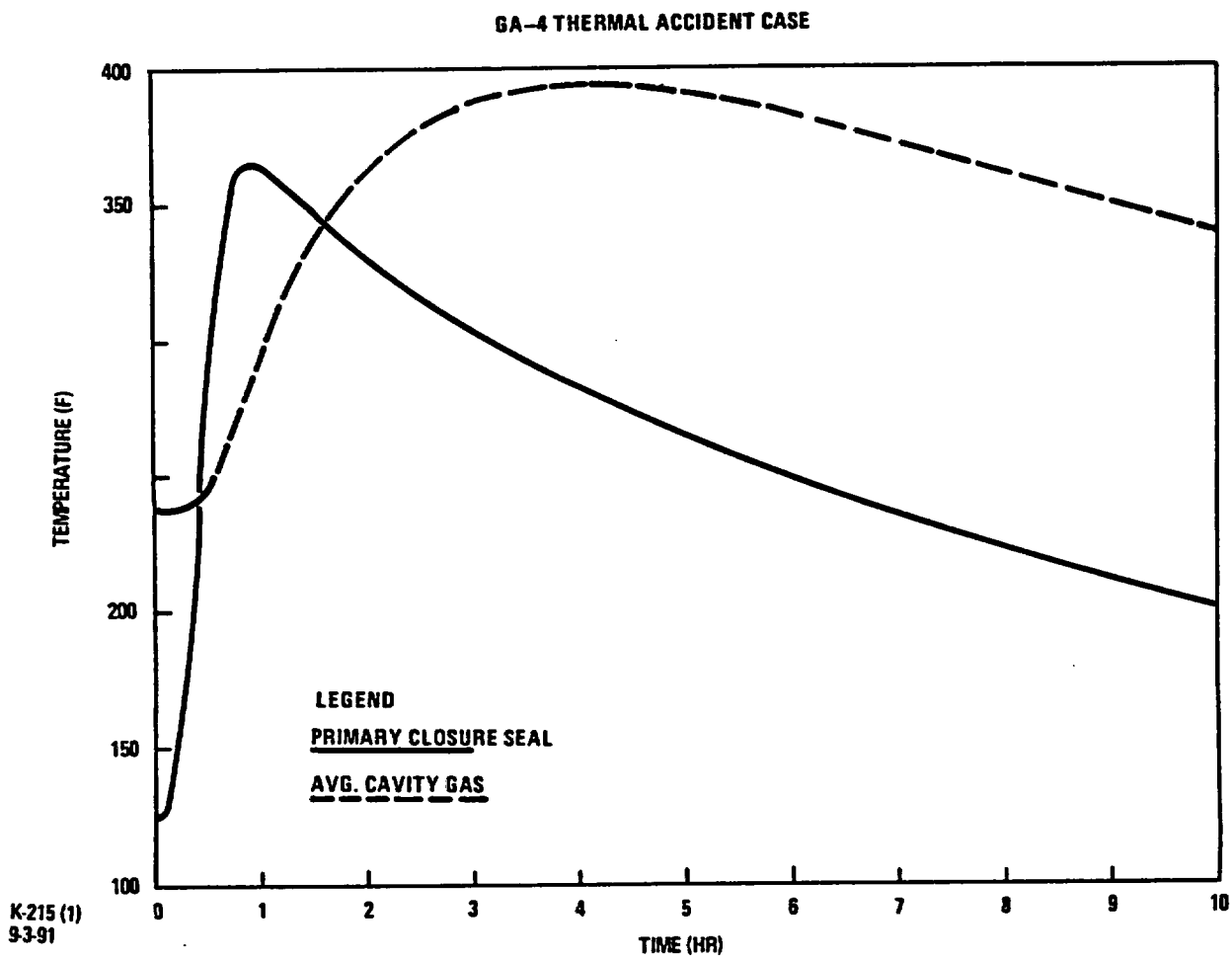


Fig. 3.5-4. TAC2D model temperatures for hypothetical accident conditions

<b>TABLE 3.5-1 MAXIMUM TEMPERATURES FOR THERMAL ACCIDENT CONDITIONS</b>			
Location	Time (hr)	Temperature (°F)	Model
Primary closure seal	0.9	365	TAC2D
Average cavity gas	4.0	393	
Closure center	0.5	720	ANSYS
Flange/taper at flats			
outer	2.5	260	
midwall	2.5	260	
inner	2.5	260	
Flange/taper at corner			
outer	1.8	270	
midwall	1.8	270	
inner	1.8	270	
Cask midlength at flats			
outer	0.5	980	
midwall	0.5	910	
inner	0.5	860	
Cask midlength at corner			
outer	0.5	1140	
midwall	0.5	1080	
inner	0.5	1060	

### 3.5.5 Maximum Thermal Stresses

The analysis to predict thermal stresses and thermal-induced distortion of the closure and flange seal interface used the ANSYS model described in Section 3.5.1. We imposed the temperature distributions from this model as loads on a separate structural model and used the ANSYS capability to interpolate between finite-element meshes. The structural model used a mesh more appropriate for stress calculations and eliminated those components that were of no interest structurally.

Sections 2.7.3 and 2.10.12 give results of the thermal stress analysis and a description of the structural model.

### 3.5.6 Evaluation of Package Performance for Hypothetical Accident Thermal Conditions

Referring to Table 3.5-1, the maximum primary closure seal temperature during the hypothetical accident is 365°F. This temperature may conservatively be used for all containment seals. The sealing ability of an elastomeric gasket is typically a function of its time-at-temperature history. The manufacturer's data for the seal material (Section 3.3) indicate that it can function for about 50 hr at 350°F and for 5 hr at 400°F. Figure 3.5-4 shows that the seal is between 350 and 365°F for less than 1 hour. We have tested the seal at 380°F, after heating for 1.5 hr above 350°F, and have shown that it will function under these conditions (Section 4.5.1).

The maximum post-accident steady-state temperatures are 155°F for the closure seal and 305°F for the cavity gas. These are well within the values of Table 3.5-1.

In Section 2.7.3 we evaluate containment boundary stresses, using a conservative internal pressure of 51.0 psig. These are found to be well within allowables for the temperatures given in Table 3.5-1.

Results of the neutron shield thermal test are discussed in detail in Section 3.6.7. In this test the back side of the test article, representing the interface between the neutron shield and the cask body, remained well below 800°C (1475°F). The maximum measured temperature, 390°C (734°F), is a less severe condition than assumed in the analysis in which the neutron shield was completely absent and the cask body was exposed directly to the accident environment.

The thermal analysis and testing thus demonstrates that the package will perform satisfactorily during hypothetical thermal accident conditions and will maintain containment integrity.

### 3.6 Appendix

#### 3.6.1 Effective Thermal Properties

The following definitions are used in this section:

$k_{\text{He}}$  = helium conductivity (Table 3.2-1)

$k_{\text{Air}}$  = air conductivity (Table 3.2-1)

$k_{\text{Steel}}$  = XM-19 steel conductivity (Table 3.2-1)

$k_{\text{NS}}$  = neutron shield conductivity (Table 3.2-1)

$f(T_1, T_2) = (T_1^2 + T_2^2)(T_1 + T_2)$  where  $T_1$  and  $T_2$  are boundary temperatures.

$h_{\text{rad}} = 4\sigma (0.667) T^3$  ( $T$  is local temperature)

$\sigma = 1.19 \times 10^{-11} \text{ Btu/hr-in.}^2\text{-}^\circ\text{R}^4$

All thermal conductivities ( $k$ ) are expressed in Btu/hr-in.- $^\circ\text{F}$  and volumetric specific heats ( $\rho c_p$ ) in Btu/in. $^3\text{-}^\circ\text{F}$  unless stated otherwise. The subscripts  $x$ ,  $y$ ,  $z$ , and  $r$  refer to coordinate directions, with  $r$  being radial. Wherever  $k$  is expressed as a function of temperature  $T$ , the temperature is assumed to be in degrees Rankine ( $^\circ\text{R}$ ).

##### 3.6.1.1 ANSYS Model, Sec. 3.4.

1. Spent fuel assembly

$$k_x = k_y = 2.5 k_{\text{He}} + 1.755 \times 10^{-11} T^3$$

$$k_z = 0.272$$

2. Gap between fuel assembly and enclosure (FSS or liner)

$$k = k_{\text{He}} + 2.051 \times 10^{-12} T^3$$

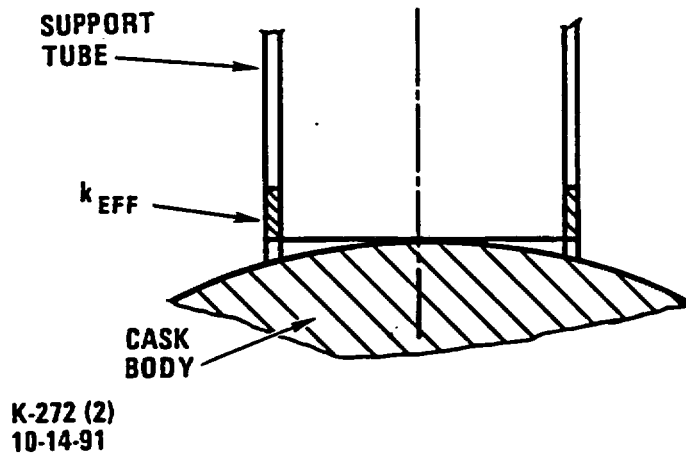
3. Fuel support structure/ $\text{B}_4\text{C}$

$$k_x = 0.462 \text{ (parallel to axis of holes and } \text{B}_4\text{C pellets)}$$

$$k_y = k_z = 0.216$$

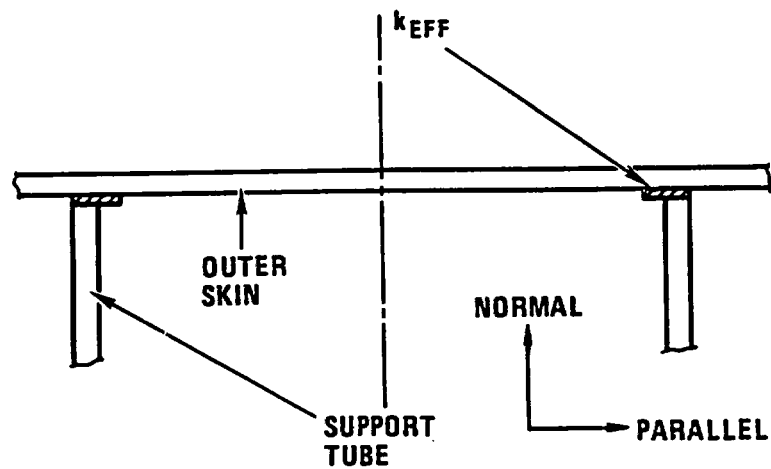
4. Neutron shield support tube contact at corner. Accounts for imperfect contact between tube and cask body at corner.

$k = 0.833$  (for shell element)



5. Neutron shield support tube flange.

$k = 0.0855$  (normal to flange) Accounts for thermal resistances of flange, contact between flange and outer skin, and outer skin. The outer skin resistance is included with the tube flange since the skin is modeled as a shell element, which has no gradient through the thickness (i.e., zero resistance).  
13.75 (parallel to flange)



6. Outer skin (XM-19 and copper. See Section 3.6.9.3.)

$$k = 2.36 \text{ (for shell element)}$$

### 3.6.1.2 TAC2D Model, Sec. 3.4.

1. Spent fuel assembly/fuel support structure/B<sub>4</sub>C

$$k_r = 1.5 [0.967(2.5 k_{\text{He}} + 1.755 \times 10^{-11} T^3) + 0.033 (0.462)]$$

$$k_z = 0.745 (0.272) + 0.053 (0.216) = 0.214$$

$$\rho c_p = 0.00810$$

2. Neutron shield/support structure

$$k_r = 0.083$$

$$k_z = 0.007$$

$$\rho c_p = 0.0148$$

3. Outer skin (XM-19/copper. See Section 3.6.9.3.)

$$k_r = k_{\text{steel}}$$

$$k_z = 0.08 (18.8) + 0.84 k_{\text{steel}}$$

$$\rho c_p = 0.0335$$

4. Void space at cavity ends (helium/FSS)

$$k_r = 0.586 [0.967 k_{\text{He}} + 0.033 (0.462)]$$

$$k_z = 1.272 [k_{\text{He}} + \sigma(0.2)(2.125) f(T_1, T_2)] + 0.0197$$

$$\rho c_p = 0.00109$$

5. Impact limiter support structures

Top:  $k_r = 0.215 k_{\text{steel}}$

$$k_z = 0.081 k_{\text{steel}}$$

$$\rho c_p = 0.0110$$

Bottom:  $k_r = 0.155 k_{\text{steel}}$

$$k_z = 0.057 k_{\text{steel}}$$

$$\rho c_p = 0.00972$$

6. Impact limiters

Inner side:  $k_r = 0.417$

$$k_z = 0.125$$

$$\rho c_p = 0.00134$$

Outer side:  $k_r = 0.314$

$$k_z = 0.0942$$

$$\rho c_p = 0.00101$$

Corner:  $k_r = 0.0795$

$$k_z = 0.138$$

$$\rho c_p = 0.000339$$

End:  $k_r = 0.125$

$$k_z = 0.417$$

$$\rho c_p = 0.00134$$

3.6.1.3 TAC2D Model, Sec. 3.5.

1. Spent fuel assembly/FSS/B<sub>4</sub>C

Properties are identical to those in 3.6.1.2 except that

$$k_z = 0.214 + 2.37 \times 10^{-11} T^3$$

2. Void space at cavity ends (helium/FSS)

Properties are identical to those in 3.6.1.2 except that

$$k_z = 1.272 [k_{\text{He}} + \sigma(0.8)(2.125)f(T_1, T_2)] + 0.0197$$

3. Impact limiter support structure (top)

$$k_r = F_1 k_{\text{steel}} + \frac{1}{\frac{1}{F_2 k_{\text{air}} + F_3 h_{\text{rad}}} + \frac{1}{F_4 k_{\text{NS}}}} + F_5 k_{\text{NS}}$$

$$k_z = G_1 k_{\text{steel}} + G_2 h_{\text{rad}}$$

Table 3.6-1 gives the values of  $F_i$ ,  $G_i$ , and  $\rho c_p$ .

#### 4. Impact limiters

Inner side:	$k_r = 0.417 + 0.0430 \sigma f(T_1, T_2)$	
	$k_z = 0.125$	
	$\rho c_p = 0.00134$	
Outer side:	$k_r = 0.315 + 0.0533 \sigma f(T_1, T_2)$	
	$k_z = 0.0942$	
	$\rho c_p = 0.00101$	
Corner (crushed):	$k_r = 0.188 + 0.04 \sigma f(T_1, T_2)$	accident
	0.205	initial conditions
	$k_z = 0.246 + 0.04 \sigma f(T_1, T_2)$	accident
	0.0536	initial conditions
	$\rho c_p = 0.000880$	
End (crushed):	$k_r = 1.17$	accident
	0.417	initial conditions
	$k_z = 1.42$	accident
	0.125	initial conditions
	$\rho c_p = 0.00446$	

TABLE 3.6-1  
CONSTANTS FOR IMPACT LIMITER SUPPORT STRUCTURE (ILSS) THERMAL PROPERTIES, TAC2D MODEL

ILSS Section		F <sub>1</sub>	F <sub>2</sub>	F <sub>3</sub> (in.)	F <sub>4</sub>	F <sub>5</sub>	G <sub>1</sub>	G <sub>2</sub> (in.)	k <sub>r</sub> @ 200°F	k <sub>z</sub> @ 200°F	ρc <sub>p</sub>
Rib Hole Dia. (in.)	Neutron Shield Thickness (in.)										
0.625	3.0	.119	8.12	2.41	.634	.385	.0571	0	.0766	.0338	.0113
0.625	1.5	.118	8.13	3.45	2.00	0	.0571	0	.0810	.0338	.00822
0.250	1.5	.222	8.14	3.46	2.00	0	.178	0	.142	.106	.0117
0.250	0 <sup>(a)</sup>	.303	8.34	3.27	∞	0	.138	3.01	.222	.123	.00637

<sup>(a)</sup>This section later filled with 1.5-in. neutron shield. Analysis is conservative to omit it.

3.6-6

TABLE 3.6-2  
THERMAL PROPERTIES FOR ILSS, ANSYS MODEL

ILSS Section		k <sub>r</sub>								k <sub>z</sub>	ρc <sub>p</sub>
		Temperature (°F)									
Rib Hole Dia. (in.)	Neutron Shield Thickness (in.)	100	300	500	700	900	1100	1300	1500		
0.625	3.0	.0713	.0820	.0923	.103	.114	.124	.160	.146	.0571 k <sub>steel</sub>	.0120
0.625	1.5	.0741	.0863	.0978	.109	.120	.130	.141	.151	.0571 k <sub>steel</sub>	.00735
0.250	1.5	.131	.153	.173	.193	.213	.233	.253	.2731	.178 k <sub>steel</sub>	.00711

### 3.6.1.4 ANSYS Model, Sec. 3.5.

1. Impact limiter support structure.

Properties are given in Table 3.6-2. They are similar to those in Table 3.6-1 for the TAC2D model and reflect differences only in model geometry.

2. Impact limiters.

These properties are identical to those given in Section 3.6.1.3 for the TAC2D model, except that the radiation term  $\sigma f(T_1, T_2) = \sigma (T_1^2 + T_2^2)(T_1 + T_2)$  in the thermal conductivity is replaced by the alternate expression  $4\sigma T^3$  in terms of the local temperature.

## 3.6.2 Heat Transfer Correlations

### 3.6.2.1 Normal Conditions, TAC2D Model.

1. Natural convection

$$h = C \left( \frac{k}{d} \right) (Gr Pr)^n$$

where

h = heat transfer coefficient  
 k = thermal conductivity of air  
 d = characteristic length  
 Gr = Grashof number  
 Pr = Prandtl number

C, n, and d are determined according to the following table (Ref. 3.6-1).

Surface	d (in.)	C		n	
		Laminar	Turbulent	Laminar	Turbulent
Outer skin	40	0.53	0.13	0.25	0.333
Personnel barrier <sup>(a)</sup>	90	0.53	0.13	0.25	0.333
Impact limiters					
Upper cylinder	90	0.53	0.13	0.25	0.333
Lower cylinder <sup>(b)</sup>	90	0.58	0.58	0.20	0.20
Flat surface	0.9 x 90	0.59	0.021	0.25	0.40

(a) Between impact limiters.  
(b) Code uses average of upper and lower h values.

## 2. Thermal radiation

$$q'' = \sigma \mathcal{F}_{1-2} (T_1^4 - T_2^4)$$

$$h = \frac{q''}{T_1 - T_2} = \sigma \mathcal{F}_{1-2} (T_1^2 + T_2^2)(T_1 + T_2)$$

where

$q''$  = heat flux

$\sigma$  = Stefan-Boltzmann constant

$\mathcal{F}_{1-2}$  = interchange factor

$T_1$  = temperature of surface 1

$T_2$  = temperature of surface 2

For all gaps the interchange factor is computed as:

$$\mathcal{F}_{1-2} = \frac{1}{\frac{1}{\epsilon_1} + \frac{1}{\epsilon_2} - 1}$$

The following table gives the interchange factor for other surface combinations:

Surface 1	Surface 2	$\epsilon_1$	$\epsilon_2$	$\mathcal{F}_{1-2}$
Personnel barrier	External environment	0.8	1.0	0.8
Impact limiter				
Cylindrical surface	External environment	0.5 <sup>(a)</sup>	1.0	0.5
Flat surface	Personnel barrier	0.2	0.8	0.18
Outer skin	Personnel barrier	0.15	0.8	0.14
<sup>(a)</sup> Top cylindrical surface wrapped by personnel barrier ( $\epsilon = 0.8$ ). Lower portion exposed ( $\epsilon = 0.2$ ). Code uses average.				

### 3.6.2.2 Accident Conditions, All Models.

1. Forced convection (0 to 30 min, heating phase)

$$h = C \left( \frac{k}{d} \right) \text{Re}^n \quad (\text{Ref. 3.6-2})$$

where

Re = Reynolds number  
d = 40 in.  
C = 0.0239  
n = 0.805

The Reynolds number is calculated on the basis of an assumed external gas velocity of 20 ft/sec. Using the above correlation, h ranges between 1.6 and 2.1 Btu/hr-ft<sup>2</sup>-°F. We used an average value of 2.0.

2. Thermal radiation (heating and cooldown)

We used the same correlation as for normal conditions. During the heating phase,  $\epsilon_1 = 0.8$  (external surfaces),  $\epsilon_2 = 0.9$  (environment), and  $T_2 = 1475^\circ\text{F}$ . Thus,

$$\mathcal{F}_{1-2} = \frac{1}{\frac{1}{.8} + \frac{1}{.9} - 1} = 0.735$$

During the cooldown portion,  $\epsilon_1 = 0.8$  and  $\epsilon_2 = 1.0$ . Thus  $\mathcal{F}_{1-2} = 0.8$ .

3. Natural convection (cooldown phase)

$$h = \frac{k}{d} \left[ C_1 + 0.387 \left( \frac{Gr Pr}{[1 + (C_2/Pr)^{9/16}]^{16/9}} \right)^{1/6} \right]^2 \quad (\text{Ref. 3.6-1})$$

where

$C_1 = 0.825$  vertical surfaces  
 $0.600$  horizontal surfaces

$C_2 = 0.492$  vertical surfaces  
 $0.559$  horizontal surfaces

4. Combined coefficient for cooldown phase.

A single coefficient was used that combined the effects of natural convection and radiation. The natural convection coefficient given in the preceding section is relatively insensitive to surface orientation (horizontal or vertical) and characteristic dimension  $d$ . The combined coefficient is then a function only of surface and environment temperatures ( $T_s$  and  $T_\infty$ ). It is given in the following table:

$T_\infty = 100^\circ\text{F}$		$T_\infty = -20^\circ\text{F}$	
$T_s$ ( $^\circ\text{F}$ )	$h$ (Btu/hr-ft <sup>2</sup> -F)	$T_s$ ( $^\circ\text{F}$ )	$h$ (Btu/hr-ft <sup>2</sup> -F)
110	1.40	-10	0.979
140	1.70	20	1.29
200	2.08	50	1.47
500	3.66	100	1.72
800	5.88	200	2.10
1000	7.92	500	3.43
1200	10.5	800	5.43
1500	15.6	1000	7.34
		1200	9.76
		1500	14.6

### 3.6.3 Air Flow inside Personnel Barrier, TAC2D Model

The natural convection air flow in the space between the outer skin and personnel barrier is computed on the basis of the following equations:

$$\Delta p = (\rho_c - \rho_h)H. \quad (3.6-1)$$

$$\Delta p = \frac{1}{2g_c} (K_1\rho_1V_1^2 + K_2\rho_2V_2^2). \quad (3.6-2)$$

where:

$\Delta p$	=	pressure loss
$\rho_1$	=	inlet density
$\rho_2$	=	outlet density
$\rho_c$	=	cold column density = $\rho_1$
$\rho_h$	=	hot column density (based on average temperature)
$K_1$	=	inlet loss coefficient
$K_2$	=	outlet loss coefficient
$V_1$	=	inlet velocity
$V_2$	=	outlet velocity
$H$	=	effective height of hot column

Since  $\dot{m} = \rho_1 A_1 V_1 = \rho_2 A_2 V_2$ , where  $\dot{m}$  and  $A$  are mass flow and area, Eq. 3.6-2 can be solved for the flow rate.

$$\dot{m} = A_1 \sqrt{\frac{\rho_1}{K_1} \left( \frac{2g_c \Delta p}{1 + F} \right)} \quad (3.6-3)$$

where

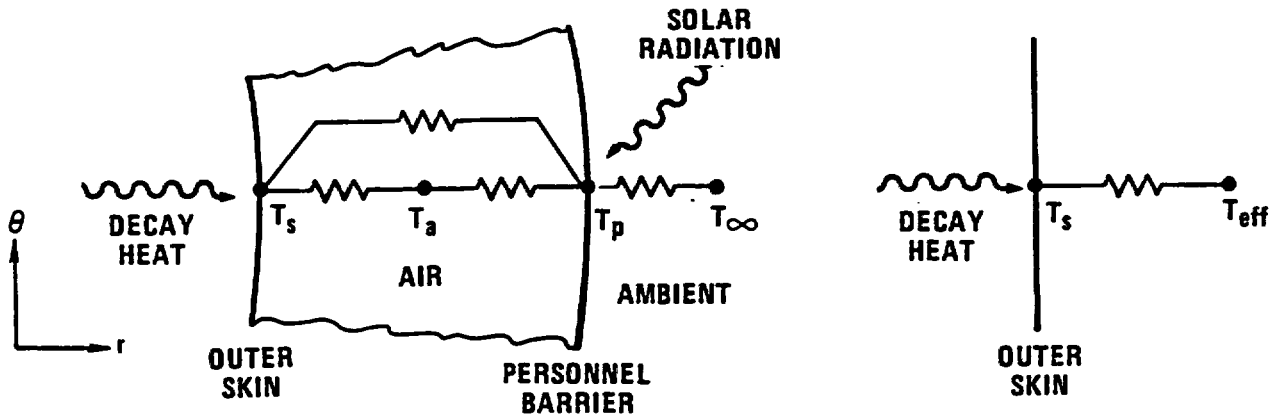
$$F = \frac{\rho_1 K_2 \left( \frac{A_1}{A_2} \right)^2}{\rho_2 K_1}$$

Eq. 3.6-1 and 3.6-3 allow calculation of the flow.

### 3.6.4 Effective Ambient Temperature for ANSYS Model, Sec. 3.4

We performed a small auxiliary TAC2D analysis to derive an effective ambient temperature for the outer skin of the ANSYS model, not including the personnel barrier. Use of this effective temperature alone yields the same heat transfer from the outer skin as if the personnel barrier were included.

The TAC2D model is in r-θ geometry and includes only the outer skin, personnel barrier, and interspace air flow.



K-234 (1)  
9-19-91

TAC2D MODEL

EFFECTIVE AMBIENT

The heat flux from the outer skin is

$$q_s'' = h(T_s - T_a) + \sigma \mathcal{F}_{s-p} (T_s^4 - T_p^4) \tag{3.6-4}$$

where

- h = convection coefficient (see Section 3.6.2.1)
- $\mathcal{F}_{s-p}$  = interchange factor (see Section 3.6.2.1)

In terms of the effective ambient temperature  $T_{eff}$ ,

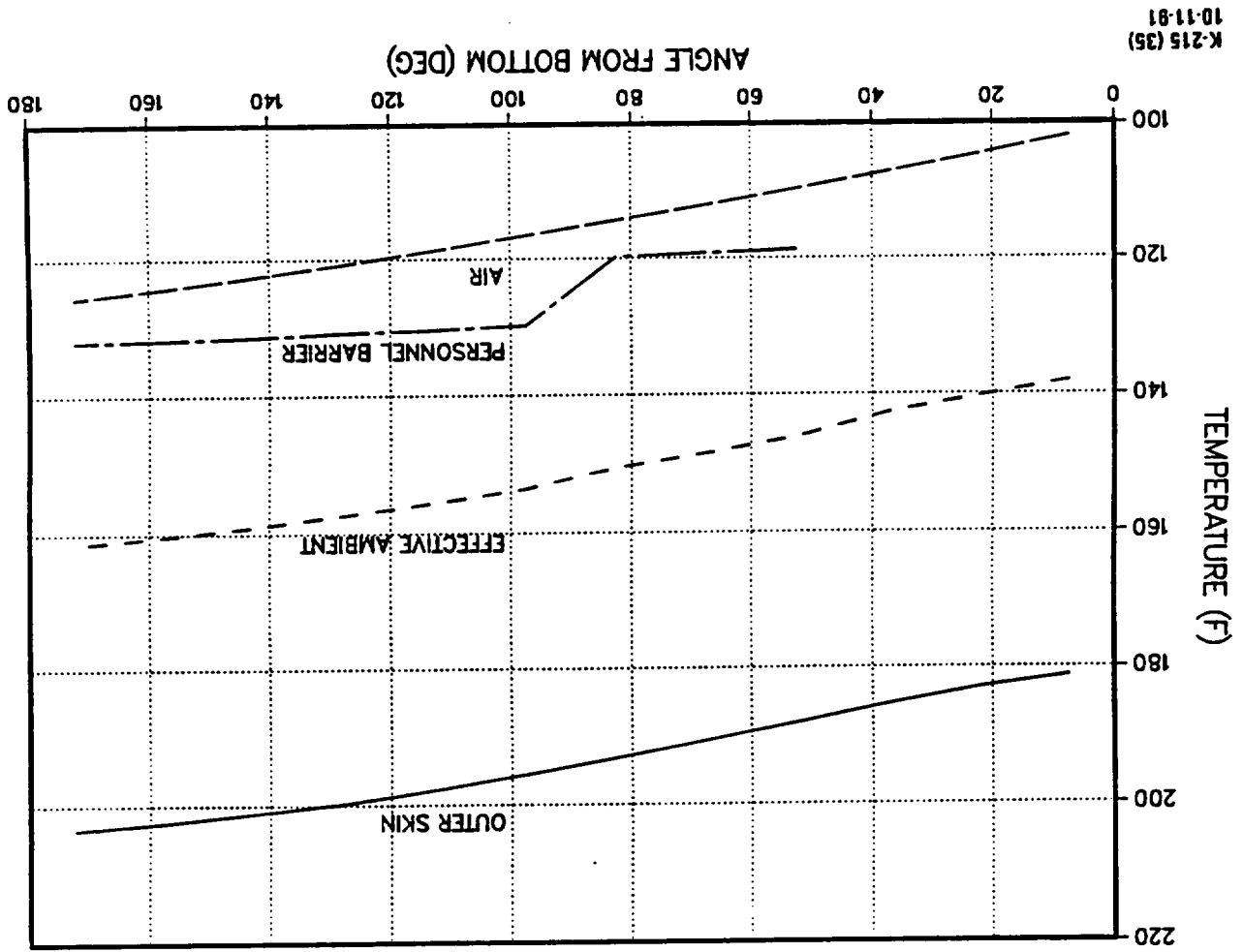
$$q_s'' = h' (T_s - T_{eff}) \tag{3.6-5}$$

The coefficient  $h'$  may be arbitrarily chosen since the calculation of  $T_{eff}$  will account for this. For simplicity of input to the ANSYS model, we chose a value of 2.0 Btu/hr-ft<sup>2</sup>-°F. Equating (3.6-4) and (3.6-5) and rearranging,

$$T_{eff} = T_s - \frac{h}{h'} (T_s - T_a) - \sigma \frac{\mathcal{F}_{s-p}}{h'} (T_s^4 - T_p^4)$$

All of the temperatures on the right side are calculated by the TAC2D model. Figure 3.6-1 is a plot of  $T_s$ ,  $T_p$ ,  $T_a$ , and  $T_{eff}$  as a function of angular position from the cask bottom.

Fig. 3.6-1. Results of effective ambient temperature model



### 3.6.5 Solar Radiation

#### 1. TAC2D Model

The TAC2D model of Fig. 3.4-2 uses two values of solar radiation on exterior surfaces. For the axial ends (flat surface not transported horizontally) covered with personnel barrier ( $\alpha = 0.8$ ), application of 10 CFR Part 71 gives the following continuous solar flux for a 24-hr period:

$$q_z'' = \frac{(0.8)(737)}{24} = 24.6 \frac{\text{Btu}}{\text{hr-ft}^2}$$

The outer radial boundary of the model actually represents the trailer (base of the package), vertical sides of the personnel barrier, and top (curved portion) of the personnel barrier. For the model, we calculate an average solar flux:

$$q_r'' = \frac{0.8 \left( \frac{0 + 737H + 1475P}{C} \right)}{24} ,$$

where

H = total height of vertical portion =  $2 \times 45 = 90$  in.

P = perimeter of curved portion =  $\frac{\pi}{2} (90) = 141.4$  in.

C = Circumference of model =  $\pi(90) = 282.7$  in.

$$\therefore q_r'' = 32.4 \frac{\text{Btu}}{\text{hr-ft}^2} .$$

#### 2. ANSYS Model

Solar radiation for the ANSYS model of Fig. 3.4-1 is accounted for in the TAC2D calculation of effective ambient temperature (Section 3.6.4). The solar flux imposed on the TAC2D model is as follows:

Base ( $\theta = 0$  to  $45^\circ$  in model)

$$q'' = 0$$

Vertical portion ( $\theta = 45$  to  $90^\circ$  in model)

$$q'' = \frac{0.8(737)}{24} \frac{H}{P_m}$$

where

H = height of vertical portion = 45 in.  
 $P_m$  = corresponding model perimeter =  $\pi(45)/4$

$$\therefore q'' = 31.3 \frac{\text{Btu}}{\text{hr-ft}^2}$$

Top (curved portion) ( $\theta = 90$  to  $180^\circ$  in model)

$$q'' = \frac{0.8(1475)}{24} = 49.2 \frac{\text{Btu}}{\text{hr-ft}^2}$$

### 3.6.6 Maximum Internal Pressure Calculation

#### 3.6.6.1 Assumptions and Bases.

1. Fuel data from Ref. 3.6-3.
2. Maximum burnup = 60,000 MWd/MTU
3. Gas fission product quantity calculated from the following formula:

$$P_1 = \frac{1.45ERT_1 f}{V'}$$

where

1.45 = total gas generation rate, gm-atoms/GWd,  
 E = burnup in GWd/MTU,  
 f = fraction of gas released from fuel pellets  
 (curve, page 152, Ref. 3.6-4),  
 R = gas law constant = 40.84 psia-in.<sup>3</sup>/gm-mole °R,  
 V' = specific gas collection volume, in.<sup>3</sup>/MTU,  
 T<sub>1</sub> = temperature at normal or accident conditions, °R.

or

$$P_1 = \frac{1.45ERT_1 fM}{V_1}$$

where

M = uranium loading, MTU/rod,  
 $V_1$  = free volume in rod,  $\pi d_i^2 L_p / 4 + \pi / 4 (d_i^2 - d_p^2) L_A$

where

$d_i$  = i.d. of cladding,  
 $d_p$  = pellet diameter,

$L_A$  = rod active length,  
 $L_p$  = plenum length,  
 $f$  = fraction of gas released, a function of the fuel local linear heating rate. The Ref. 3.6-3 local linear heating rates were multiplied by a peaking factor of 1.2.

4. 100% failure of fuel rod cladding for normal and accident conditions.
5. Cask backfilled with helium to 14.7 psia.
6. Temperature when cask closed = 100°F.

### 3.6.6.2 MNOP Analysis. GA-4 cask, B&W 15 x 15 Mark B fuel element

Linear heating rate = 6.3 kW/ft x 1.2 = 7.56 kW/ft,

where

$f$  = 0.019,  
 $V_1$  = 2.01 in.<sup>3</sup>,  
 $P_o$  = initial fill pressure = 430 psia,  
 $E$  = 60 GWd/MTU,  
 $M$  = 2.23 x 10<sup>-3</sup> MTU/rod,  
 $T_1$  = normal condition cavity temperature = 262°F (Table 3.4-3).

1. Rod gas pressure at normal-condition temperature due to initial fill pressure,

$$\begin{aligned}
 P_1 &= \frac{722^\circ\text{R}}{530^\circ\text{R}} \times P_o \\
 &= \frac{722^\circ\text{R}}{530^\circ\text{R}} \times 430 \text{ psia} \\
 &= 586 \text{ psia.}
 \end{aligned}$$

2. Rod gas pressure at normal-condition temperature due to gas fission products,

$$\begin{aligned}
 P_2 &= \frac{1.45 E T_1 f M}{V_1} \\
 &= [1.45 (60 \text{ GWd/MTU})(40.84 \text{ psia-in.}^3/\text{g mole } ^\circ\text{R}) \\
 &\quad (722^\circ\text{R})(0.019)(2.23 \times 10^{-3} \text{ MTU/rod})] / 2.01 \text{ in.}^3 \\
 &= 54.1 \text{ psia.}
 \end{aligned}$$

3. Gas g moles in fuel rod,

$$N_1 = \frac{(P_1 + P_2) V_1}{R T_1}$$

$$= \frac{(586 \text{ psia} + 54.1 \text{ psia})(2.01 \text{ in.}^3)}{(40.84 \text{ psia-in.}^3/\text{g mole } ^\circ\text{R})(722^\circ\text{R})}$$

$$= 4.36 \times 10^{-2} \text{ g moles/rod}$$

$$4.36 \times 10^{-2} (208 \text{ rods/element})(4 \text{ elements})$$

$$= 36.28 \text{ g moles.}$$

4. Gas g moles in cask cavity,

$$N_2 = \frac{14.7(V_2)}{R T_o}$$

$$= \frac{14.7 \text{ psia}(30,137 \text{ in.}^3)}{(40.84 \text{ psia-in.}^3/\text{g mole } ^\circ\text{R})(560^\circ\text{R})}$$

$$= 19.4 \text{ g moles,}$$

where

$$V_2 = 30,137 \text{ in.}^3 = \text{cask cavity void volume,}$$

$$T_o = \text{temperature when cask is closed} = 560^\circ\text{R.}$$

5. Cavity pressure.

Normal condition:

$$P_N = \frac{(N_1 + N_2)(R)(T_1)}{V_2 + X(V_1)(4)}$$

$$= \frac{(36.28 + 19.4)(40.84)(722)}{30,137 + 208(2.01)(4)}$$

$$= 51.6 \text{ psia}$$

$$\text{MNOP} = 36.9 \text{ psig}$$

where

X = number of rods per element.

**3.6.6.3 Accident Analysis.** The maximum internal pressure for the GA-4 cask during hypothetical accident conditions results from an increase in cavity temperature, which is caused by the 800°C (1472°F) 30-min thermal event. The initial condition for the thermal event is MNOP calculated in the previous section.

$$\begin{aligned}
 P_A &= \frac{(N_1 + N_2)(R)(T_1)}{V_2 + X(V_1)(4)} \\
 &= \frac{(36.28 + 19.4)(40.84)(853)}{30,137 + 208(2.01)(4)} \\
 &= 61.0 \text{ psia} \\
 &= 46.3 \text{ psig,}
 \end{aligned}$$

where

$$\begin{aligned}
 T_1 &= 853^\circ\text{R (Table 3.5-1),} \\
 X &= \text{Number of rods/element.}
 \end{aligned}$$

### 3.6.7 Neutron Shield Test

In the thermal accident specified in 10 CFR Part 71, the cask is subjected to an 800°C (1472°F) environment for 30 minutes. No artificial cooling may be applied thereafter, and any combustion of materials must be allowed to proceed until it terminates naturally. The neutron shield need not perform any shielding function during or after the thermal accident, but the thermal behavior of the shield must not compromise the ability of the cask to contain the radioactive contents.

This section describes the procedure and results of the fire test performed on the KOBESH PP-R01 borated-polypropylene neutron shield to qualify the material for use on the GA-4 cask; the material was fabricated by Kobe Steel, Ltd. An alternate material, Type 216A polyethylene, fabricated by Reactor Experiments, Inc., was also tested and qualified.

**3.6.7.1 Set-up and Description.** Figure 3.6-2 shows the test article together with thermocouple locations. The test article represents a 3-ft-square section of the cask's neutron shield material and outer skin. The neutron shield consists of 72 6-in. by 6-in. by 2.25-in. blocks that have been assembled into an 11-gage Type 304L welded stainless steel box. Mineral fiber insulation covers all sides of the box except one of the 3-ft-square faces. Damage to the outer skin of the cask, which occurs in the hypothetical drop accident, is accounted for in the test article. A cut 6 in. wide by 12 in. high is made at the center of the front face, exposing the neutron shield directly to the fire. The cut penetrates 1.5 in. into the shielding material and is the only place where the neutron shield is directly exposed to the environment.



Although a representative full-scale thickness of neutron shield is used, the test is not intended to be a reproduction of the cask configuration. The sole purpose of the test is to qualify the thermal performance of the neutron shield material by demonstrating that its presence will not cause a more severe thermal environment than the 800°C regulatory environment impinging directly on the cask body. This is the boundary condition used in the thermal analysis.

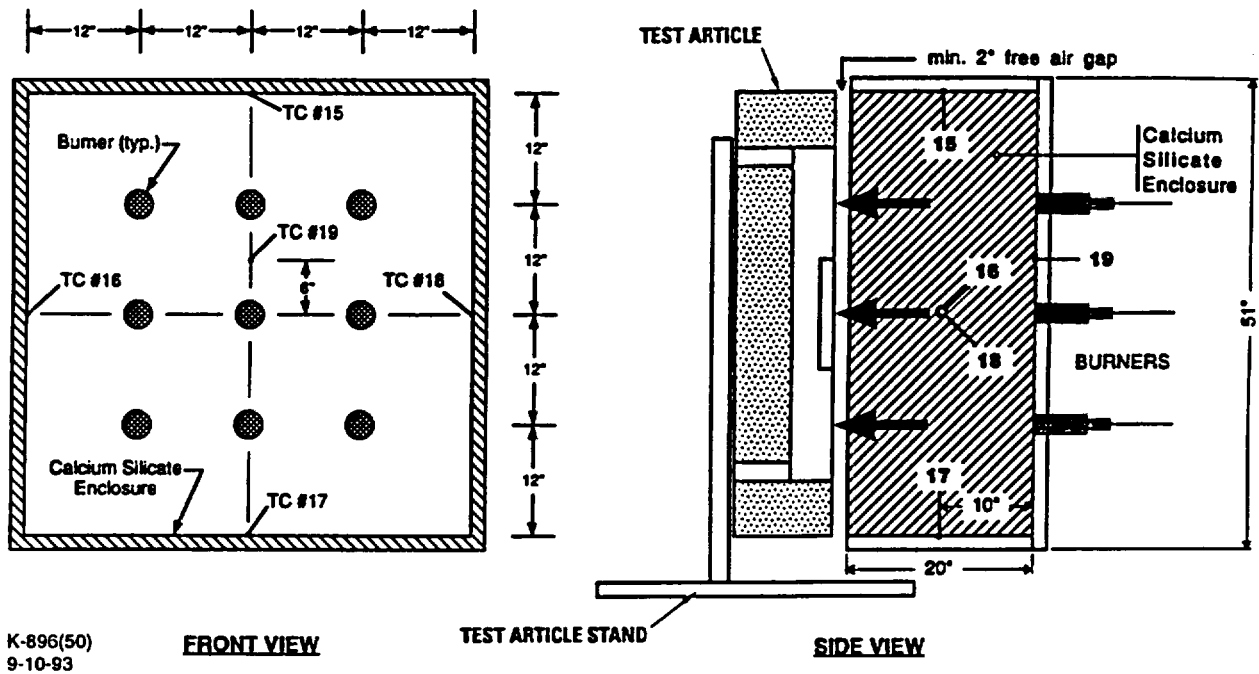
Nine Type K chrome-alumel 20-gage thermocouples (TCs) are attached to the test article at the locations shown in Fig. 3.6-2. The environment temperatures are measured with five thermocouples of the same type as on the test article but shielded from the test article surface. These thermocouples are positioned 6 in. from the test article surface. In addition, five thermocouples measure the interior surface temperature of the burner. See Fig. 3.6-3.

The test article is conditioned at room temperature for at least 24 hr and then moved into position in front of the burners, as shown in Fig. 3.6-3. Recording of thermocouple data begins 5 min before the burners are ignited. After the burners are lit and the average environment temperature (i.e., average of the five thermocouples 10 through 14) shows at least 800°C (1475°F) for 30 min, the burners are shut off and the test article is pulled away to cool in ambient air. When all temperatures have peaked, the test article is again conditioned at room temperature for at least 24 hr and then disassembled for inspection.

**3.6.7.2 Results.** Figure 3.6-4 gives the average environment temperature (average of TCs 10–14) during the heating phase of the KOBESH test. Approximately 30 sec after ignition of the furnace burners, flames began issuing from the front face hole in the test article, and within 3 min flames were issuing from the 2-in. space between the enclosure and test article along the top and sides. The burners were adjusted to control the environment to the specified 800°C as ignition of the neutron shield material began to raise the interior temperature. At about 7 min, the heat from combustion of this material — confined within the burner enclosure — was sufficient to maintain the desired temperature, and the burners were shut off for the duration of the test. As seen from Fig. 3.6-4, the environment temperature continued to maintain its minimum required value without severe excursions. The flames continued throughout the test with approximately the same intensity, accompanied by very heavy smoke. Molten material was observed flowing into a water-filled catch pan underneath the test article.

When the test article was pulled away from the hot enclosure and exposed to ambient air after 30 min, the flames issuing from the hole in the front face began to subside immediately. Material flowing out of the hole was observed burning. All flames were completely extinguished after 26 min. No artificial cooling was used on the test article.

After complete cooling in ambient air, the total neutron shield weight loss was determined to be 81.5 lb from an initial 196 lb, about 42%. Disassembly of the test article revealed that the remaining material had separated into two characteristic regions. Below a line even with the bottom edge of the 6-in. by 12-in. hole, the material had fused into a solid, uniform mass. Some boundary lines between original blocks were identifiable, but the material was not easily separated into individual blocks. Above the hole's bottom edge, the blocks had melted together at horizontal interfaces, but the vertical interfaces were still distinct. The material thus appeared as six vertical columns extending essentially



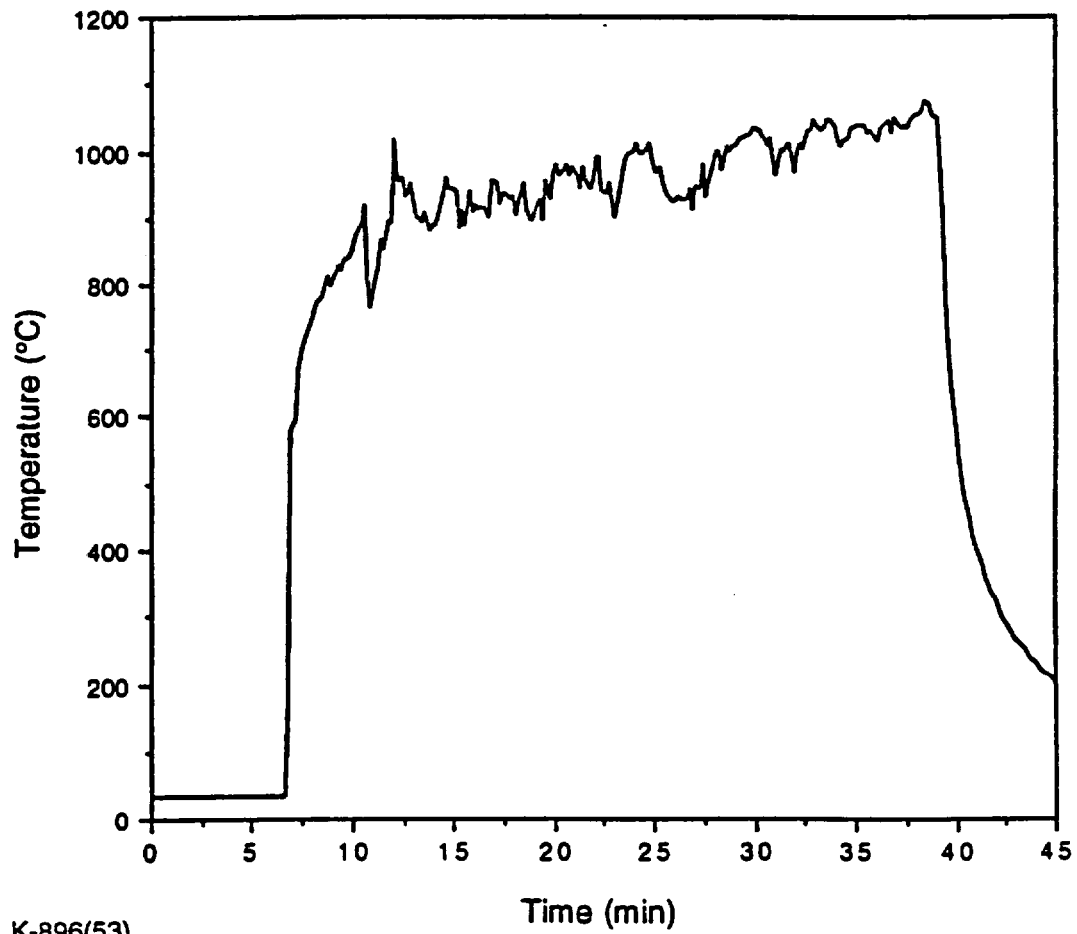
K-896(50)  
9-10-93

**FRONT VIEW**

TEST ARTICLE STAND

**SIDE VIEW**

Fig. 3.6-3. Neutron shield test furnace



K-896(53)  
8-16-93

Fig. 3.6-4. Average environment temperature

to the top edge of the test article. Each column was about one block thick (i.e., 2.25 in.) except near the top where the thickness was reduced to about half a block. When viewed from the top, the columns were skewed, occupying the back half of the test article on the right side and the front half on the left side. Overall there was very little loose material and no obvious char layer.

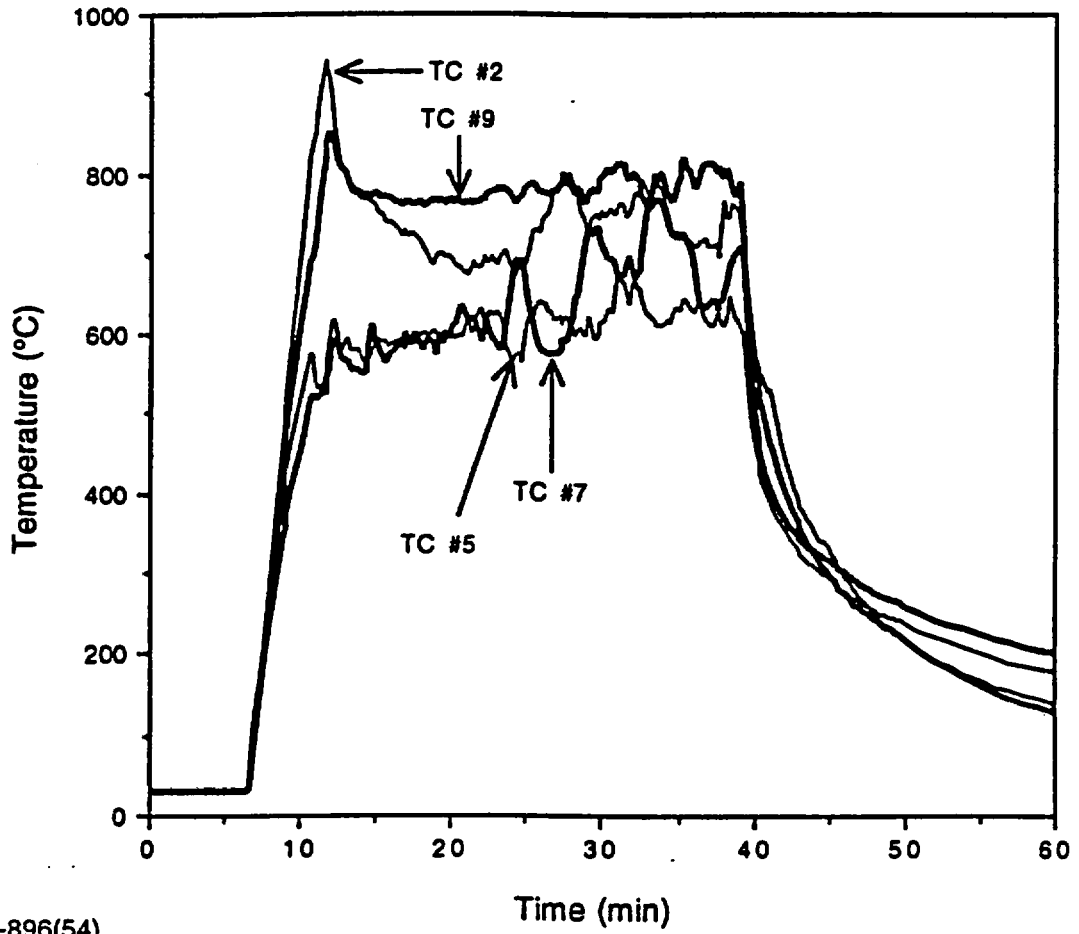
Temperatures on the front face of the test article are shown in Fig. 3.6-5, and Fig. 3.6-6 shows temperatures on the back face.

The thermal performance of the alternate material, Type 216A polyethylene, was very similar to the KOBESH PP-R01. About 5 minutes following burner ignition combustion of the material was sufficient to maintain the required 800°C and the burners were shut off. After moving the test article away from the furnace enclosure, however, the combustion subsided and all flames ceased within 34 minutes. The material lost 62% of its original weight. The peak temperature on the back surface of the test article attained 294°C.

**3.6.7.3 Conclusions.** Regulations in 10 CFR Part 71 require that the test article be exposed to an 800°C radiant environment for 30 minutes, with no artificial cooling thereafter. Any combustion of materials must be allowed to proceed until it terminates naturally. These conditions were met in both tests.

In order to qualify a neutron shield material, it must be shown to perform in such a manner that during and after the thermal accident there is no effect that impairs the function of the cask. The specific criteria for acceptability of the neutron shield are that (1) temperatures on the back surface do not at any time exceed the maximum temperature of the thermal accident environment, and (2) it shows no evidence of prolonged combustion (i.e., combustion lasting for a period of several hours) following the thermal accident. These criteria ensure that combustion of the neutron shield material does not present a worse situation than if the cask body were exposed directly to the accident environment. This condition has been shown by analysis to be acceptable for the cask.

The temperatures on the back surface of either test article never exceeded 800°C. In fact, both peak temperatures were well below this, with 390°C for the KOBESH and 294°C for the Type 216A. After being heated for 30 minutes, each material self-extinguished well within several hours without severe temperature excursions. This self-extinguishing supports the thermal analysis that shows the regulations are satisfied. On the basis of the thermocouple data and visual observations, both materials are thermally qualified as neutron shields for the GA-4 cask.



K-896(54)  
8-16-93

Fig. 3.6-5. Front side thermocouple response

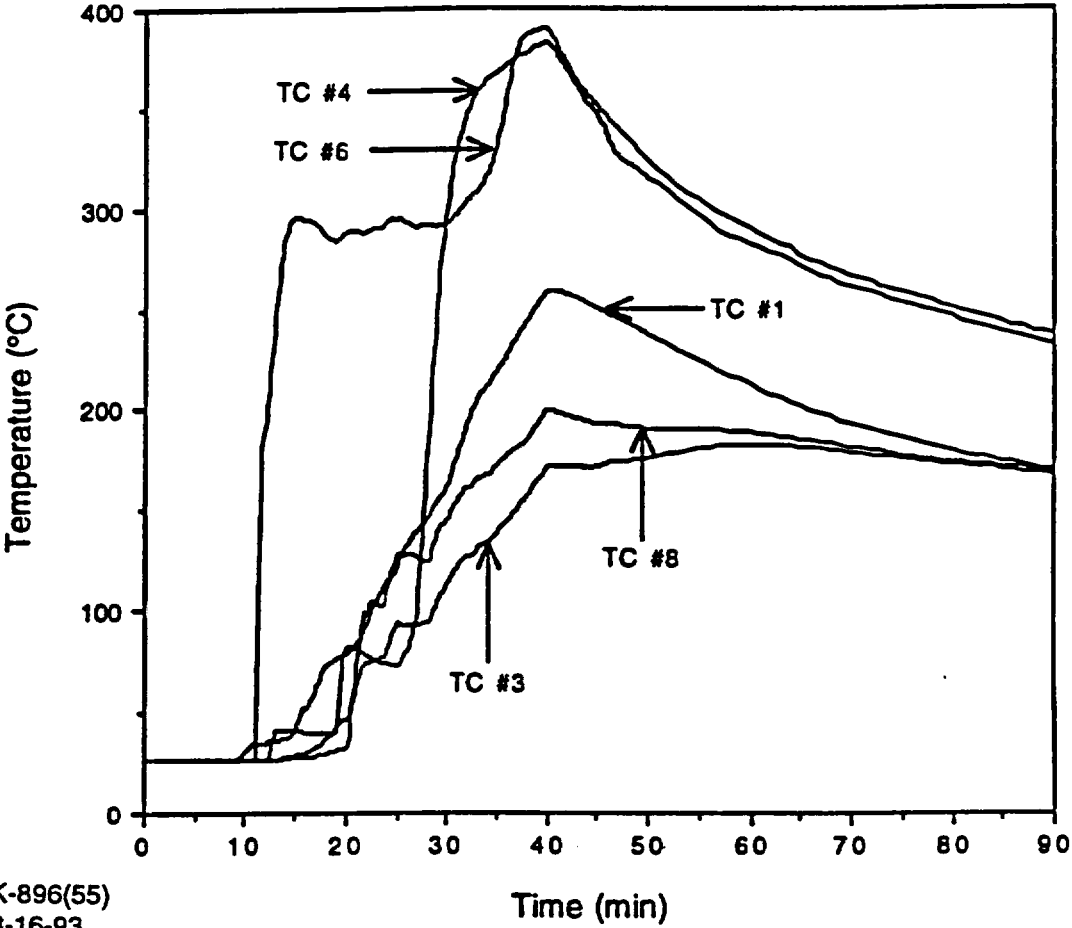


Fig. 3.6-6. Back side thermocouple response

### 3.6.8 Thermal Evaluation with Hotter Fuel

3.6.8.1 Summary. The GA-4 cask can ship a payload of a different configuration than the reference case of four assemblies, each generating 617 W. We extended the analyses presented in Sections 3.4 and 3.5 to consider configurations in which some assemblies generate more than the reference decay heat of 617 W. The table below shows the decay heat limits which must be followed. Both the per-assembly and total decay heat limits must be observed.

No. Assemblies	Maximum Allowed Decay Heat per Assembly (W)	Maximum Allowed Total Decay Heat (W)
2-4	617	2468
	740	2220
	845	2078
1-2 <sup>(a)</sup>	1234	2468
<sup>(a)</sup> Special configuration with inserts in diagonal cavities.		

3.6.8.2 Analysis Method. We constructed a TAC2D (version 0002, Ref. 3.6-5) model of the cask cross section to analyze assembly-to-assembly variations in decay heat that may arise when off-reference payloads are shipped. The model (shown in Fig. 3.6-7) treats four fuel assemblies, the fuel support structure (FSS), the cavity liner, and the depleted uranium (DU) gamma shielding. Properties were taken from Sections 3.2 and 3.6.1.1. In the case of only two assemblies, the empty cavities were assumed to be occupied by steel shielding inserts and helium gas. The model terminates with the DU and uses an overall heat transfer coefficient from the DU to the ambient temperature. Temperatures outside the model envelope can be hand-calculated satisfactorily by ratioing reference temperatures on the basis of total decay heat.

The boundary condition temperature for the model is 118°F, which represents the effective temperature seen by the outer skin, including the effects of solar radiation and the personnel barrier. We established the ambient temperature by running the TAC2D model of Section 3.6.4 with decay heats ranging from 50% to 120% of the reference value of 2468 W. In that section the effective ambient temperature for the reference case was calculated to be an average of about 150°F (see Fig. 3.6-1). This was based on an arbitrary skin heat transfer coefficient  $h'$  of 2 Btu/hr-ft<sup>2</sup>-°F. Although using this arbitrary  $h'$  is correct, as explained in Section 3.6.4, it is not optimum because the effective ambient of 150°F is strictly valid only for the reference condition and will vary with decay heat. To avoid this difficulty, the heat transfer coefficient  $h'$  was changed to a value that yielded an effective ambient temperature essentially independent of decay heat. The new  $h'$  is 1.15 Btu/hr-ft<sup>2</sup>-°F, and the corresponding effective ambient temperature is 118°F.

**3.6.8.3 Base Case.** The TAC2D model (Fig. 3.6-7) was first run for the reference condition to establish a base case from which various perturbations could be made. The DU-to-ambient heat transfer coefficient  $h_{DU}$  must include the thermal resistances of the gap between the DU and the cask body; the cask body; the neutron shield supports; and the outer skin. It must also include the skin heat transfer coefficient  $h'$  of 1.15 Btu/hr-ft<sup>2</sup>-°F. Rather than calculating  $h_{DU}$ , we simply varied it in the model by trial and error until the temperature distribution matched as closely as possible the ANSYS-predicted results of Fig. 3.4-3. This gave an  $h_{DU}$  of 0.910 Btu/hr-ft<sup>2</sup>-°F, which was then used in all subsequent cases. The base case temperature distribution is shown in Fig. 3.6-8.

**3.6.8.4 Other Cases.** Off-reference cases were then run with local increases or decreases in decay heat. Three cases were considered as shown in Fig. 3.6-9, and the TAC2D results are given in Figs. 3.6-10 through 3.6-12. Cases 2 and 3 represent the configurations giving the highest temperatures possible for the assembly and total decay heats that were used. All other configurations will result in lower temperatures, provided that the assembly and total decay heats are within the values shown. Case 4 is a special configuration that requires shielding inserts in diagonal cavities.

Since the TAC2D model is two-dimensional with adiabatic ends, axial conduction is not accounted for and the TAC2D temperatures are not taken as final results. We used several methods to calculate actual cask temperatures that can be compared directly to those presented in Table 3.4-3.

$$1. \quad T = T_{ref} + \Delta T - \left( \frac{Q}{Q_{ref}} - 1 \right) \Delta T_a$$

where

T	=	temperature
$T_{ref}$	=	reference temperature from Table 3.4-3
$\Delta T$	=	change from reference as indicated by comparing base case (Fig. 3.6-8) with current case (Figs. 3.6-10 - 3.6-12)
Q	=	decay heat
$Q_{ref}$	=	reference decay heat = 2468 W
$\Delta T_a$	=	axial conduction effect from Table 3.4-2. (The axial conduction effect is adjusted since it is proportional to the decay heat.)

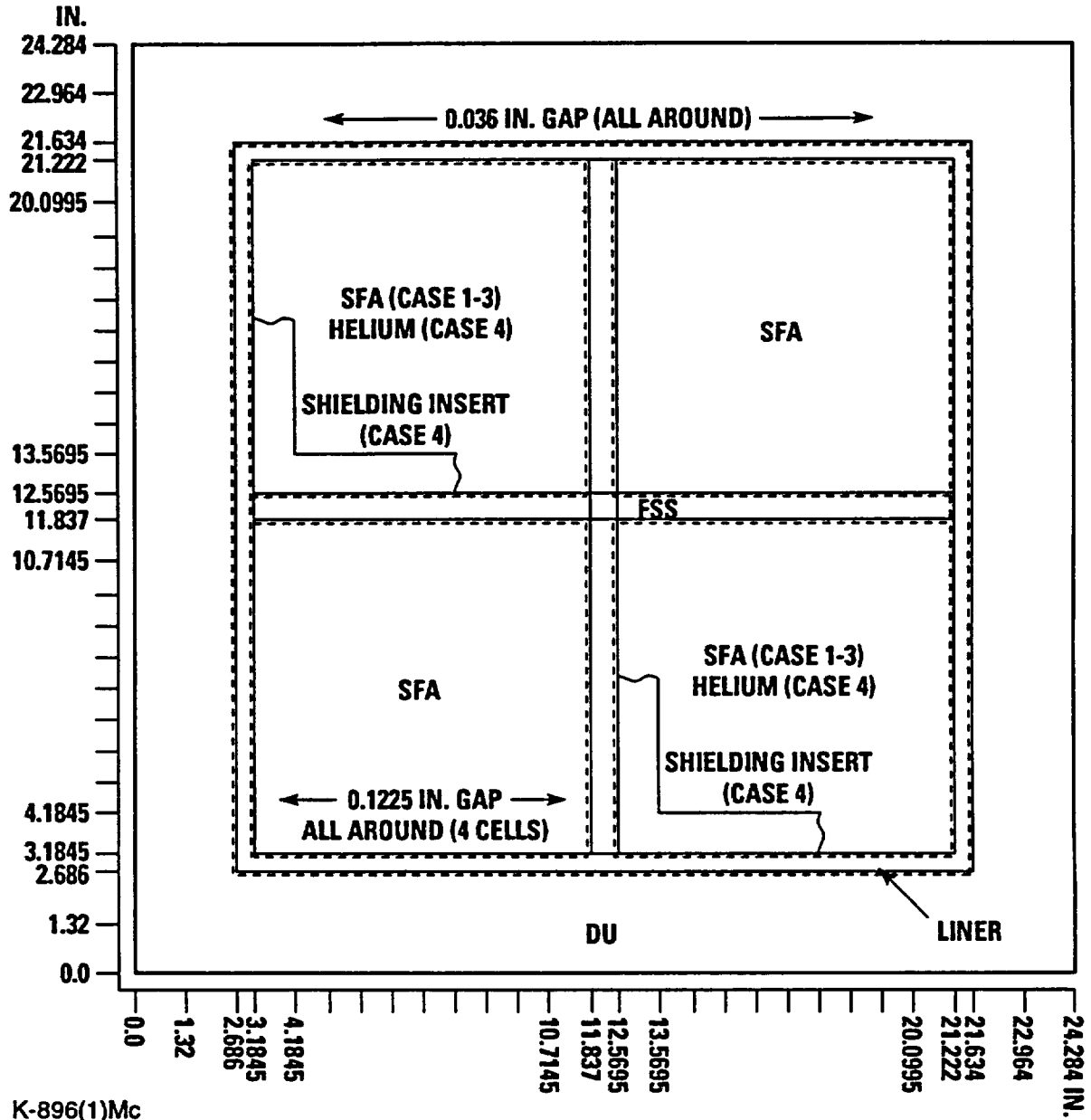
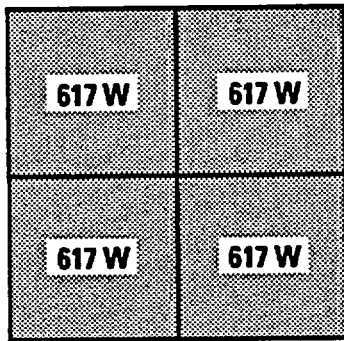
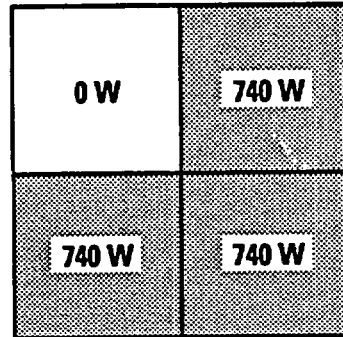


Fig. 3.6-7. TAC2D model for hotter fuel cases

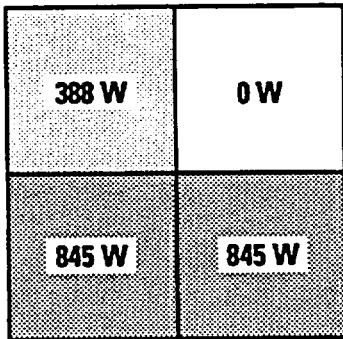




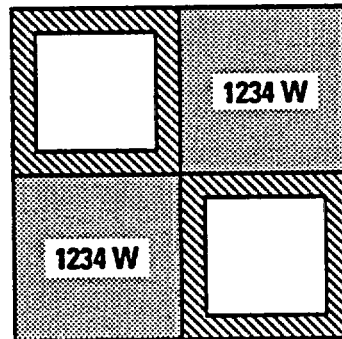
**CASE 1 (BASE)**



**CASE 2**



**CASE 3**



**CASE 4**

K-896(15)Mc  
6-22-93

Fig. 3.6-9. Decay heat configurations for hotter fuel cases







$$2. \quad \frac{T_1 - 118}{T_2 - 118} = \left( \frac{T_1 - 118}{T_2 - 118} \right)_{\text{ref}}$$

where

$$\begin{aligned} T_1 &= \text{temperature at location 1} \\ T_2 &= \text{temperature at location 2} \end{aligned}$$

and the subscript "ref" has the same meaning as before.

$$3. \quad \frac{T - 118}{T_{\text{ref}} - 118} = \frac{Q}{Q_{\text{ref}}}$$

Method 1 uses the TAC2D results and accounts for local variations in temperature caused by concentrations in the decay heat. This is typically significant for determining maximum FSS and liner temperatures. Method 2 extrapolates to those areas outside the TAC2D model based on reference temperature profiles. Method 3 is the simplest and is satisfactory for those areas where the temperature is a function only of total decay heat.

Using these methods, results for the three cases are shown in Tables 3.6-3 through 3.6-5. By comparing with Table 3.4-3 it may be seen that all temperatures except fuel cladding are less than or equal to reference values. The fuel cladding temperature increases but is still well below the allowable of 716°F. In fact, cases 2 and 3 were specifically chosen to determine the assembly versus total decay heat envelope within which cask temperatures would not increase over reference.

Note that although case 4 has the same total reference decay heat, FSS and cavity temperatures have actually dropped. This is due to the effect of the shielding inserts, which slightly increase the overall cavity conductance.

**3.6.8.5 Effect of Empty Fuel Cavities.** Although the analyses for cases 2 and 3 assumed the "0 W" cavities were fuel assemblies generating no heat, virtually identical results are obtained if the cavities are empty, that is, helium-filled with radiation across the boundaries. The axial conduction effect  $\Delta T_a$  will be reduced if a fuel cavity is empty, owing to a lower axial conductivity, but the overall conductivity decreases by only about 6%.

If a shielding insert is placed in an empty cavity, FSS temperatures will be slightly lowered since the steel insert will enhance the effective radial (x and y) conductivities of the contents (versus that of no insert or of a fuel assembly), and the effective axial (z) conductivity of an insert is greater than that of a fuel assembly.

**TABLE 3.6-3  
TEMPERATURES FOR NORMAL CONDITIONS, CASE 2 (°F)**

Component	Maximum		Cross-section Average		Axial Average
	Midlength	End	Midlength	End	
FSS	330 <sup>(a)</sup>	228 <sup>(c)</sup>	296 <sup>(a)</sup>	218 <sup>(c)</sup>	271 <sup>(c)</sup>
Cavity liner	270 <sup>(a)</sup>	212 <sup>(c)</sup>	235	182	206
Gamma shield (DU)	228 <sup>(a)</sup>	183 <sup>(c)</sup>	216	174	193
Cask wall	217 <sup>(b)</sup>	178 <sup>(c)</sup>	202	165	183
Neutron shield	210 <sup>(b)</sup>	178 <sup>(c)</sup>	189	159	176
Outer skin	189	168	176	155	169

Fuel cladding (max.)	349 <sup>(a)</sup>
Cavity gas (avg.)	248
Closure seal	140
Drain seal	151
Closure (plug)	144
Impact limiters	142
Trunnions	183
Personnel barrier	134

(a) Calculated as $T_{ref} + \Delta T + 0.1\Delta T_a$	(Method 1)
(b) Calculated as $(T_{DU} - 118) \left( \frac{T - 118}{T_{DU} - 118} \right)_{ref} + 118$	(Method 2)
(c) Calculated as $(T_{mid} - 118) \left( \frac{T - 118}{T_{mid} - 118} \right)_{ref} + 118$	(Method 2)
where $T_{mid}$ = midlength (max. or avg.) temperature	
All other temperatures are calculated as $0.9 (T_{ref} - 118) + 118$ .	(Method 3)

**TABLE 3.6-4  
TEMPERATURES FOR NORMAL CONDITIONS, CASE 3 (°F)**

Component	Maximum		Cross-section Average		Axial Average
	Midlength	End	Midlength	End	
FSS	326 <sup>(a)</sup>	226 <sup>(c)</sup>	284 <sup>(a)</sup>	211 <sup>(c)</sup>	260 <sup>(c)</sup>
Cavity liner	271 <sup>(a)</sup>	213 <sup>(c)</sup>	227	178	200
Gamma shield (DU)	227 <sup>(a)</sup>	182 <sup>(c)</sup>	210	170	188
Cask wall	216 <sup>(b)</sup>	177 <sup>(c)</sup>	196	162	178
Neutron shield	209 <sup>(b)</sup>	177 <sup>(c)</sup>	184	157	173
Outer skin	184	164	172	152	166

Fuel cladding (max.)	350 <sup>(a)</sup>
Cavity gas (avg.)	239
Closure seal	139
Drain seal	149
Closure (plug)	142
Impact limiters	141
Trunnions	178
Personnel barrier	133

(a) Calculated as $T_{ref} + \Delta T + 0.16\Delta T_a$	(Method 1)
(b) Calculated as $(T_{DU} - 118) \left( \frac{T - 118}{T_{DU} - 118} \right)_{ref} + 118$	(Method 2)
(c) Calculated as $(T_{mid} - 118) \left( \frac{T - 118}{T_{mid} - 118} \right)_{ref} + 118$	(Method 2)
where $T_{mid}$ = midlength (max. or avg.) temperature	
All other temperatures are calculated as $0.84 (T_{ref} - 118) + 118$ .	(Method 3)

**TABLE 3.6-5  
TEMPERATURES FOR NORMAL CONDITIONS, CASE 4 (°F)**

Component	Maximum		Cross-section Average		Axial Average
	Midlength	End	Midlength	End	
FSS	303 <sup>(a)</sup>	214 <sup>(b)</sup>	284 <sup>(a)</sup>	211 <sup>(b)</sup>	260 <sup>(b)</sup>
Cavity liner	267 <sup>(a)</sup>	210 <sup>(b)</sup>	248	189	216
Gamma shield (DU)	232 <sup>(a)</sup>	185	227	180	201
Cask wall	221	180	211	170	190
Neutron shield	213	180	197	164	183
Outer skin	197	173	182	158	175

Fuel cladding (max.)	373 <sup>(a)</sup>
Cavity gas (avg.)	262
Closure seal	143
Drain seal	155
Closure (plug)	147
Impact limiters	145
Trunnions	190
Personnel barrier	136

<sup>(a)</sup>Calculated as  $T_{ref} + \Delta T$  (Method 1)

<sup>(b)</sup>Calculated as  $(T_{mid} - 118) \left( \frac{T - 118}{T_{mid} - 118} \right)_{ref} + 118$  (Method 2)

where  $T_{mid}$  = midlength (max. or avg.) temperature

All other temperatures calculated as  $T_{ref}$  since the total decay heat is unchanged. (Method 3)

**3.6.8.6 Hypothetical Accident Conditions.** Temperatures given in Table 3.5-1 will not increase due to these cases using hotter fuel assemblies. The peak seal temperature is driven by the accident environment and the local geometry and thermal properties; it will be unaffected by changes in the cask contents. Since the total decay heat does not increase, the average cavity gas temperature during the accident will not increase for cases 2 and 3. It will actually drop for case 4, since the heat capacity of the shielding inserts is about 50 percent greater than that of the fuel assemblies.

The ANSYS model containment boundary temperatures given in Table 3.5-1 were calculated on the basis of an adiabatic surface at the cavity liner. The temperatures are, therefore, the maximum possible and are independent of the cask contents.

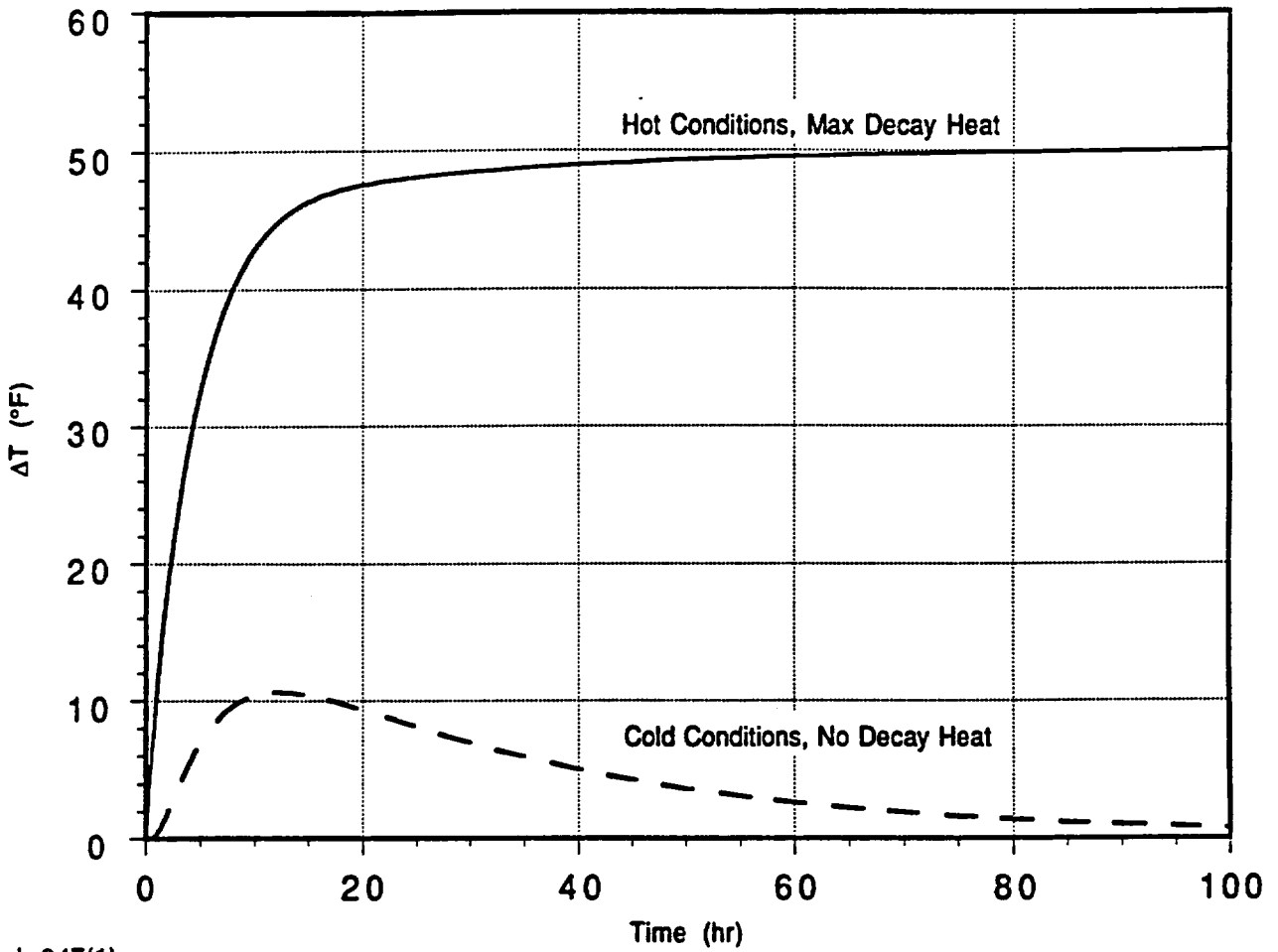
If fewer than four assemblies are shipped and the cavities without assemblies are empty (no inserts), the effective heat capacity of the contents will be reduced and the average cavity gas temperature will experience a greater rise during the thermal accident. However, this greater rise will be offset by the lower initial temperature due to a lower total decay heat. We considered the GA-4 cask containing 3, 2, and 1 assemblies with no inserts. The highest gas temperature during the thermal accident resulted from 3 assemblies but was only 3°F higher than for the reference case (Fig. 3.5-4).

### **3.6.9 Other Thermal Considerations**

**3.6.9.1 Welded Fuel Support Structure (FSS).** All analysis presented thus far has assumed a removable FSS, with a thermal contact resistance at the junction of the FSS and the cavity liner. As a result of a design modification, the FSS and liner are now welded together. This change has very little effect on cask temperatures. The FSS decreases by about 4°F and temperatures outside the FSS are essentially unchanged.

Two additional thermal calculations were performed to support the structural evaluation for the welded FSS. The first was concerned with the gap between the cavity liner and the depleted uranium gamma shielding (DU). This gap is important since there must be no interference between these components. Using the TAC2D model of Sec. 3.4.1, we determined that the maximum difference between the average FSS/liner temperature and the DU temperature during normal transients with decay heat occurs at steady-state conditions. In other words, calculating the gap at steady-state conditions, as done in Table 2.6-2, will give the minimum gap. For cold transport conditions without decay heat this temperature difference peaks within 20 hr but is only about 10°F. At steady-state the temperature difference is 0. See Fig. 3.6-13.

A second calculation generated a 3-dimensional temperature distribution for use in an ANSYS thermal stress model of the FSS and liner. To produce this temperature distribution we combined results of the ANSYS model of Fig. 3.4-1 with the TAC2D results of Fig. 3.4-4. The ANSYS model gives detailed temperatures at the hottest cross-section of the cask but does not show axial variation. The TAC2D model gives axial temperature variations but does not explicitly represent the FSS and does not show circumferential variations. Results of the two models were combined by first noting which two radially adjacent TAC2D temperatures at the hottest axial position (J=21 in Fig. 3.4-4) bracketed the ANSYS-predicted FSS or liner temperature, corrected for axial conduction. A normalized linear combination of these two



L-047(1)  
10-19-93

Fig. 3.6-13. Temperature difference between FSS/liner and DU

temperatures was then derived:

$$T_A(x,y) - \Delta T_a = fT_{i,21} + (1-f)T_{i+1,21}$$

where

$T_A(x,y)$	=	ANSYS model temperature
$\Delta T_a$	=	axial conduction effect (Table 3.4-2)
$f$	=	coefficient ( $0 < f < 1$ )
$T_{i,21}$	=	TAC2D temperature
$T_{i+1,21}$	=	adjacent TAC2D temperature

This formula was then applied over the whole length of the FSS and liner using the TAC2D temperatures of Fig. 3.4-4 at the same two radial ( $i$  and  $i+1$ ) positions:

$$T(x,y,z) = fT_{i,j} + (1-f)T_{i+1,j}$$

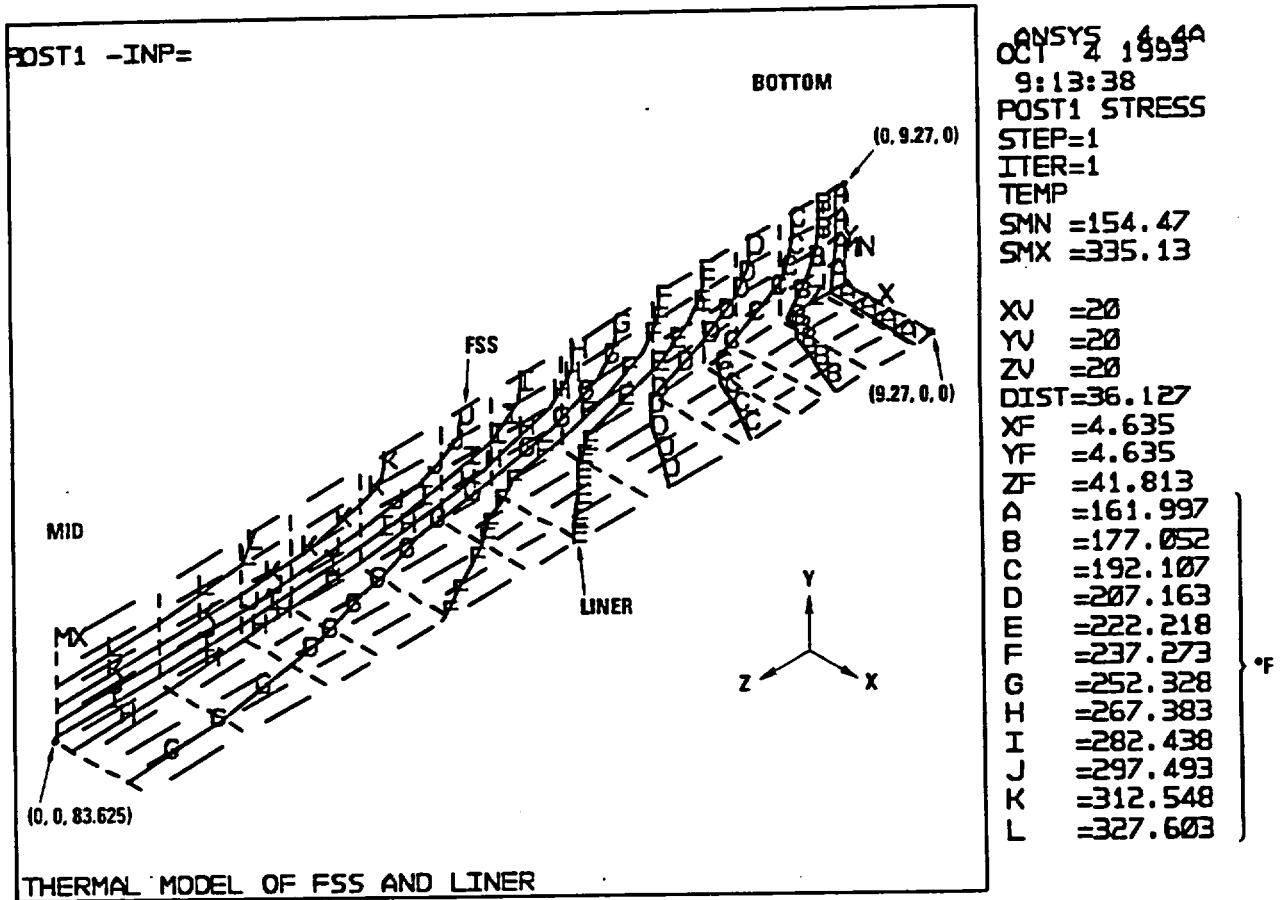
where the subscript  $j$  now ranges over all values in the cavity (9 to 36). In this way we produced temperatures at discrete  $(x,y,z)$  points in the FSS and liner.

The thermal stress analysis modeled a one-eighth cross section of the FSS and cavity liner and extended half the cavity length. For conservatism, we used the hottest one-eighth section from the ANSYS thermal results when generating the temperature distribution. In the axial direction, the temperatures are not quite symmetric as the decay heat profile causes the peak temperature to occur below the cavity midpoint. For input into the thermal stress model, we adjusted the temperature distribution slightly so that the midpoint coincided with the peak temperature. Temperatures in the lower half of the cavity were then used in the thermal stress model.

Figure 3.6-14 shows the final temperature distribution imposed on an ANSYS model having the same envelope as the thermal stress model. Section 2.10.9 documents the actual thermal stress analysis.

**3.6.9.2 Sensitivity to Tube/Skin Contact.** The normal conditions ANSYS model of the cask (Sec. 3.4.1) uses a coefficient of 900 Btu/hr-ft<sup>2</sup>-°F for contact between the neutron shield support tubes and the outer skin. The effect of a reduction of this coefficient was examined and is discussed here.

The design coefficient is taken from Ref. 3.6-6 and is based on a contact pressure of 10 psi and a pair of aluminum surfaces with a 65  $\mu$ -in. finish. If the surface finishes are taken to be 120  $\mu$ -in., the coefficient is reduced to about 450. The data also indicate that the coefficient is not very sensitive to contact pressure provided there is air in the gap. A contact pressure of 5 psi will reduce the coefficient by about 10%.



L-047(2)  
 10-19-93

Fig. 3.6-14. Temperature distribution in FSS and liner

To assess the effect of varying contact, a local TAC2D model of the cask body, tube, and outer skin was constructed. We imposed a heat flux on the cask body based on the maximum decay heat of 2,468 W. The heat sink on the outer skin was an effective ambient temperature of 118°F with a coefficient of 1.15 Btu/hr-ft<sup>2</sup>-°F (Sec. 3.6.8.2.1). The model was then run with tube/skin contact coefficients of 900, 450 and 225 Btu/hr-ft<sup>2</sup>-°F. The results show that the cask body temperature increases by only about 1°F when the contact coefficient is reduced to 450 and by some 5°F if it drops to 225. The data in Ref. 3.6-6 show that contact coefficients for gaps with air in them are all at least 300 Btu/hr-ft<sup>2</sup>-°F even at a contact pressure of 5 psi.

It is therefore concluded that cask temperatures will be affected by no more than 5°F by variations in tube/skin thermal contact.

**3.6.9.3 Aluminum vs. Copper on Outer Skin.** All analysis has assumed the 0.105-in. outer skin is plated with 0.010 in. of copper on its interior surface, except for areas near welding. By reducing thermal gradients on the skin the copper causes the cask to transfer heat more efficiently and minimize interior temperatures. In the cask design the copper has since been replaced with 0.020 in. of aluminum. This change renders the analysis slightly conservative since, in the direction parallel to the skin, the effective conductance of the skin with aluminum is approximately 10% higher than with copper. In the direction normal to the skin the change to aluminum makes no appreciable difference in the conductance.

**3.6.9.4 Melting of Impact Limiters.** We imposed a modification on the TAC2D model of Section 3.5.1.1 to check the effect of melting of the aluminum honeycomb impact limiters. The melting model assumed that the 0.04-in. steel skin surrounding the impact limiters remained intact except in the vicinity of the punch where it would be torn off. Impact limiter material retaining a skin was replaced with air after it melted, and the heat transfer across the void occurred by convection and thermal radiation. Impact limiter material without a skin was simply replaced by the fire environment upon melting (as in ablation).

The melting point of the aluminum 5052 alloy is 1100°F (Ref. 3.2-9) and the latent heat of fusion was taken to be 171 Btu/lb (Ref. 3.6-7). The specific heat during melting is theoretically infinite as the material absorbs the latent heat of fusion at a constant temperature. For numerical purposes a finite temperature interval of ±10°F about the melting point was taken within which the material was considered to be melting. The effective Al specific heat during melting is thus:

$$c_p = \frac{\Delta h}{\Delta T} = \frac{171}{20} = 8.55 \text{ Btu/lb-}^\circ\text{F}$$

Results for the hypothetical accident with this modification show that the peak seal temperature is 10°F less than if melting is not considered. There is no significant difference (~1°F) in the average cavity gas temperature. The lower seal temperature results from the impact limiter absorbing heat during melting while the subsequent void region presents a thermal resistance. The assumption of no melting is therefore conservative.

**3.6.9.5 Verification of Fuel Assembly Temperature Method.** The method used to calculate fuel assembly temperatures compares favorably to test data and also to the Wooten-Epstein correlation as shown below.

**3.6.9.5.1 Test Data Comparison.** Reference 3.6-8 presents experimental measurements of temperatures of standard Westinghouse 15x15 spent fuel assemblies in a 21-assembly PWR storage cask. Test run 4 utilized helium as the backfill with the cask in a horizontal configuration. Using the HYDRA (thermal analysis computer code) post-test predictions to fill in the temperatures between the data points (Fig. 5-21 of Ref. 3.6-8), the peak clad temperature was found to be 375°C (707°F) (assembly A1) and the corresponding enclosure temperature was 353°C (667°F). The decay heat for the assembly with these temperatures was 1 kW (3413 Btu/hr) over a 12-ft active length, or 284.4 Btu/hr-ft.

Using the GA method, the maximum rod temperature for this configuration would be calculated as follows.

Temperature rise across the gap from enclosure to edge of assembly ( $\Delta T_2$ ):

$$\Delta T_2 = \frac{Q' \Delta x}{k_g P}$$

where  $Q'$  = heat rate per unit length = 284.4 Btu/hr-ft,  $\Delta x$  = gap from wall to assembly edge = 0.1745 in.,  $k_g$  = gap (helium and radiation) conductivity, and  $P$  = average wall perimeter = 4 x 8.6 = 34.4 in. From Section 3.6.1.1, the gap conductivity evaluated at 667°F = 1127°R is 0.181 Btu/hr-ft-°F. Thus:

$$\Delta T_2 = 8^\circ\text{F}$$

For heat generation in a square assembly, the temperature rise  $\Delta T_1$  from the edge to the center is (Ref. 3.6-9):

$$\Delta T_1 = \frac{0.294 q'' L^2}{k_{fa}}$$

where  $q''$  is the heat generation per unit volume,  $L$  is the half-side length, and  $k_{fa}$  is the fuel assembly effective conductivity. Since  $Q' = (2L)^2 q''$ ,

$$\Delta T_1 = \frac{0.0735 Q'}{k_{fa}}$$

From Sec. 3.6.1.1 and evaluating at the mean assembly temperature  $0.5 \cdot (707 + 667 + 8) = 691^\circ\text{F} = 1151^\circ\text{R}$ , we obtain  $k_{fa} = 0.692$  Btu/hr-ft-°F. Thus:

$$\Delta T_1 = 30.2^\circ\text{F}$$

The center temperature is predicted to be  $667 + 8 + 30 = 705^\circ\text{F}$ , in good agreement with the measured value.

**3.6.9.5.2 Wooten-Epstein Comparison.** The Wooten-Epstein (WE) correlation was developed for spent fuel assemblies in air, whereas the GA method presumes helium. In order to facilitate a meaningful comparison, the GA method will be converted to an air medium. We will assume a 15 x 15 assembly with a rod pitch of 0.563 in. The decay heat will be taken as 617 W over an active length of 12 ft. A typical enclosure temperature of  $250^\circ\text{F}$  is used.

#### 1. WE Method

$$q'' = \sigma \left[ \frac{C_1}{\frac{1}{\epsilon_1} + \frac{1}{\epsilon_2} - 1} \right] \left( T_1^4 - T_2^4 \right) + C_2 (T_1 - T_2)^{\frac{4}{3}}$$

where

$q''$  = heat flux based on assembly envelope area (Btu/hr-ft<sup>2</sup>)  
 $\sigma$  =  $0.1714 \times 10^{-8}$  Btu/hr-ft<sup>2</sup>-°R<sup>4</sup>  
 $\epsilon_1, \epsilon_2$  = cladding and enclosure emissivities = 0.7, 0.2 (Table 3.2-2)  
 $C_1$  = regression constant

$$= \frac{4N}{(N+1)^2} \quad \text{for odd values of } N$$

$$= \frac{4}{N+2} \quad \text{for even values of } N$$

$N$  = number of rows in assembly  
 $C_2$  = regression constant = 0.118  
 $T_1, T_2$  = cladding and enclosure temperatures (°R)

The length of the assembly edge is  $15 \times \text{pitch} = 15 \times 0.563 = 8.445$  in., and the length is 12 ft. The heat flux is then

$$q'' = \frac{(617)(3.413)}{(12)(4) \left( \frac{8.445}{12} \right)} = 62.3$$

With a 15 x 15 assembly,  $C_1 = 0.234$ . The enclosure temperature  $T_2$  is  $250^\circ\text{F} = 710^\circ\text{R}$ . Inserting all the values, the WE correlation gives:

$$62.3 = 7.39 \times 10^{-11} (T_1^4 - 710^4) + 0.118 (T_1 - 710)^{\frac{4}{3}}$$

Solving by iteration gives  $T_1 = 804^\circ\text{R} = \underline{344^\circ\text{F}}$ .

## 2. GA Method

Temperature rise across the gap from enclosure to edge of assembly:

$$\Delta T_2 = \frac{Q' \Delta x}{k_g P}$$

where  $Q' = (617)(3.413)/12 = 175.5$  Btu/hr-ft,  $\Delta x = 0.1745$  in.,  $k_g =$  gap (air and radiation) conductivity, and  $P =$  average wall perimeter  $= 4 \times 8.6 = 34.4$  in. From Section 3.6.1.1 and substituting air for helium, the gap conductivity evaluated at  $250^\circ\text{F} = 710^\circ\text{R}$  is 0.0271 Btu/hr-ft- $^\circ\text{F}$ . Thus:

$$\Delta T_2 = 32.8^\circ\text{F}$$

Temperature rise from the assembly edge to center:

$$\Delta T_1 = \frac{0.0735 Q'}{k_{fa}}$$

If the expression for the fuel assembly effective conductivity from Sec. 3.6.1.1 is modified for air (substitute  $k_{\text{Air}}$  for  $k_{\text{He}}$ ) and evaluated at the estimated mean temperature  $300^\circ\text{F} = 760^\circ\text{R}$ , we obtain  $k_{fa} = 0.140$  Btu/hr-ft- $^\circ\text{F}$ . Thus:

$$\Delta T_1 = 92.1^\circ\text{F}$$

The center temperature is predicted to be  $250 + 32.8 + 92.1 = \underline{375^\circ\text{F}}$ . Thus, the GA method is conservative when compared to the WE correlation.

### 3.6.10 References for Sections 3.2 through 3.6

- 3.2-1 Glasstone, S., and A. Sesonske, *Nuclear Reactor Engineering*, D. Van Nostrand, 1963, p. 814.
- 3.2-2 *Thermophysical Properties of Matter*, Thermophysical Properties Research Center, Purdue University, IFI/Plenum, 1970, Vol. 1, pp. 887-889.
- 3.2-3 Kreith, F., *Principles of Heat Transfer*, 2nd ed., International Textbook, 1968, pp. 215, 593-595.

- 3.2-4 ASME Code, 1986 Edition, Section III, Division 1, Appendix I, Table I-4.0.
- 3.2-5 Armco, Inc., Bulletin No. S-45e, p. 9.
- 3.2-6 "Final Design for Fort St. Vrain Fuel Shipping Cask," GADR-55, General Atomics, Addendum I, 1978.
- 3.2-7 *Thermophysical Properties of High Temperature Solid Materials*, Thermophysical Properties Research Center, Purdue University, Macmillan, 1967, Vol. 6, pp. 1078-1081; Vol. 5, p. 35.
- 3.2-8 Deem, H. W., and C. F. Lucks, "Thermal Conductivity of Boron Carbide from 100°C to 800°C," BMI-713, Battelle Memorial Institute, December 10, 1951.
- 3.2-9 "Materials Selector," *Materials Engineering*, December 1990, pp. 70, 72, 82.
- 3.2-10 Goodman et al., "The Thermodynamic and Transport Properties of Helium," GA-A13400, General Atomic Company, October 1975.
- 3.2-11 "Heat Transfer in a Dry, Horizontal LWR Spent Fuel Assembly," PATRAM-83, Vol. II, pp. 1087-1094.
- 3.2-12 "MODREX Application Study to Support the Sequoyah Nuclear Power Plant," GA-A16673, General Atomics, March 1982, pp. 5-36.
- 3.2-13 "The CASTOR-V/21 PWR Spent Fuel Storage Cask: Testing and Analysis," EPRI NP-4887, November 1986, pp. 5-6.
- 3.2-14 "The TN-24P PWR Spent Fuel Storage Cask: Testing and Analysis," EPRI NP-5128, April 1987, pp. 5-17.
- 3.2-15 "Comparison of HYDRA-II Predictions to Temperature Data from Consolidated and Unconsolidated Model Spent Fuel Predictions," PNL-6630, September 1988.
- 3.2-16 Gubareff, G. G., J. E. Janssen, and R. H. Torborg, *Thermal Radiation Properties Survey*, Honeywell Research Center, 1960, p. 206.
- 3.3-1 *Parker O-Ring Handbook*, Parker Seal Company, pp. A3-4, A3-36, 1991.
- 3.4-1 "ANSYS, Engineering Analysis System User's Manual," Version 4.4, Swanson Analysis Systems, May 1989.
- 3.4-2 "PATRAN Plus User's Manual," Release 2.4, PDA Engineering, September 1989.
- 3.4-3 "TAC2D Version 1.0 Verification Report and Independent Review," Document 910351, General Atomics, September 1991.
- 3.4-4 "PAT/ANSYS Interface Guide," Release 2.2, PDA Engineering, September 1989.

- 3.4-5 "Quality Assurance Data Package for Polypropylene Neutron Shield," General Atomics Purchase Order M307505, Item 1, June 16, 1993.
- 3.6-1 Holman, J. P., *Heat Transfer*, 5th ed., McGraw-Hill, 1981, pp. 275, 281.
- 3.6-2 Kreith, F., *Principles of Heat Transfer*, 2nd ed., International Textbook, 1968, p. 411.
- 3.6-3 "Characteristics of Spent Fuel, High-Level Waste, and Other Radioactive Wastes Which May Require Long-Term Isolation," DOE/RW-0184, U. S. Department of Energy, Vol. 3, Appendix 2A ("Physical Descriptions of LWR Fuel Assemblies"), December 1987.
- 3.6-4 "A Guide for the Design, Fabrication, and Operation of Shipping Casks for Nuclear Applications," ORNL-NSIC-68, February 1970.
- 3.6-5 "Validation Document for TAC2D\_0002," Document 910513, General Atomics, May 1992.
- 3.6-6 Rohsenow, W. M., and J. P. Hartnett (ed.), *Handbook of Heat Transfer*, McGraw-Hill, 1973, p. 3-16.
- 3.6-7 *Marks' Standard Handbook for Mechanical Engineers*, McGraw-Hill, 8th ed., 1978, p. 4-12.
- 3.6-8 "The CASTOR-V/21 PWR Spent Fuel Storage Cask: Testing and Analysis," EPRI NP-4887, November 1986.
- 3.6-9 Arpaci, V. S., *Conduction Heat Transfer*, Addison-Wesley, 1966, p. 465.

THIS PAGE LEFT BLANK INTENTIONALLY

**CHAPTER 4  
TABLE OF CONTENTS**

<b>4. CONTAINMENT</b> .....	<b>4.1-1</b>
4.1 Containment Boundary .....	4.1-1
4.1.1 Containment Vessel .....	4.1-1
4.1.2 Containment Penetrations .....	4.1-1
4.1.3 Seals and Welds .....	4.1-1
4.1.3.1 Containment Boundary O-ring Seals .....	4.1-1
4.1.3.2 Containment Boundary Welds .....	4.1-1
4.1.4 Closure .....	4.1-3
4.2 Requirements for Normal Conditions of Transport .....	4.2-1
4.2.1 Containment of Radioactive Material .....	4.2-1
4.2.2 Pressurization of Containment Vessel .....	4.2-1
4.2.3 Containment Criterion .....	4.2-1
4.3 Requirements of the Hypothetical Accident Conditions .....	4.3-1
4.3.1 Fission Gas Products .....	4.3-1
4.3.2 Containment of Radioactive Materials .....	4.3-1
4.3.3 Containment Criterion .....	4.3-1
4.4 Special Requirements .....	4.4-1
4.5 Appendix .....	4.5-1
4.5.1 Full-scale Closure Seal Tests .....	4.5-1
4.5.1.1 Summary .....	4.5-1
4.5.1.2 Test Set-up .....	4.5-1
4.5.1.3 Test Results .....	4.5-4
4.5.1.4 Conclusions .....	4.5-5
4.5.2 References for Sections 4.1 through 4.2 .....	4.5-8

**FIGURES**

4.1-1 Containment boundary .....	4.1-2
4.5-1 Test set-up for ambient conditions .....	4.5-2
4.5-2 Schematic of test arrangement .....	4.5-3
4.5-3 Test results, 0.010-in. gap, ambient temperature .....	4.5-6
4.5-4 Test results, 0.038-in. gap, 250°F .....	4.5-7
4.5-5 Test results, zero-gap, 380°F .....	4.5-8

THIS PAGE LEFT BLANK INTENTIONALLY

## 4. CONTAINMENT

### 4.1 Containment Boundary

The containment boundary consists of the cask body (cask body wall, flange and bottom plate), cask closure, closure bolts (with threaded inserts), gas sample port, drain valve and the primary O-ring seals. One O-ring, located in the inner dovetail groove in the cask closure, seals the interface between the cask body and the cask closure. A second O-ring is located on the gas sample port in the closure, and a third on the drain valve in the bottom head of the cask. Figure 4.1-1 shows the structural components and the O-ring seals that form the containment boundary.

#### 4.1.1 Containment Vessel

The cask body and closure for the GA-4 cask are fabricated from SA-240, Type XM-19 stainless steel. The cask body wall is 1.5 in. thick. The bottom plate is 9.5 in. thick. The closure is 11.0 in. thick.

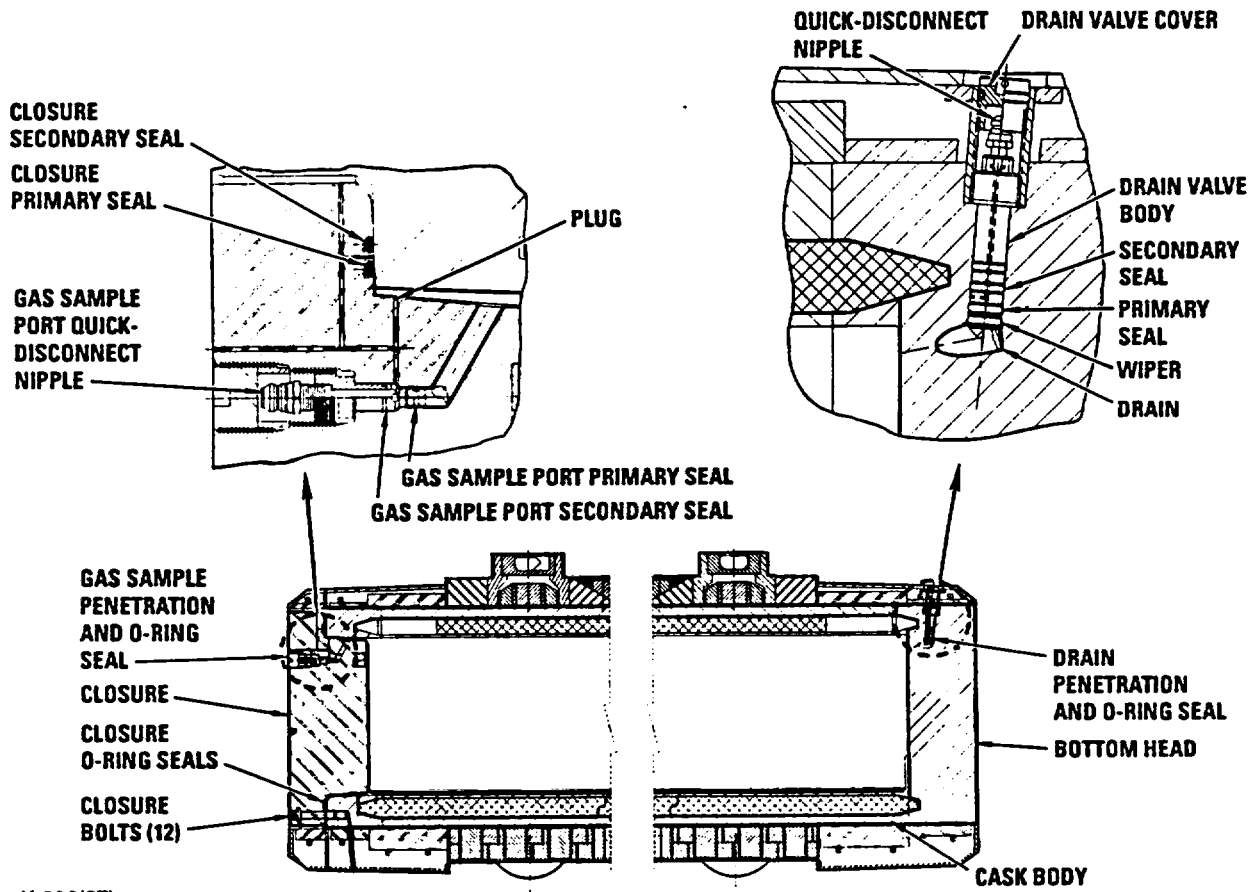
#### 4.1.2 Containment Penetrations

A gas sample port in the closure and a drain valve in the bottom plate are the only two penetrations into the containment vessel (see Fig. 4.1-1). All ports are made from SA-240, Type XM-19 stainless steel. We designed all components of the ports to maintain the required leaktight ( $1 \times 10^{-7}$  std-cm<sup>3</sup>/s) containment during both normal conditions of transport and hypothetical accident conditions.

#### 4.1.3 Seals and Welds

**4.1.3.1 Containment Boundary O-ring Seals.** The O-ring seals must function properly between -40°F and 155°F during normal conditions of transport. During the hypothetical accident condition thermal event, the O-ring seals must function properly at a temperature above 350°F for as much as an hour, with a maximum of 365°F. The closure primary O-ring is 0.375 in. in diameter and is compressed 25%, nominal. This amount of squeeze, 0.093 in., allows the O-ring seal to function properly during the maximum expected displacement of the cask closure and cask body interface; see Section 4.3. Close-tolerance O-ring seals and special dovetail groove dimensions are used in order to obtain the specified squeeze. The closure seals are Parker E-0740-75 ethylene propylene elastomer.

**4.1.3.2 Containment Boundary Welds.** We have designed and will qualify, fabricate, inspect, and accept all containment boundary welds in accordance with the requirements of Section III, Subsection NB, of the ASME Code (Ref. 4.1-1); NUREG/CR-3019, "Recommended Welding Criteria for Use in the Fabrication of Shipping Containers for Radioactive Materials"; and NUREG/CR-3854, "Fabrication Criteria for Shipping Containers." Chapter 9 describes the Quality Assurance Program.



K-896(87)  
10-22-93

Fig. 4.1-1. Containment boundary

4.1.4 Closure

The cask closure consists of a Type XM-19 stainless steel plate which is attached to the cask body with 12 1-in. bolts having threaded inserts. The material specification for the bolts is ASME SB-637, Alloy N07718. Each bolt is torqued to  $235 \pm 15$  ft-lb.

THIS PAGE LEFT BLANK INTENTIONALLY

## 4.2 Requirements for Normal Conditions of Transport

We designed all components of the containment boundary in accordance with established criteria and then performed tests and analysis to verify compliance with the criteria. Analysis shows that, during all normal conditions, the containment vessel meets the structural criteria in Section 2.1 and the O-ring seals remain below allowable temperatures and maintain sufficient compression. We have verified the seal design by performing a test on a full-scale closure and seal configuration (Section 4.5.1).

### 4.2.1 Containment of Radioactive Material

The cask design permits no release of radioactive material, demonstrated to a sensitivity of  $A_2 \times 10^{-6}$  Ci/hr. This criterion is met by maintaining a leaktight containment boundary as defined in ANSI N14.5-1987 (Ref. 4.2-1).

### 4.2.2 Pressurization of Containment Vessel

We calculated the maximum normal operating pressure (MNOP) in Section 3.4.4. We included this pressure in the loading combinations that were defined in Section 2.1 and evaluated in Section 2.6. The results show that the structural allowable stresses are met.

### 4.2.3 Containment Criterion

The verifiable containment criterion for a leaktight containment is a leakage test that shows leakage to be less than  $1 \times 10^{-7}$  std-cm<sup>3</sup>/s (air) or  $1.96 \times 10^{-7}$  cm<sup>3</sup>/s (helium). The cask is designed to a leaktight capability as defined in ANSI N14.5. Section 4.5.1 discusses full-scale closure seal tests, which demonstrate that the primary seal is leaktight for normal conditions of transport. The test procedure for the containment system assembly verification and for periodic leakage tests will be described in the Operation and Maintenance Manual. Results from half-scale model testing will also be used to confirm leaktightness.

For the containment system assembly verification pre-shipment test, ANSI N14.5-1987 requires a leakage test with a sensitivity of  $1 \times 10^{-3}$  std-cm<sup>3</sup>/s. A pressure rise test is adequate for this purpose. For the containment system fabrication and periodic verification tests, ANSI N14.5-1987 requires that the leakage test procedure have a sensitivity of  $5 \times 10^{-8}$  std-cm<sup>3</sup>/s to demonstrate that the package is leaktight. Section 8.1.3.2 contains a description of the procedure for the containment system fabrication and periodic verification tests.

THIS PAGE LEFT BLANK INTENTIONALLY

### 4.3 Requirements of the Hypothetical Accident Conditions

We designed all components of the containment boundary in accordance with established criteria and then performed tests and analysis to verify that the criteria were met. Conservative analysis shows (1) that during all hypothetical accident conditions, the containment boundary meets the structural criteria in Section 2.1 and, (2) that the O-ring seals remain below allowable temperatures and maintain sufficient compression. According to the manufacturer's data (Section 3.3), the maximum O-ring temperature of 365°F during the hypothetical accident condition thermal event allows the seal to function for at least 10 hr. Section 3.5.3 shows that the seal is between 350 and 365°F for at most 1 hr. The maximum O-ring transient local decompression due to bending of the closure caused by a thermal gradient during the thermal event is equal to 0.035 in. (see Sec. 2.7.3) out of an initial minimum nominal compression of 0.093 in. We have verified the seal design by performing a test on a full-scale closure and seal configuration (Section 4.5.1).

#### 4.3.1 Fission Gas Products

Since the containment criterion is a leaktight cask, the quantity of gas fission products is not necessary for containment analysis.

#### 4.3.2 Containment of Radioactive Materials

The GA-4 cask design allows no release of krypton-85 exceeding  $10A_2$  in one week and no escape of radioactive material exceeding a total amount  $A_2$  in one week. We meet this criterion by maintaining a leaktight containment boundary as defined in ANSI N14.5-1987 (Ref. 4.2-1).

#### 4.3.3 Containment Criterion

The verifiable containment criterion for a leaktight containment is a leakage test that shows leakage to be less than  $1 \times 10^{-7}$  std-cm<sup>3</sup>/s (air) or  $1.96 \times 10^{-7}$  cm<sup>3</sup>/s (helium). The cask is designed to a leaktight capability as defined in ANSI N14.5. Section 4.5.1 discusses full-scale closure seal tests and demonstrates that the primary seal is leaktight for hypothetical accident conditions of transport. The test procedure for the containment system assembly verification and for periodic verification leakage tests will be described in the Operation and Maintenance Manual. Results from half-scale model testing will be used to confirm leaktightness.

For the containment system assembly verification pre-shipment test, ANSI N14.5-1987 requires a leakage test with a sensitivity of  $1 \times 10^{-3}$  std-cm<sup>3</sup>/s. A pressure rise test is adequate for this purpose. For the containment system fabrication and periodic verification tests, ANSI N14.5-1987 requires that the leakage test procedure have a sensitivity of  $5 \times 10^{-8}$  std-cm<sup>3</sup>/s to demonstrate that the package is leaktight. Section 8.1.3.2 contains a description of the procedure for the containment system fabrication and periodic verification tests.

THIS PAGE LEFT BLANK INTENTIONALLY

#### 4.4 Special Requirements

Four PWR fuel elements contain more than 20 curies of plutonium. However, reactor fuel elements are exempt from the requirements of 10 CFR Part 71.63(b); therefore, we have not included a separate inner container.

THIS PAGE LEFT BLANK INTENTIONALLY

## 4.5 Appendix

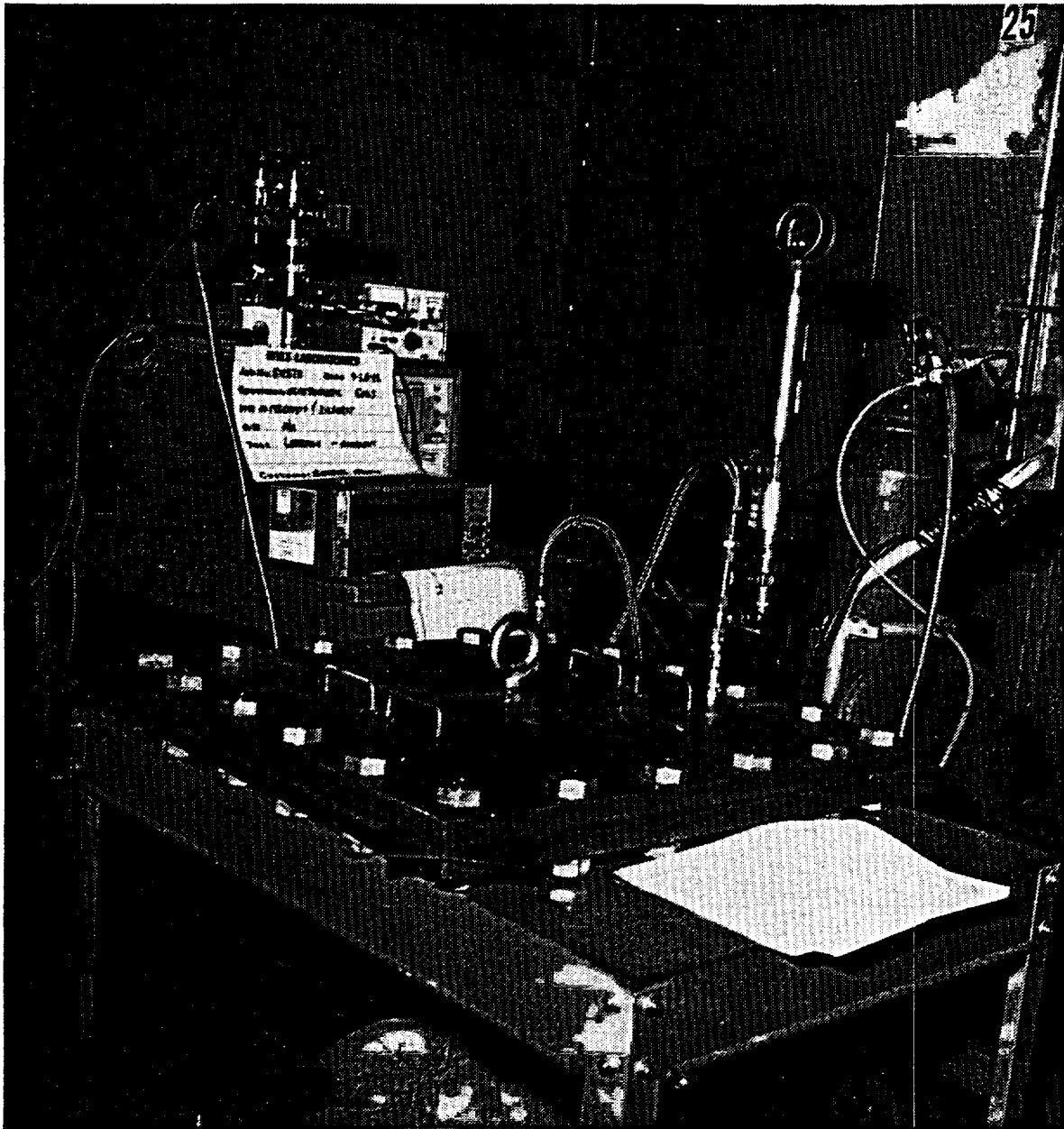
### 4.5.1 Full-scale Closure Seal Tests

4.5.1.1 Summary. The primary O-ring seal of the cask was tested for leakage using a full-scale mockup of the cask closure and flange. The seal material was E-0740-75, an ethylene propylene compound supplied by Parker Seal Group, Parker Hannifin Corporation. The tests were performed at temperatures of ambient,  $-42^{\circ}$ ,  $250^{\circ}$ , and  $380^{\circ}$ F. Shim plates between the fixture lid and flange, ranging from 0 to 0.038 in., simulated gaps resulting from thermal-induced distortion. The leakage testing was carried out by means of a helium mass spectrometer leak detector (MSLD), following ANSI N14.5-1987 (Ref. 4.2-1). All tests were performed at Wyle Laboratories, Norco, California.

Results showed that the primary seal maintained leaktightness for all test conditions. After pressurization of the test fixture, permeation of the helium gas through the seal was observed to begin in about 20 minutes for the ambient test and in 1–2 minutes for the tests at elevated temperatures. To verify that the MSLD readings were due to permeation and not real leakage, a response check was conducted in which a calibrated leak source of approximately  $1 \times 10^{-7}$  std  $\text{cm}^3/\text{s}$  was inserted in the detector line near the seal. When the leak source was activated, the detector responded within seconds.

4.5.1.2 Test Set-up. A typical test set-up is shown in Fig. 4.5-1 and illustrated schematically in Fig. 4.5-2. The test fixture consists of a lid and flange and is a full-scale representation of the cross section of the cask closure end. Two dovetail grooves in the lid hold the primary and secondary O-ring seals. The grooves and O-ring seals precisely model the full-scale cask. All fixture materials are fabricated from 304 stainless steel. The fixture lid weighs approximately 170 lb and the flange 180 lb. The fixture lid attaches to the flange with 20 1-in. bolts that thread into nuts tack-welded to the bottom of the flange. The bolts are torqued to 100 ft-lb. Shim plates extending all around the fixture's perimeter maintain uniform specified gaps between the lid and flange.

From operational and handling considerations it was not feasible to fabricate the test lid to the actual closure thickness of 11 in. The thicknesses of the lid and flange, the number of bolts and the bolt torque are not critical. Since the purpose of the test is to verify the seal performance under predicted conditions of temperature and seal compression, the critical dimensions are those of the seal and groove. The test closure precisely models these dimensions as in the full-scale cask, and the temperatures and amount of seal compression imposed encompass those predicted by analysis. The number of bolts is increased to compensate for a reduced closure stiffness and ensure a uniform gap around the perimeter. The bolt torque, although less than specified for the actual cask, is sufficient to compress the seals by the desired amount.



K-885(17)  
5-26-93

Fig. 4-5.1. Test set-up for ambient conditions

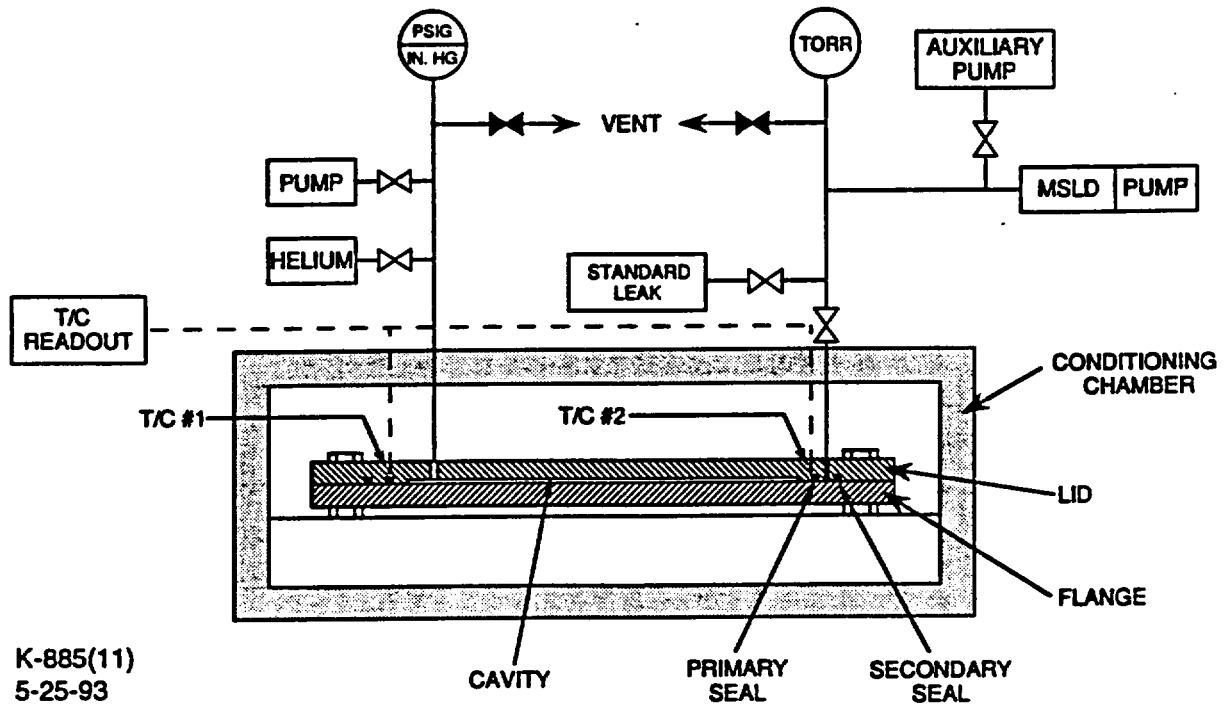


Fig. 4.5-2. Schematic of test arrangement

Prior to testing, the small volume between the flange and lid is initially evacuated. When the test begins, this volume is filled with helium to atmospheric pressure. A second port located between the O-rings is continuously evacuated by the MSLD, and the detector measures the helium leakage past the primary (inner) O-ring. The detector output is recorded by a conventional strip chart recorder.

For the tests carried out in the conditioning chamber, the fixture temperatures near the inner seal are measured by two thermocouples (Type T) and recorded.

**4.5.1.3 Test Results.** Four tests were carried out with E-0740-75 seals and the results are shown in the following table. One set of seals was used for the test at  $-40^{\circ}\text{F}$ , and another set was used for the other three tests. The first two tests simulated normal conditions of transport, while the last two represented hypothetical accident conditions. For the latter conditions, the thermal and thermal stress analyses (Sections 3.5 and 2.7.3) predict a maximum lid/flange gap of 0.035 in., corresponding to a temperature of  $250^{\circ}\text{F}$ , while  $365^{\circ}\text{F}$  is the maximum seal temperature, corresponding to a zero-gap. The conditions used in the test are therefore conservative.

Gap (in.)	Temp. ( $^{\circ}\text{F}$ )	Background (atm $\text{cm}^3/\text{s}$ )	Leakage <sup>(a)</sup> (atm $\text{cm}^3/\text{s}$ )	Permeation time (min) <sup>(b)</sup>
0	-42	$9.3 \times 10^{-9}$	$7.1 \times 10^{-10}$	> 5
0.010	Ambient (~75)	$3.0 \times 10^{-8}$	$< 1 \times 10^{-7}$	23
0.038	15 hr @ 250	$4.8 \times 10^{-8}$	"	2
0	380 1 hr above 365 1.5 hr above 350	$3.0 \times 10^{-10}$	$2 \times 10^{-10}$	1
<sup>(a)</sup> Before onset of permeation <sup>(b)</sup> After achieving 1 atm cavity pressure				

Test data are summarized above. Results are given in terms of test conditions, i.e., helium leakage at the test temperature with an upstream pressure of 1 atm in the fixture cavity and a downstream pressure of less than 0.01 atm (typically 2–5 millitorr) in the detector line or seal interspace. The definition of leaktight in ANSI N14.5-1987 (Ref. 4.2-1) assumes air at a standard temperature of  $77^{\circ}\text{F}$  (298 K) as the leakage gas. No conversion of test results to air standard conditions was made. Such a conversion would give leakage rates less than the helium rate, and the helium rate is therefore conservative.

The test at  $-42^{\circ}\text{F}$  was allowed to proceed for 5 minutes, while the remaining tests were carried out for longer times to investigate the effect of permeation. Figures 4.5-3 through 4.5-5 show the leakage plotted against time for the tests at ambient,  $250^{\circ}$ , and  $380^{\circ}\text{F}$ . Time 0 corresponds to 1 atm helium pressure in the fixture cavity. (Typically, less than 30 seconds were required to achieve this from the time the valve was first opened.) In Fig. 4.5-3 permeation is clearly evident from the slow rise in detector output following some 20 minutes of no indicated leakage. Figures 4.5-4 and 4.5-5 show permeation beginning much more rapidly, as expected with higher temperatures, with the leakage showing no change for 1–2 minutes after pressurization.

Following the last test, a response check was carried out to verify that an actual leak would be observed within a time much less than 1 minute. The calibrated standard leak of  $1.7 \times 10^{-7}$  was connected to the detector line where it entered the test fixture. With the leak standard valve open, an arbitrary reference point of time 0 was marked and the valve was closed one minute later. The detector responded virtually instantaneously. After another minute the valve was opened again, producing another immediate response. The entire sequence was then repeated, with the same results.

**4.5.1.4 Conclusions.** The tests carried out confirmed the leaktightness of the E-0740-75 inner (primary) seal under normal and hypothetical accident conditions of transport for the GA-4 cask. The leaktightness is inferred by observing that for ambient conditions the MSLD reading did not increase by more than  $1 \times 10^{-7}$  during a 20-minute period following pressurization of the fixture cavity to 1 atm helium. For elevated temperatures the indicated leakage increased after holding at background for at least one minute. Since a response check showed that an actual leak would be observed within seconds, the indicated "leakage" is actually permeation.

#### **4.5.2 References**

- 4.1-1 American Society of Mechanical Engineers (ASME), *Boiler and Pressure Vessel Code*.
- 4.2-1 American National Standards Institute, "American National Standard for Leakage Tests on Packages for Shipment of Radioactive Material," ANSI N14.5-1987.

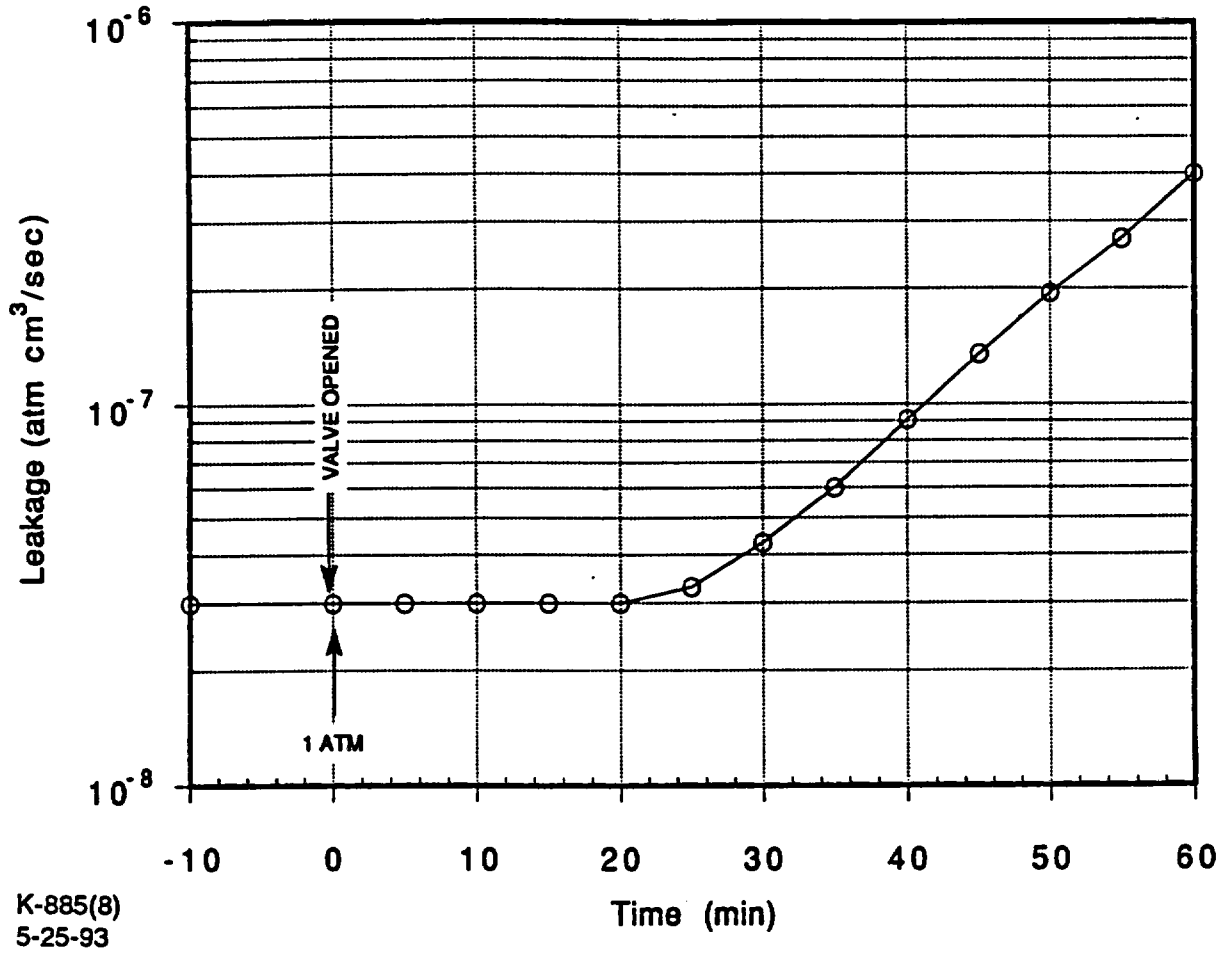


Fig. 4.5-3. Test results, 0.010-in. gap, ambient temperature

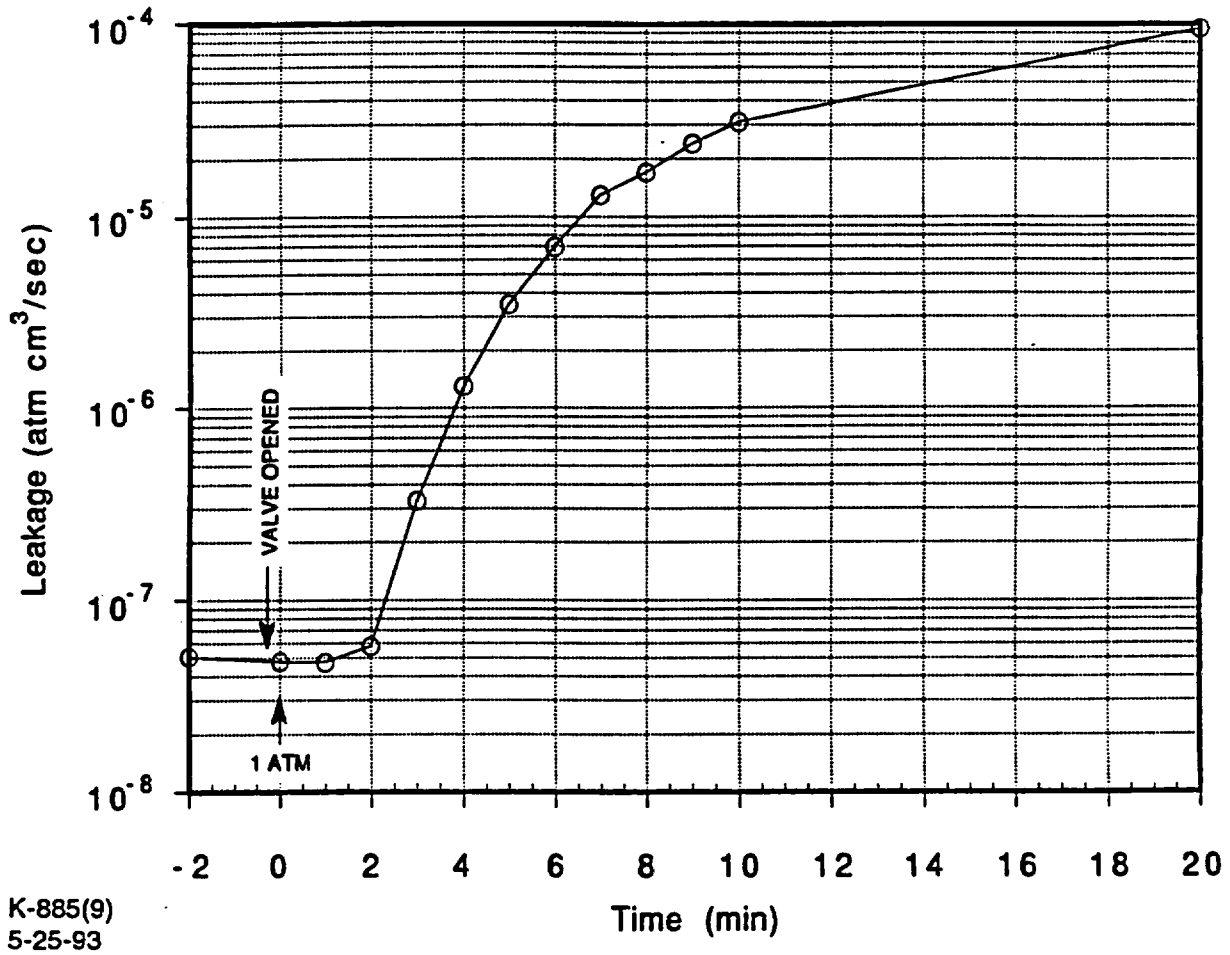


Fig. 4.5-4. Test results, 0.038-in. gap, 250°F

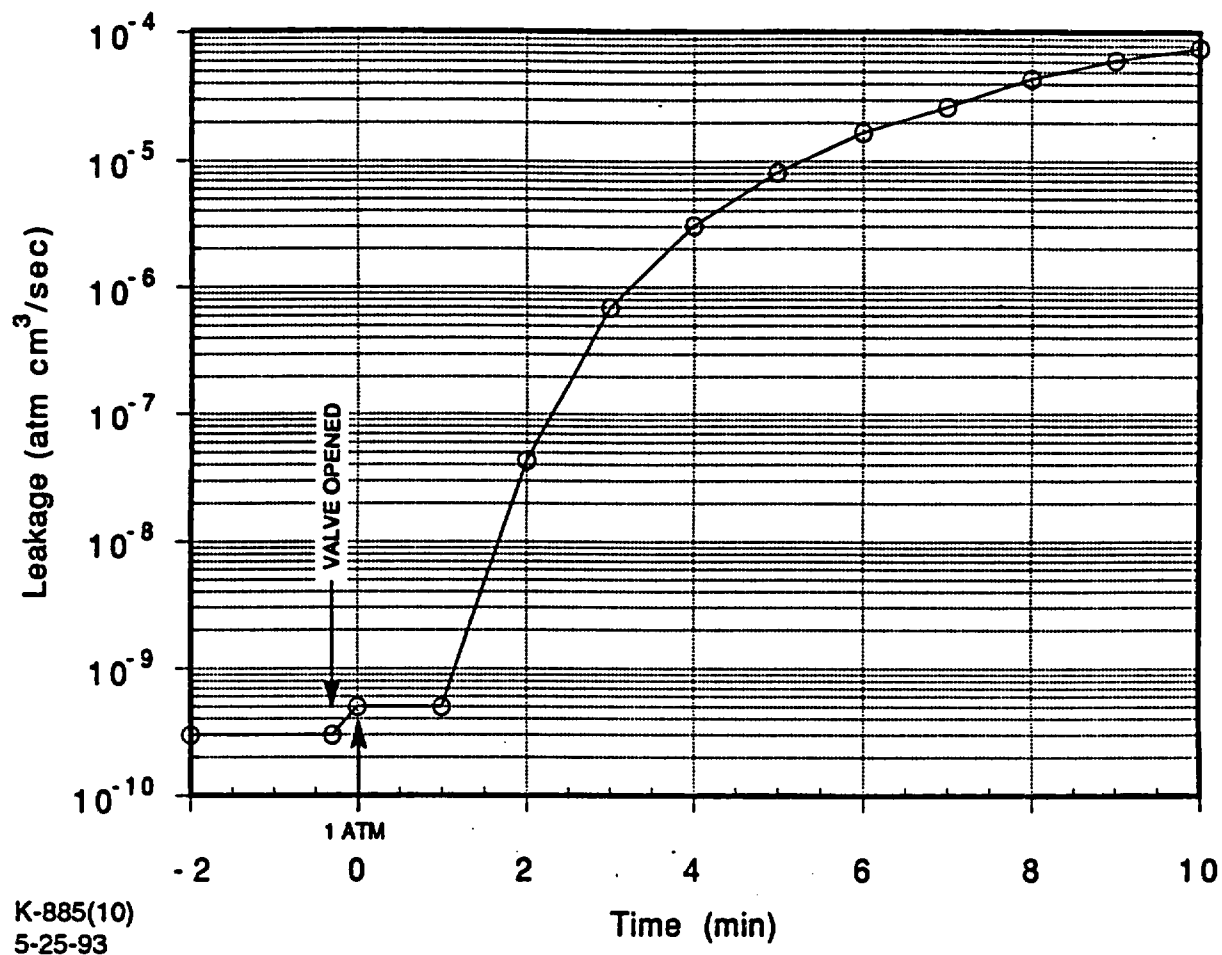


Fig. 4.5-5. Test results, zero-gap, 380°F

**CHAPTER 5  
TABLE OF CONTENTS**

<b>5. SHIELDING EVALUATION</b> .....	<b>5.1-1</b>
5.1 Discussion and Results .....	5.1-1
5.2 Source Specification .....	5.2-1
5.2.1 Gamma Source .....	5.2-3
5.2.2 Neutron Source .....	5.2-6
5.3 Model Specification .....	5.3-1
5.3.1 Description of Radial and Axial Shielding Configuration .....	5.3-1
5.3.2 Shield Regional Densities .....	5.3-1
5.4 Shielding Evaluation .....	5.4-1
5.4.1 Assumptions .....	5.4-1
5.4.2 Cross-section Data .....	5.4-1
5.4.3 Dose Rate Conversion Factors .....	5.4-2
5.4.4 Computer Code Selection .....	5.4-2
5.4.5 Shielding Calculations .....	5.4-5
5.4.5.1 Gamma Analysis .....	5.4-5
5.4.5.2 Neutron Analysis .....	5.4-6
5.4.5.3 Gap Analysis .....	5.4-7
5.4.5.4 Ground Scattering Analysis .....	5.4-7
5.4.6 Shielding Results for Normal Transport Conditions .....	5.4-8
5.4.6.1 Azimuthal Dose Rate Profile .....	5.4-8
5.4.6.2 Dose Rate Maps .....	5.4-8
5.4.7 Shielding Results for Hypothetical Accident Conditions .....	5.4-8
5.4.8 Correlation of Accident Dose Rate to Measured Dose Rate .....	5.4-8
5.5 Appendices .....	5.5-1
5.5.1 Additional Burnup and Age Shielding Analysis .....	5.5-1
5.5.1.1 Source Specification .....	5.5-1
5.5.1.2 Model Specification .....	5.5-16
5.5.1.3 Shielding Evaluation .....	5.5-16
5.5.2 References for Sections 5.2 through 5.5 .....	5.5-20

**FIGURES**

5.2-1	Representative PWR axial burnup distribution .....	5.2-2
5.3-1	Axial shielding configuration on flats .....	5.3-2
5.3-2	Radial shielding configuration at midsction .....	5.3-3
5.4-1	Azimuthal midplane dose rate profile for GA-4 cask .....	5.4-9
5.4-2	Total dose rate around GA-4 cask for normal conditions .....	5.4-10
5.4-3	Total dose rate around GA-4 cask for hypothetical accident conditions .....	5.4-12
5.5-1	Minimum cooling time for four or fewer fuel assemblies .....	5.5-2
5.5-2	Minimum cooling time for two fuel assemblies with two shield inserts .....	5.5-3
5.5-3	Down-loaded GA-4 cask configuration with shield inserts .....	5.5-4
5.5-4	GA-4 cask dose rate points for normal conditions of transport .....	5.5-17

## TABLES

5.1-1	SUMMARY OF MAXIMUM REGULATORY DOSE RATES FOR GA-4 CASK .....	5.1-2
5.2-1	BASIS FOR SOURCE SPECIFICATION .....	5.2-1
5.2-2	PWR FUEL ASSEMBLY AND EXPOSURE DATA FOR SAS2 MODULE IN SCALE ...	5.2-4
5.2-3	PWR FUEL GAMMA SOURCE DATA .....	5.2-5
5.2-4	PWR NON-FUEL REGION GAMMA SOURCE TERMS .....	5.2-6
5.2-5	PWR FUEL NEUTRON SOURCE DATA .....	5.2-6
5.3-1	SHIELDING THICKNESS OF GA-4 CASK .....	5.3-4
5.3-2	MATERIAL PROPERTY DATA .....	5.3-6
5.3-3	PWR FUEL ASSEMBLY MATERIAL DATA .....	5.3-7
5.4-1	MULTIGROUP FLUX-TO-DOSE CONVERSION FACTORS .....	5.4-3
5.4-2	POINTWISE ENERGY FLUX-TO-DOSE CONVERSION FACTORS .....	5.4-4
5.4-3	EQUIVALENT SHIELDING CODES .....	5.4-5
5.4-4	GA-4 CASK DOSE RATES FOR NORMAL CONDITIONS .....	5.4-11
5.4-5	GA-4 CASK DOSE RATES FOR HYPOTHETICAL ACCIDENT CONDITIONS .....	5.4-13
5.4-6	CORRELATION DATA FOR ACCIDENT CONDITIONS .....	5.4-14
5.5-1	PWR FUEL ASSEMBLY AND EXPOSURE DATA FOR SAS2 .....	5.5-5
5.5-2	PWR FUEL GAMMA SOURCE DATA FOR 35 GWd/MTU AND 5-YEAR-COOLED ...	5.5-6
5.5-3	PWR FUEL GAMMA SOURCE DATA FOR 45 GWd/MTU AND 7-YEAR-COOLED ...	5.5-6
5.5-4	PWR FUEL GAMMA SOURCE DATA FOR 45 GWd/MTU AND 15-YEAR-COOLED ...	5.5-7
5.5-5	PWR FUEL GAMMA SOURCE DATA FOR 55 GWd/MTU AND 10-YEAR-COOLED ...	5.5-7
5.5-6	PWR FUEL GAMMA SOURCE DATA FOR 55 GWd/MTU AND 20-YEAR-COOLED ...	5.5-8
5.5-7	PWR FUEL GAMMA SOURCE DATA FOR 60 GWd/MTU AND 11-YEAR-COOLED ...	5.5-8
5.5-8	PWR FUEL GAMMA SOURCE DATA FOR 60 GWd/MTU AND 25-YEAR-COOLED ...	5.5-9
5.5-9	PWR NON-FUEL REGION GAMMA SOURCE TERMS .....	5.5-9
5.5-10	PWR FUEL NEUTRON SOURCE DATA FOR 35 GWd/MTU AND 5-YEAR-COOLED .....	5.5-10
5.5-11	PWR FUEL NEUTRON SOURCE DATA FOR 45 GWd/MTU AND 7-YEAR-COOLED .....	5.5-11
5.5-12	PWR FUEL NEUTRON SOURCE DATA FOR 45 GWd/MTU AND 15-YEAR-COOLED .....	5.5-12
5.5-13	PWR FUEL NEUTRON SOURCE DATA FOR 55 GWd/MTU AND 10-YEAR-COOLED .....	5.5-13
5.5-14	PWR FUEL NEUTRON SOURCE DATA FOR 55 GWd/MTU AND 20-YEAR-COOLED .....	5.5-14
5.5-15	PWR FUEL NEUTRON SOURCE DATA FOR 60 GWd/MTU AND 11-YEAR-COOLED .....	5.5-15
5.5-16	PWR FUEL NEUTRON SOURCE DATA FOR 60 GWd/MTU AND 25-YEAR-COOLED .....	5.5-16
5.5-17	FULLY LOADED GA-4 CASK, DOSE RATES FOR NORMAL CONDITIONS .....	5.5-18
5.5-18	TWO-ELEMENT GA-4 CASK WITH SHIELD INSERTS, DOSE RATES FOR NORMAL CONDITIONS .....	5.5-19

## 5. SHIELDING EVALUATION

The GA-4 legal weight truck cask utilizes a combination of depleted uranium (DU) and stainless steel, primarily for gamma shielding, and solid modified polypropylene (with 1% boron by weight, to minimize secondary gamma production within the material) as neutron shielding. Optimum amounts and thicknesses of neutron and gamma shielding, with the densest material placed toward the inside of the cask, are provided to achieve the most efficient cask geometry. For simplicity in design and ease of fabrication, the top and bottom ends of the cask use a solid stainless steel structure that provides sufficient shielding for both neutrons and gammas.

### 5.1 Discussion and Results

The GA-4 cask provides radiation shielding engineered to meet the regulatory requirements of 10 CFR Part 71 for both normal conditions of transport and hypothetical accident conditions. Our approach to shielding design is to optimize the cask shielding configuration for minimum weights and maximum payloads. The optimization method involves use of the most effective shielding materials, square cross-section geometry with rounded corners, and tapered shielding sections in the non-fuel regions. In addition, the trade-off between the thicknesses of the neutron and gamma shields enables us to select an optimum design in which the cask weight is at a minimum.

The main shielding analysis is based on four pressurized-water reactor (PWR) assemblies with a fuel burnup of 35 GWd/MTU and a cooling time of 10 years. This analysis is presented in Sections 5.1 through 5.4. Appendix 5.5.1 presents the shielding analyses for PWR assemblies with higher burnup levels. Fully loaded cask configurations with high burnup, long cooling time fuel were analyzed. Partially loaded (2 elements) casks with shorter cooling time fuel were also considered. We generated the neutron and gamma source data with the SAS2 (SAS2H) module of SCALE-4.1, using a representative burnup profile for the active fuel region. The gamma source terms for the non-fuel regions were obtained by using activation ratios related to the active fuel region.

The shielding analyses considered both normal and hypothetical accident conditions to comply with 10 CFR Part 71. The shielding models for these two conditions differ only in the assumption that the neutron shield and outer skin remain intact during normal transport but completely disappear following a hypothetical accident condition thermal event.

The results of the analyses (including the high-burnup fuel analyses) are shown in Table 5.1-1. These results show that radiation levels outside the cask are all within the regulatory dose rate limits for transportation. In these tables the package surface is defined as the surface of the top and bottom impact limiters and the cylindrical personnel

5.1-2

**TABLE 5.1-1  
SUMMARY OF MAXIMUM REGULATORY DOSE RATES FOR GA-4 CASK**

Burnup (GWd/MTU)	35	45	55	60	35	45	55	60																	
Cooling time (years)	10	15	20	25	5	7	10	11																	
Number of assemblies	4	4	4	4	2	2	2	2																	
Number of shield inserts	0	0	0	0	0	0	0	0																	
<b>NORMAL CONDITIONS</b>																									
Package surface	$\gamma$	n	Total	Reg.																					
Side	59	14	73	45	28	73	35	41	76	26	43	69	77	8	85	67	18	86	53	28	81	52	35	87	200
Top	12	6	18	9	12	21	7	17	24	5	18	23	13	3	16	11	8	19	9	12	21	9	14	23	200
Bottom	38	6	44	27	12	39	20	17	37	14	18	32	43	4	47	38	9	47	30	14	44	30	17	47	200
2 m from vehicle	$\gamma$	n	Total	Reg.																					
Side	7.6	1.8	9.4	5.7	3.8	9.5	4.4	5.4	9.8	3.1	5.8	8.9	8.8	0.8	9.6	7.7	1.8	9.5	6.1	2.8	8.9	6.0	3.5	9.5	10
Rear	0.96	0.16	1.11	0.68	0.32	1.00	0.50	0.46	0.96	0.35	0.49	0.84	1.1	0.1	1.2	0.96	0.24	1.2	0.76	0.37	1.13	0.75	0.46	1.21	10
Back of cab	0.20	0.04	0.24	0.13	0.08	0.21	0.12	0.12	0.24	0.06	0.12	0.18	0.21	0.03	0.24	0.18	0.06	0.24	0.15	0.09	0.24	0.14	0.11	0.26	2
<b>HYPOTHETICAL ACCIDENT CONDITIONS</b>																									
1 m from damaged cask	$\gamma$	n	Total	Reg.																					
Side (peak)	103	194	297	75	398	473	56	571	627	38	608	646	131	115	246	114	269	383	88	414	502	86	514	600	1000

barrier that extends between them. The dose rate for the side of the package is the peak dose rate that occurs on the personnel barrier. The "top" and "bottom" package surface dose rates are the peak dose rates found anywhere on the top and bottom impact limiters respectively. The "2 m from vehicle, side" dose rate is the peak dose rate found anywhere on a vertical plane 2 m from the trailer's side edge. The rear dose rate refers to a point 2 m behind the back end of the trailer along the axis of the cask. The "back of cab" dose rate is that found on the back of the tractor cab along the central axis of the cask. The tables intentionally omit the dose rate 2 m in front of the trailer (when the tractor is not attached), since the 2-mR/h dose rate limit at the rear of the tractor cab is more restrictive.

Table 5.1-1 presents the dose rate results with two and three significant digits to be consistent with the results shown on the dose rate maps in Sections 5.4 and 5.5.1. The results are based on three-dimensional (3-D) Monte Carlo calculations. There is a statistical uncertainty of about 5% (one sigma) for the 2-m dose rates. Other calculational uncertainties due to physical modeling and cross sections are relatively small, as demonstrated by validation of the shielding analysis calculational methods.

THIS PAGE LEFT BLANK INTENTIONALLY

## 5.2 Source Specification

GA used the SAS2 (SAS2H) module of SCALE-4.1 (Ref. 5.2-1) to generate the neutron and gamma source terms for PWR fuels. The SAS2 module uses ORIGEN-S, to generate the necessary source term data for shielding and thermal evaluations of spent fuel shipping casks. Table 5.2-1 presents the basis for the source terms used in the shielding analysis for the GA-4 cask. The source specification for the shielding design assumes an axial distribution in the active fuel region; this was obtained from Ref. 5.2-2. This section presents the details of the source term generation, including the SAS2 models and the resulting neutron and gamma source terms for representative PWR spent fuel.

TABLE 5.2-1 BASIS FOR SOURCE SPECIFICATION	
Description	GA-4 (PWR)
Initial enrichment (wt % U-235)	3.00
Fuel burnup (MWd/MTU)	35,000
Cooling time (years)	10
Fuel loading (MTU per assembly)	0.469
Assembly type	W 15 x 15

### SAS2 Models

We generated the source term data by using the SAS2 control module in SCALE-4.1. The SAS2 control module (sometimes referred to as SAS2H) computes gamma and neutron source terms for fuel assemblies of a given reactor history and cooling time. Time-dependent cross sections for a given set of reactor characteristics are computed from two-dimensional simulations, with one dimensional transport neutronics models that account for resonance self-shielding. The functional modules of SCALE-4 called by SAS2 are BONAMI-S, NITAWL-S, XSDRNPM-S, COUPLE, ORIGEN-S, and XSDOSE.

The PWR model represents a standard Westinghouse 15 X 15 PWR fuel assembly with an axial burnup distribution (Ref. 5.2-2). Six separate SAS2 calculations were performed, one for each burnup level used to approximate the axial distribution, as shown in Fig. 5.2-1. For each case an initial enrichment of 3.0 wt % U-235 was used.

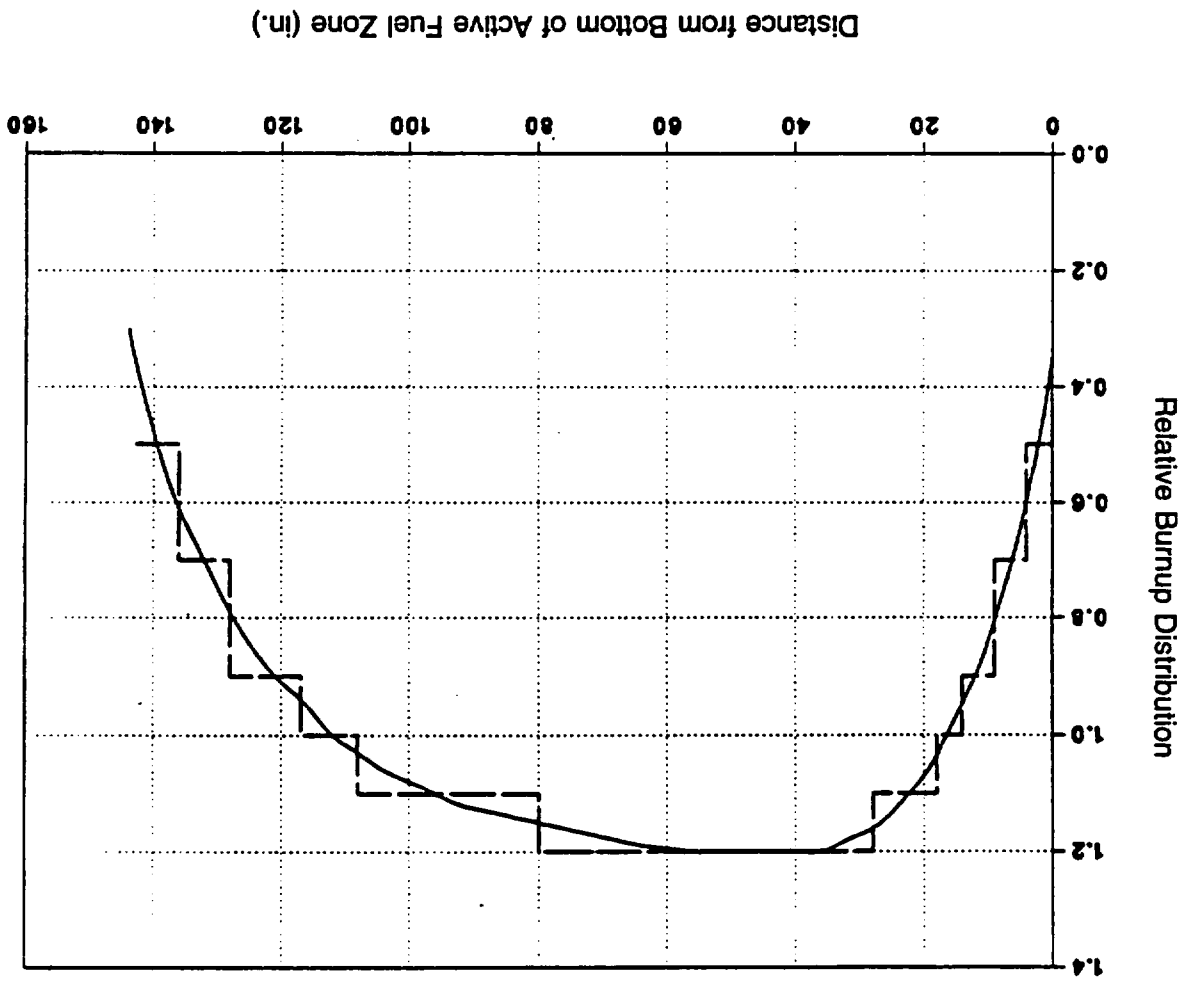


Fig. 5.2-1. Representative PWR axial burnup distribution

For a given burnup, this enrichment produces a conservative source as compared to higher initial enrichments. The fuel is burned for three cycles (313.5 days each), with 78.4 days cooling between the cycles and 10 years cooling after the last cycle. The SAS2 models include soluble boron to control excess reactivity. Table 5.2-2 lists the input parameters for the SAS2 models.

The radiation sources in a spent fuel assembly come from four basic regions: the active fuel (including such components as fuel, cladding, spacer grids, and instrument or guide tubes); the bottom tie plate and skirt; the plenum (including spring); and the top tie plate. The active fuel region includes both gamma and neutron sources while the other three non-fuel regions only include gamma sources. Only the Co-60 source, from activation of the Co-59 in the non-fueled regions, contributes to the dose rates outside the cask; it is therefore the only activation product considered in these regions.

### 5.2.1 Gamma Source

The gamma source for the fuel region includes primary gammas, X rays, conversion photons, ( $\alpha,n$ ) photons, prompt and fission-product gammas from spontaneous fission, and bremsstrahlung radiation. The non-fuel region source terms were obtained by using activation ratios related to the fuel region (given in Ref. 5.2-3, developed by Croff). Tables 5.2-3 and 5.2-4 provide the gamma source terms for the fuel and non-fuel regions, respectively. Only gamma groups 10-13 contribute significantly to gamma dose rates outside the cask, so only these gamma groups are treated in the shielding analyses.

**TABLE 5.2-2**  
**PWR FUEL ASSEMBLY AND EXPOSURE DATA FOR SAS2 MODULE IN SCALE**

Assembly type	W15x15
Initial heavy metal loading, MTU	0.469
Initial U-235 enrichment, weight percent	3.0
Number of fuel rods per assembly	204
Fuel temperature during operation, K	1000
Clad temperature during operation, K	605
Moderator temperature during operation, K	581
Number of cycles	3
Exposure time per cycle, days	313.5
Shutdown time between cycles, days	78.4
Cooling time after discharge, days	3650
Soluble boron-10 concentration, atoms/b-cm	
Cycle 1	4.388E-6
Cycle 2	4.169E-6
Cycle 3	4.037E-6
Moderator density, g/cm <sup>3</sup>	0.7113
Fuel rod	
Pellet diameter, in.	0.366
Gap, in.	0.0037
Rod o.d., in.	0.422
Fuel rod pitch, in.	0.563
Clad material	Zr-4
Active fuel length, in.	144
Burnup, GWd/MTU	
Relative power = 0.3	10.5
Relative power = 0.5	17.5
Relative power = 0.7	24.5
Relative power = 0.9	31.5
Relative power = 1.0	35.0
Relative power = 1.1	38.5
Relative power = 1.2	42.0
Light elements, kg per assembly	
O	62.6
Fe	4.6
Co	0.033
Ni	4.4
Zr	102
Nb	0.33
B	0.036

**TABLE 5.2-3  
PWR FUEL GAMMA SOURCE DATA  
(10-yr Cooling)**

		Gamma Source Strength (MeV/s per assembly)						
Group No.	Energy Range (MeV)	RP=0.5	RP=0.7	RP=0.9	RP=1.0	RP=1.1	RP=1.2	Total
1	0.0-0.02	4.509E+11	5.606E+11	9.292E+11	8.261E+11	2.619E+12	3.857E+12	9.243E+12
2	0.02-0.03	2.315E+11	2.871E+11	4.739E+11	4.202E+11	1.328E+12	1.950E+12	4.691E+12
3	0.03-0.045	4.514E+11	5.819E+11	9.965E+11	8.988E+11	2.886E+12	4.299E+12	1.011E+13
4	0.045-0.07	4.631E+11	5.821E+11	9.670E+11	8.587E+11	2.715E+12	3.985E+12	9.570E+12
5	0.07-0.1	4.468E+11	5.609E+11	9.399E+11	8.398E+11	2.673E+12	3.950E+12	9.411E+12
6	0.1-0.15	6.256E+11	8.463E+11	1.511E+12	1.386E+12	4.518E+12	6.815E+12	1.570E+13
7	0.15-0.3	1.002E+12	1.254E+12	2.088E+12	1.859E+12	5.895E+12	8.681E+12	2.078E+13
8	0.3-0.45	7.526E+11	9.360E+11	1.549E+12	1.376E+12	4.353E+12	6.397E+12	1.536E+13
9	0.45-0.70	4.190E+13	5.509E+13	9.595E+13	8.726E+13	2.825E+14	4.246E+14	9.873E+14
10	0.70-1.0	6.925E+12	9.902E+12	1.847E+13	1.727E+13	5.730E+13	8.787E+13	1.318E+14
11	1.0-1.5	3.038E+12	5.339E+12	1.140E+13	1.122E+13	3.889E+13	6.194E+13	1.977E+14
12	1.5-2.0	9.001E+10	1.557E+11	3.263E+11	3.175E+11	1.085E+12	1.703E+12	3.677E+12
13	2.0-2.5	4.106E+09	5.516E+09	9.776E+09	8.956E+09	2.919E+10	4.413E+10	1.017E+11
14	2.5-3.0	2.136E+08	3.277E+08	6.396E+08	6.094E+08	2.057E+09	3.206E+09	7.053E+09
15	3.0-4.0	3.378E+07	5.246E+07	1.042E+08	1.004E+08	3.431E+08	5.422E+08	1.176E+09
16	4.0-6.0	1.181E+05	5.130E+05	2.139E+06	2.758E+06	1.211E+07	2.378E+07	4.142E+07
17	6.0-8.0	1.898E+04	8.263E+04	3.448E+05	4.447E+05	1.953E+06	3.835E+06	6.679E+06
18	8.0-10.0	2.957E+03	1.289E+04	5.381E+04	6.941E+04	3.048E+05	5.986E+05	1.043E+06
<b>Total</b>		<b>5.638E+13</b>	<b>7.610E+13</b>	<b>1.356E+14</b>	<b>1.246E+14</b>	<b>4.068E+14</b>	<b>6.161E+14</b>	<b>1.416E+15</b>

NOTE: RP = relative power

TABLE 5.2-4 PWR NON-FUEL REGION GAMMA SOURCE TERMS (MeV/s)				
Group	Energy Range (MeV)	Bottom Tie Plate	Plenum	Top Tie Plate
9	1.0 to 1.33	3.450E+11	6.310E+11	9.450E+11

5.2.2 Neutron Source

The neutron source terms consist of the contributions from (α,n) and spontaneous fission. Table 5.2-5 lists the neutron source spectrum as provided by SAS2 for each fuel region.

TABLE 5.2-5 PWR FUEL NEUTRON SOURCE DATA (10-yr Cooling)								
		Neutron Source Strength (n/s per assembly)						
Group No.	Energy Range (MeV)	RP=0.5	RP=0.7	RP=0.9	RP=1.0	RP=1.1	RP=1.2	Total
1	6.43 - 20.0	9.732E+03	4.339E+04	1.822E+05	2.354E+05	1.035E+06	2.035E+06	3.541E+06
2	3.00 - 6.43	1.243E+05	5.116E+05	2.096E+06	2.691E+06	1.179E+07	2.310E+07	4.030E+07
3	1.85 - 3.00	1.598E+05	5.954E+05	2.357E+06	3.002E+06	1.308E+07	2.553E+07	4.472E+07
4	1.40 - 1.85	7.897E+04	3.208E+05	1.309E+06	1.680E+06	7.355E+06	1.441E+07	2.515E+07
5	0.90 - 1.40	9.894E+04	4.237E+05	1.759E+06	2.265E+06	9.941E+06	1.951E+07	3.400E+07
6	0.40 - 0.90	1.035E+05	4.563E+05	1.910E+06	2.466E+06	1.084E+07	2.129E+07	3.707E+07
7	0.10 - 0.40	2.020E+04	8.925E+04	3.739E+05	4.827E+05	2.121E+06	4.167E+06	7.255E+06
8	0.0 - 0.1	0.000E+00	0.000E+00	0.000E+00	0.000E+00	0.000E+00	0.000E+00	0.000E+00
<b>Total</b>		<b>5.954E+05</b>	<b>2.440E+06</b>	<b>9.986E+06</b>	<b>1.282E+07</b>	<b>5.615E+07</b>	<b>1.100E+08</b>	<b>1.920E+08</b>

### 5.3 Model Specification

#### 5.3.1 Description of Radial and Axial Shielding Configuration

Figures 5.3-1 and 5.3-2 show the axial and radial (at midplane) shielding configurations of the GA-4 cask. Table 5.3-1 lists the pertinent shielding thicknesses for the cask. Each layer of structure and shielding is shaped to fit closely around the fuel cavity to minimize weight. The flat and corner portions of the sidewall have different shielding thicknesses for weight optimization. The neutron shielding is tapered at the upper and lower sections of the sidewall (beyond the active fuel region) to save additional weight.

The cask weight is further optimized by placing the densest materials toward the inside of the cask. The first layer outside the cavity liner is the DU gamma shielding. The next layer is the Type XM-19 austenitic stainless steel containment boundary wall, followed by the solid borated modified polypropylene neutron shield material. Finally, the entire cask is encased in a smooth Type XM-19 stainless steel skin, to ensure ease of decontamination after contact with the fuel pool water.

The cask closure and bottom plate of the cask use XM-19 stainless steel with sufficient thickness for both neutron and gamma shielding. The impact limiter housing is taken into account for the impact limiter surface dose rates and 2-m dose rates. The shielding effect of the impact limiters on both ends of the cask is disregarded for conservatism.

The shielding configurations for normal transport and hypothetical accident conditions are different only with regard to the neutron shielding. The neutron shielding remains intact for normal conditions of transport, whereas complete loss of the neutron shield is assumed for hypothetical accident conditions. The outer stainless steel skin, which encases the neutron shielding, is also disregarded in the accident condition model.

For normal conditions, the dose rate points are placed at the surface of the package, at 2 m from the edge of the transporter, and at the rear of the tractor cab. The dose rate points for hypothetical accident conditions are located at 1 m from the damaged cask surface after loss of the neutron shield and the impact limiters as well. The locations of the dose rate points used for the normal and hypothetical accident conditions are shown in Section 5.4, along with the dose rate maps.

#### 5.3.2 Shield Regional Densities

Standard reference handbooks and material suppliers provided the material property data for shielding analysis. The ORNL SCALE-4.1 code package (Ref. 5.2-1) contains a standard material data library for common elements, compounds, and mixtures. Suppliers provided the data for other materials.

**FIGURE WITHHELD UNDER 10 CFR 2.390**

Fig. 5.3-1. Axial shielding configuration on flats

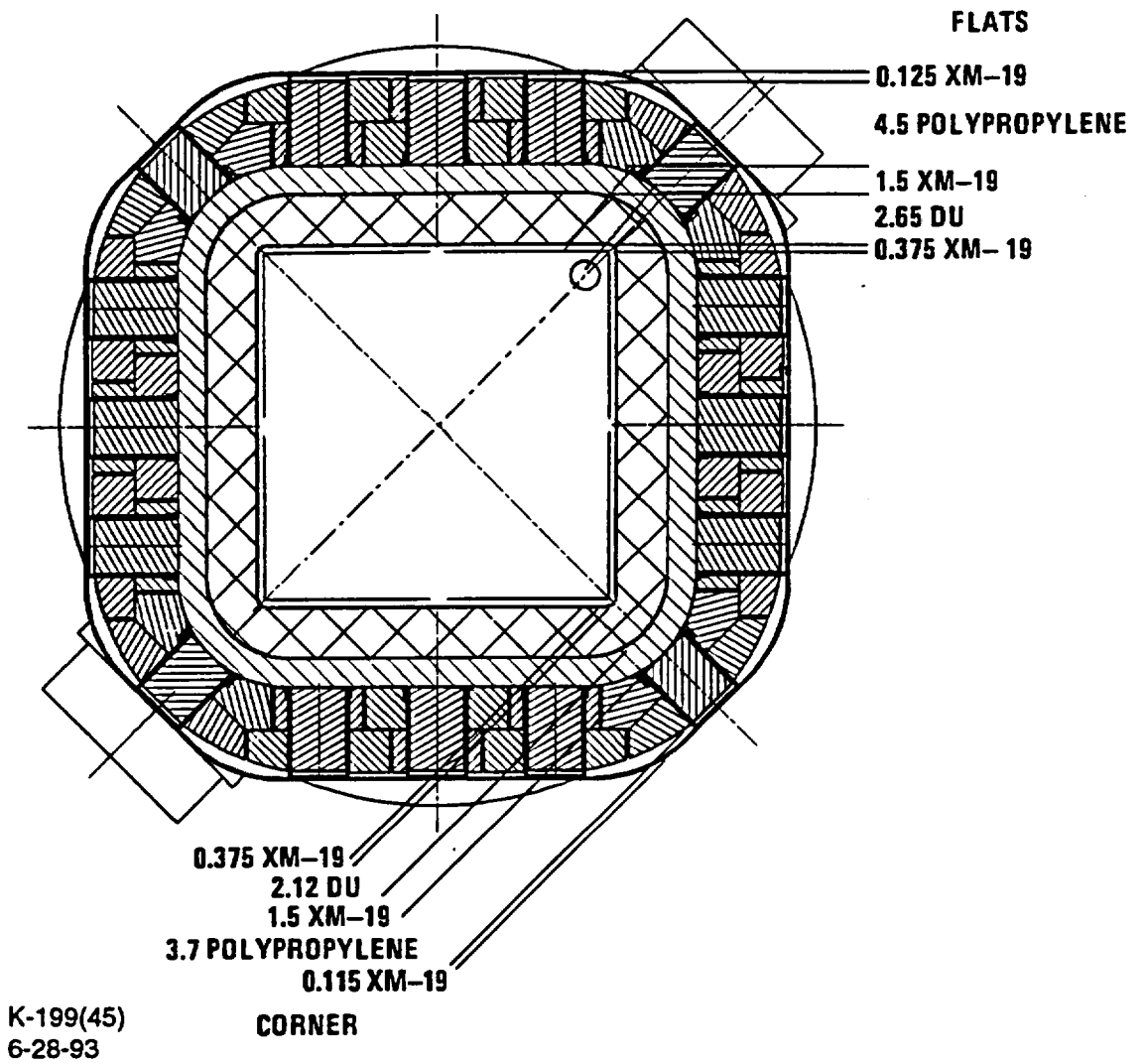


Fig. 5.3-2. Radial shielding configuration at midsection

<b>TABLE 5.3-1 SHIELDING THICKNESS OF GA-4 CASK</b>	
Component	Thickness <sup>(a)</sup> (in.)
<b>Upper section (top 12.5 in. of cask cavity)</b>	
Cavity liner (XM-19)	0.375/0.375
Gamma shield (DU)	2.65/2.12
Cask body wall (XM-19)	1.5/1.5
Neutron shield (polypropylene)	3.0/2.2
Outer skin (XM-19)	0.4/0.4
<b>Main body (middle 140.75 in. of cask cavity)</b>	
Cavity liner (XM-19)	0.375/0.375
Gamma shield (DU)	2.65/2.12
Cask body wall (XM-19)	1.5/1.5
Neutron shield (polypropylene)	4.5/3.7
Outer skin (XM-19)	0.115/0.115
<b>Lower section (bottom 14 in. of cask cavity)</b>	
Cavity liner (XM-19)	0.375/0.375
Gamma shield (DU)	2.65/2.12
Cask body wall (XM-19)	1.5/1.5
Neutron shield (polypropylene)	3.0/2.2
Outer skin (XM-19)	0.4/0.4
Cask closure (XM-19)	11.0
Bottom plate (XM-19)	9.5

<sup>(a)</sup>Flats/corner thicknesses for side wall

Table 5.3-2 provides a compilation of all the relevant materials used for the GA-4 cask. The fuel region of the PWR assemblies is modeled as a homogeneous  $\text{UO}_2$  mixture, with the uranium density being equal to the fuel loading (MTU) divided by the volume of the cask cavity fuel region. We conservatively neglected the shielding properties of all other materials in the fuel region. The gas plenum regions were treated as a homogeneous smear of the Zircaloy cladding over the entire plenum region. The top- and bottom-end-fitting regions were modeled as air, thus neglecting all shielding properties of the end-fitting materials. Table 5.3-3 provides the smeared PWR fuel assembly material data used in the analyses.

For shielding analysis we used the same shield regional densities for both normal conditions of transport and hypothetical accident conditions, except for the neutron shield material. The neutron shield region and its associated outer skin is assumed to become a void region after a hypothetical accident thermal event.

Some minor changes have been made to the design since the shielding analysis was performed. These changes (aluminum posts rather than copper, higher neutron shield hydrogen and gram density with slightly large gaps) have little effect on the dose rates; therefore, reanalysis or adjustment is not necessary.

TABLE 5.3-2  
MATERIAL PROPERTY DATA

Material	Density, g/cm <sup>3</sup> (lb/in. <sup>3</sup> )	Element	Wt %	Atom Density (atoms/barn-cm)
B <sub>4</sub> C	2.495 (0.0901)	B-10	14.32	2.14995E-2
		B-11	63.94	8.72818E-2
		C	21.73	2.71953E-2
SS304 or XM-19	7.92 (0.286)	Cr	19.0	1.74286E-2
		Mn	2.0	1.73633E-3
		Fe	69.5	5.93579E-2
		Ni	9.5	7.72074E-3
DU	19.00 (0.686)	U-235	0.20	9.6134E-5
		U-238	99.8	4.7971E-2
Polypropylene-1% boron	0.92 <sup>(a)</sup> (0.0332)	H <sup>(a)</sup>	12.56 <sup>(a)</sup>	6.9000E-2 <sup>(a)</sup>
		B-10	0.278	1.5376E-4
		B-11	1.223	6.1504E-4
		C	85.94	3.9625E-2
Air dry, 0°C, 1 atm	0.001293 (0.0000467)	N	75.53	4.1988E-5
		O	23.18	1.1281E-5
		Ar	0.0129	2.5135E-7
Ground soil U.S. average (dry)	1.5 (0.05419)	O	50.2	2.8332E-2
		Si	26.5	8.5202E-3
		Al	6.7	2.2423E-3
		Fe	5.5	8.8930E-4
		Mn	0.07	1.1506E-5
		Ti	0.45	8.4833E-5
		Ca	5.0	1.1265E-3
		Mg	1.3	4.8299E-4
		K	1.4	3.2334E-4
		Na	0.6	2.3567E-4

<sup>(a)</sup>Density and composition of polyethylene shown and used in shielding analysis for conservatism. The values for polypropylene are: Density 0.942 g/cm<sup>3</sup>; Hydrogen content: 13.49 wt% or 7.59 x 10<sup>-2</sup> atoms/barn-cm.

**TABLE 5.3-3  
PWR FUEL ASSEMBLY MATERIAL DATA**

Material <sup>(a)</sup>	Density, g/cm <sup>3</sup> (lb/in. <sup>3</sup> )	Element	Wt %	Atom Density (atoms/barn-cm)
Top nozzle, height = 6.3 in.	0.0	--	--	--
Gas plenum, height = 9.449 in.	0.7044 (0.0254)	Zr	100.0	4.6510E-3
Active fuel, pitch = 0.563 in. height = 144 in. 0.469 MTU	3.169 (0.114)	U-235 U-238 0	2.6 85.5 11.9	2.1217E-4 6.8600E-3 1.4143E-2
Bottom nozzle, height = 3.75 in.	0.0	--	--	--

<sup>(a)</sup>Sequentially from the top to the bottom of a fuel assembly, with an 8.434-in. by 8.434-in. cross section.

THIS PAGE LEFT BLANK INTENTIONALLY

## 5.4 Shielding Evaluation

Shielding evaluation, which considered both normal and hypothetical accident conditions, consisted of neutron and gamma shielding analysis to demonstrate shielding adequacy and compliance with 10 CFR Part 71. This section presents the details of the shielding evaluations, including assumptions, cross-section data, flux-to-dose conversion factors, and computer codes used.

### 5.4.1 Assumptions

We made the following assumptions in the shielding analysis:

1. The radiation sources are uniformly distributed in fourteen separate axial homogenized regions inside the fuel cavity liner. The analysis models the top hardware, gas plenum, eleven active fuel regions, and bottom hardware.
2. No credit is taken for the shielding properties of the end nozzles of PWR fuel assemblies.
3. The model includes shield materials at nominal thickness.
4. A 43-ft-long by 8-ft-wide semitrailer is used, with 5.5 ft between the front of the semitrailer and the rear of the tractor's cab.
5. The center of the cask is centered on the trailer.
6. The cask is mounted on the trailer with the corner facing downwards.
7. The impact limiters on the top and bottom ends of the cask are treated as void regions, except for the 0.25-in. XM-11 or XM-19 impact limiter housing for the impact limiter surface and 2-m dose rates.
8. The fuel assemblies are assumed to be at the ends of the cask cavity in the dose rate calculations for both the top and the bottom of the cask.

### 5.4.2 Cross-section Data

The computer codes used for shielding analysis include the PATH point-kernel integration code (Ref 5.4-1), ONEDANT and TWODANT transport codes (Refs. 5.4-2 and 5.4-3), and MCNP Monte Carlo Code (Ref. 5.4-4). The cross-section data required for these codes are described below.

The PATH code is a gamma shielding program, based on the common point-kernel integration attenuation coefficients for gamma shielding analysis. No additional cross-section data need be supplied.

For the transport calculations with ONEDANT and TWODANT, the standard CASK-81 cross-section set (Ref. 5.4.5) for a 40-group structure (22 neutron groups and 18 gamma groups) was selected for calculations of neutron dose rates and secondary gamma contributions. The primary gamma contributions were treated separately with either PATH or MCNP.

MCNP is a complete shielding code with built-in cross-section data for neutrons and gammas. The code eliminates the need for external cross-section generation, as required for the transport codes, since MCNP uses a pointwise energy grid for the cross-section data.

#### 5.4.3 Dose Rate Conversion Factors

A standard set of the flux-to-dose conversion factors is provided in ANSI/ANS 6.1.1-1977 (Ref. 5.4-6) for both neutrons and gammas as a function of energy. This set was selected for converting the calculated neutron gamma fluxes from the transport and Monte Carlo codes to the respective dose rates.

Table 5.4-1 gives the conversion factors for the transport calculations with ONEDANT and TWODANT by energy group, corresponding to the 40-group structure for the cask cross-section data. The MCNP Monte Carlo calculations use pointwise energy conversion factors as provided in Table 5.4-2.

#### 5.4.4 Computer Code Selection

Shielding analysis used a variety of validated computer codes, including the one-dimensional (1-D) ONEDANT (Ref. 5.4-2) and 2-D TWODANT (Ref. 5.4-3) transport codes, the 3-D PATH point-kernel code (Ref. 5.4-1), and the 3-D Monte Carlo MCNP code (Ref. 5.4-4). ONEDANT and TWODANT have been combined by Los Alamos National Laboratory (LANL) into a single program commonly know as TWODANT with the ONEDANT option. These codes have been benchmarked and validated in accordance with Quality Assurance Program Requirements for Nuclear Facilities, ASME NQA-1-1989 Edition, Supplementary Requirements for Computer Program Testing Supplement 11S-2.

TABLE 5.4-1  
MULTIGROUP FLUX-TO-DOSE CONVERSION FACTORS

Neutron Group	Upper Energy (eV)	Flux-to-Dose Conversion [(mR/h)/(n/cm <sup>2</sup> -s)]	Gamma Group	Upper Energy (eV)	Flux-to-Dose Conversion [(mR/h)/(γ/cm <sup>2</sup> -s)]
1	1.492E+7	1.95E-1	23	1.00E+7	9.79E-3
2	1.220E+7	1.64E-1	24	8.00E+6	8.28E-3
3	1.000E+7	1.47E-1	25	6.50E+6	6.38E-3
4	8.180E+6	1.47E-1	26	5.00E+6	5.41E-3
5	6.360E+6	1.53E-1	27	4.00E+6	4.62E-3
6	4.960E+6	1.63E-1	28	3.00E+6	4.00E-3
7	4.060E+6	1.51E-1	29	2.50E+6	3.45E-3
8	3.010E+6	1.40E-1	30	2.00E+6	3.00E-3
9	2.460E+6	1.28E-1	31	1.66E+6	2.60E-3
10	2.350E+6	1.26E-1	32	1.33E+6	2.10E-3
11	1.183E+6	1.29E-1	33	1.00E+6	1.80E-3
12	1.110E+6	1.20E-1	34	8.00E+5	1.52E-3
13	5.500E+5	6.38E-2	35	6.00E+5	1.17E-3
14	1.110E+5	1.39E-2	36	4.00E+5	8.78E-4
15	3.350E+3	3.66E-3	37	3.00E+5	6.31E-4
16	5.830E+2	3.94E-3	38	2.00E+5	3.79E-4
17	1.010E+2	4.26E-3	39	1.00E+5	2.60E-4
18	2.900E+1	4.46E-3	40	5.00E+4	5.84E-4
19	1.010E+1	4.57E-3		1.00E+4	
20	3.060E+0	4.55E-3			
21	1.120E+0	4.40E-3			
22	4.140E-1	3.67E-3			
	1.000E-2				

TABLE 5.4-2  
POINTWISE ENERGY FLUX-TO-DOSE  
CONVERSION FACTORS

Neutron Energy (MeV)	Flux-to-Dose Conversion [(mR/h)/(n/cm <sup>2</sup> -s)]	Gamma Energy (MeV)	Flux-to-Dose Conversion [(mR/h)/(γ/cm <sup>2</sup> -s)]
2.5E-8	3.67E-3	0.01	3.96E-3
		0.03	5.82E-4
1.0E-8	3.67E-3	0.05	2.90E-4
		0.07	2.58E-4
1.0E-6	4.46E-3	0.15	3.79E-4
		0.2	5.01E-4
1.0E-5	4.54E-3	0.25	6.31E-4
		0.3	7.59E-4
1.0E-4	4.18E-3	0.35	8.78E-4
		0.4	9.85E-4
1.0E-3	3.76E-3	0.45	1.08E-3
		0.5	1.17E-3
1.0E-2	3.56E-3	0.55	1.27E-3
		0.6	1.36E-3
0.1	2.17E-2	0.65	1.44E-3
		0.7	1.52E-3
0.5	9.26E-2	0.8	1.68E-3
		1.0	1.98E-3
1.0	1.32E-1	1.4	2.51E-3
		1.8	2.99E-3
2.5	1.25E-1	2.2	3.42E-3
		2.6	3.82E-3
5.0	1.56E-1	2.8	4.01E-3
		3.25	4.41E-3
7.0	1.47E-1	3.75	4.83E-3
		4.25	5.23E-3
10.0	1.47E-1	4.75	5.90E-3
		5.0	5.80E-3
14.0	2.08E-1	5.25	6.01E-3
		5.75	6.38E-3
20.0	2.27E-1	6.25	6.74E-3
		6.75	7.11E-3
		7.5	7.66E-3
		9.0	8.77E-3
		11.0	1.02E-2
		13.0	1.18E-2
		15.0	1.33E-2

TABLE 5.4-3 EQUIVALENT SHIELDING CODES		
Calculation	Code Used	Equivalent Code
1-D Transport	ONEDANT	ANISN
2-D Transport	TWODANT	DOT
3-D Point-kernel	PATH	QAD
3-D Monte Carlo	MCNP	MORSE

#### 5.4.5 Shielding Calculations

We performed shielding calculations to obtain the total dose rate from all contributing source components:

1. Primary neutron source (and subcritical multiplication) from spent fuel.
2. Secondary neutron source from additional fission in fuel and DU.
3. Primary gamma source from fuel and associated hardware.
4. Secondary gamma source from neutron interactions with the fuel assemblies and cask materials.
5. Scattering source from air and ground.
6. Gaps in neutron and gamma shields.

The analytical procedures for determination of the various dose rate contributions are described below.

**5.4.5.1 Gamma Analysis.** We used two codes, MCNP and PATH, to treat the primary gamma source in the active fuel region. The primary gamma source in the associated hardware was analyzed with PATH only.

The MCNP code was first used to calculate the gamma dose rates at the cask midplane. MCNP explicitly models the unconventional cask geometry with its variable shield thicknesses. In the MCNP model, the DU shield and the neutron shield in the cask body were subdivided into several subregions to obtain the radial dependence of the dose rates on the material thicknesses. Dose rates were calculated over several azimuthal regions (1) to determine the azimuthal variation of the dose rates on the cask surface and at 2 m from the edge of the transporter and (2) to ensure adequate shielding.

The PATH point-kernel gamma shielding code was used to supplement the MCNP code. PATH calculates the exponential attenuation of gamma rays and applies single-medium buildup factors to produce the final results. PATH employs certain approximations as necessitated by the point-kernel integration method and therefore requires corrections to the results. The PATH results were normalized to the MCNP results for a comparable calculation in order to obtain an overall correction factor.

The PATH code enabled us to specify as many dose rate points as desired around the cask. The explicit MCNP 3-D physical model was used to normalize the PATH calculations. The dose rate points were specified at various locations on the package surface, at 2 m from the edge of the transporter, and at the back of the cab. The results at these points encompassed the radial, axial, and azimuthal variations of the dose rates external to the cask.

Corrections to the PATH results were made at the side of the cask to account for the buildup factors through the composite shields, the normalization factor used to correct the PATH results was based on the MCNP results. No corrections were required for the PATH results at the top and bottom of the cask, since stainless steel is the only shielding material used.

The PATH results included the contribution from the primary gamma source in the active fuel and hardware regions. At the midplane of the cask, the dose rate contribution is predominantly from the active fuel. The hardware sources contribute appreciably to the dose rate points at the top and bottom ends of the cask.

**5.4.5.2 Neutron Analysis.** MCNP was also used to calculate the neutron dose rates from the primary neutron source in spent fuel, together with (1) the secondary neutron sources from additional fission reactions in the fuel and DU shield, and (2) the secondary gamma dose rates from (n, $\gamma$ ) reactions.

The MCNP model for the neutron analysis at the cask midplane was very similar to that for the gamma analysis. The neutron model used a different regional subdivision for the DU and neutron shield regions because of differences in neutron and gamma attenuation characteristics. The radial model for MCNP represented the exact cask geometry to obtain the azimuthal variation of the dose rates at the cask surface and at 2 m from the edge of the transporter.

An axial MCNP model was also developed to accurately describe the lower end of the cask bottom. The model was used to determine the neutron dose rates on the cask surface under the bottom impact limiters, on the bottom impact limiter surface, and 2 m behind the back of the trailer. The neutron source peaks toward the lower end of the fuel assembly. Also, the cask closure is thicker than the cask bottom plate. This will lead to lower neutron dose rates on the top end of the cask. A simple cylindrical MCNP model of the cask was used to determine the dose rate ratio between the top and bottom end surfaces of the cask. Neutron dose rates on the top end surface of the cask, on the end of the top impact limiter, and at the tractor cab are found by multiplying this ratio times the dose rates at equivalent locations on the bottom end of the cask. Dose rates on the sides of the top impact limiter and on the sides of the top end of the cask are conservatively set equal to the corresponding dose rates on the cask bottom end.

**5.4.5.3 Gap Analysis.** The depleted uranium shield is divided (with lap joints) into five pieces. The cavity in the cask body for the DU shield is 0.25 inches longer than the DU itself. To minimize the gaps between the pieces, the sections are fastened together with DU pins. Due to fabrication tolerances, small gaps are expected at the lap joints. We used an infinite length TWODANT model to analyze the effects of one of these gaps. In this model, the gap appears as a line gap of infinite length. The width of the model is equal to the width of one DU segment. This model yields a conservatively large estimate of the increase in the dose rate due to the gaps. The largest gamma dose rate increase for any point on the cask surface is 12%. The largest increase on the 2-m dose rate plane is 1.7%. We increased the peak gamma dose rate on the cask surface by 12% (thus assuming that the peak dose rate location occurs directly over the gap). The peak gamma dose rate on the 2-m dose rate plane is increased by 1.7%. Other locations on the 2-m plane are increased by 1.0%. For the accident case, the peak 1-m gamma dose rate was increased by 1.7%. If under accident conditions the pins break and the DU rings slide apart, sufficient margin in the accident dose rates exists to meet the 1 R/hr limit at 1-m from the damaged package.

The neutron shield consists of overlapping modified polypropylene blocks, which are anchored to the cask body by aluminum tubes. Gaps of 0.125 in. must exist between the blocks to accommodate thermal expansion. Smaller gaps (0.01 in.) that go completely through the neutron shield exist around the aluminum tubes. The effects of these gaps were analyzed with an infinite plane MCNP model similar to the TWODANT model described above. This model also yields a conservatively large estimate of the increase in the neutron dose rate. The increase at the 2-m dose rate plane (as well as over the cask surface) was found to be 24.4%. We therefore increased all neutron dose rates by 24.4% to account for neutron shield gaps.

**5.4.5.4 Ground Scattering Analysis.** Ground scattering is a significant component of the total dose rate external to the cask, especially at 2 m from the transporter. The ground scattering factor is normally greater for neutrons than for gammas because of a higher albedo for neutrons.

Separate ground scattering analyses were performed with MCNP for neutrons and gammas. Since the ground scattering factor is insensitive to the cask geometry, we used an equivalent cylindrical cask model without loss of its generality or applicability.

For each analysis, three MCNP cases were run, (1) without the ground present, (2) with the ground parallel to the cask axis at 3.5 ft below the cask surface to simulate the cask positioned on the semitrailer, and (3) with the ground against the cask sidewall to simulate the cask lying on the ground. The MCNP results with the two ground locations were compared with the corresponding results in the absence of the ground to quantify the increases in the dose rate caused by ground scattering.

The results at the 2-m location were conservatively applied to all dose rate points. The factors were 1.4 for neutrons and 1.1 for gammas.

#### 5.4.6 Shielding Results For Normal Transport Conditions

5.4.6.1 Azimuthal Dose Rate Profile. MCNP results give the azimuthal dose rate profile at the midplane of each cask for normal conditions. Figure 5.4-1 shows the azimuthal dose rate variations at the surfaces of the GA-4 cask for 1/8 segments of the cross section. The statistical uncertainty associated with the MCNP results is between 2 percent and 5 percent (one sigma).

The results in Fig. 5.4-1 show that the dose rates on the surface of the personnel barrier are considerably below the regulatory limit of 200 mR/h and the 2-m limit controls the shielding requirements for the cask.

5.4.6.2 Dose Rate Maps. Figure 5.4-2 depicts the dose rate maps for normal conditions of transport as generated with the PATH code, including the effects of gaps, peaking, and ground scatter, with appropriate normalization to the MCNP results. The dose rate at each point includes both neutron and gamma contributions. Table 5.4-4 shows the neutron and gamma dose rate components. The calculated total dose rates are all below the 10 CFR Part 71 limits.

#### 5.4.7 Shielding Results for Hypothetical Accident Conditions

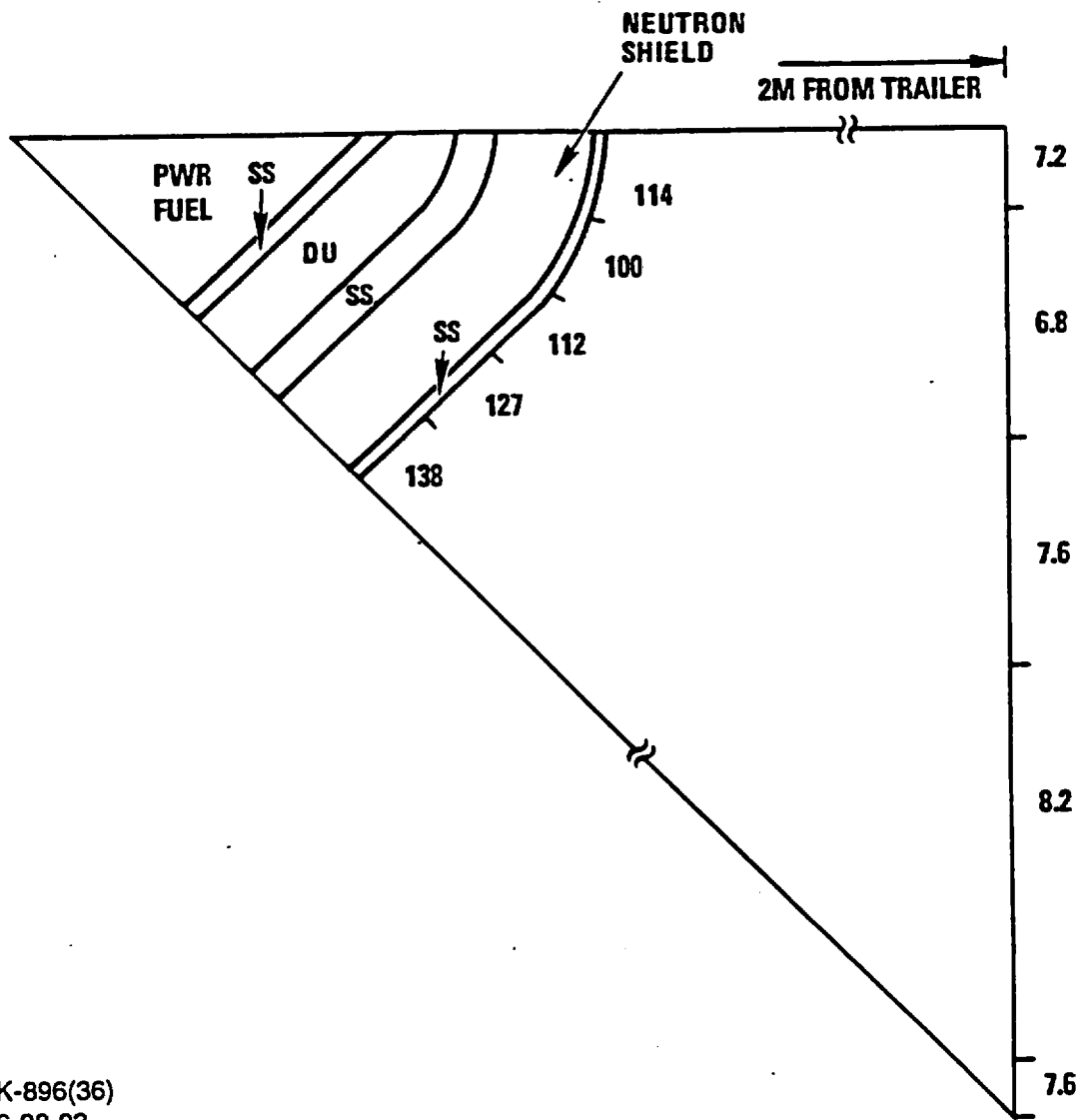
The dose rate map for hypothetical accident conditions was obtained in the same manner as for normal transport conditions. Figure 5.4-3 shows the resulting total dose rates. Table 5.4-5 gives the neutron and gamma dose rate breakdown. Note that the impact limiters are not shown in Fig. 5.4-3. Although they are designed to remain attached during a severe accident, the accident case shielding analysis conservatively assumes their absence.

#### 5.4.8 Correlation of Accident Dose Rate to Measured Dose Rate

Since the hypothetical accident conditions cannot be tested before each fuel shipment, GA proposes the following dose rate condition for each shipment.

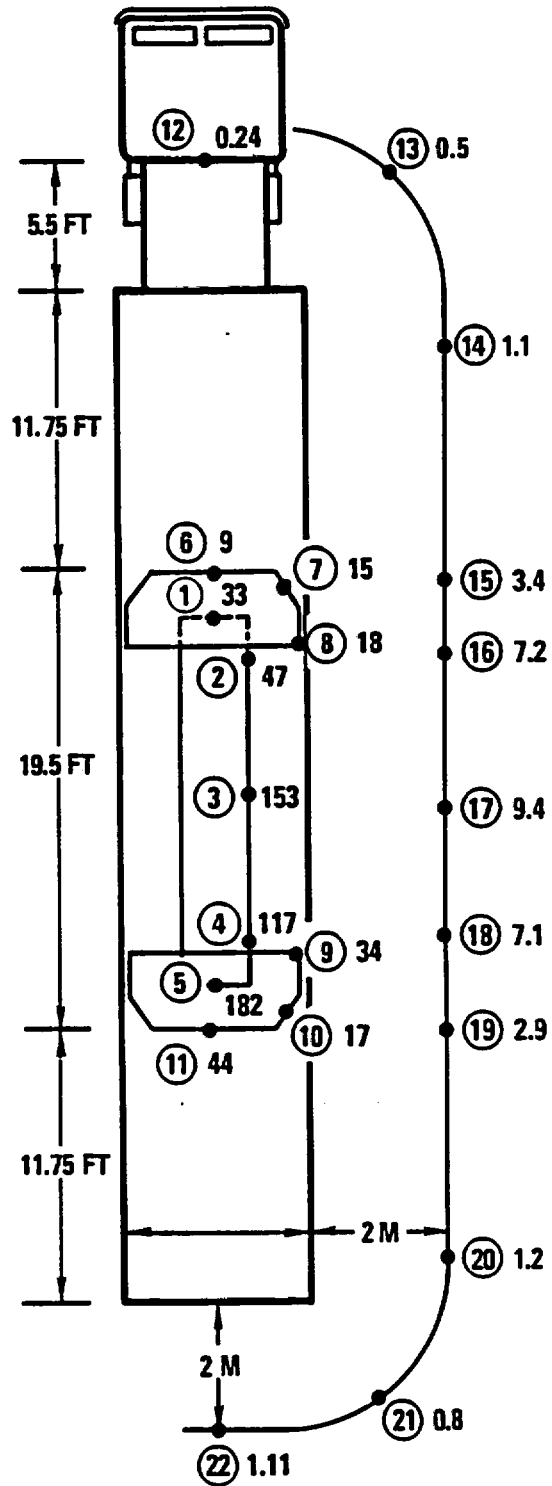
The cask contents shall be so limited that 4.8 times the peak neutron dose rate at any point on the surface of the cask at its midlength plus 0.9 times the gamma dose rate at that location does not exceed 1000 mR/h.

This formula was derived by determining two ratios: the ratio of the calculated peak 1-m accident neutron dose rate to the calculated peak cask surface normal transport neutron dose rate and the ratio of the respective gamma dose rates at the same point. Table 5.4-6 is a compilation of the data used to calculate the ratios. The table also includes references to the tables in this report from which the data were obtained. The maximum neutron dose rate occurs near the midplane of the cask. The maximum ratios for the neutron dose rate (4.8) and gamma dose rate (0.9) were used for conservatism to apply to all configurations. The neutron ratio is from the 50 GWd/MTU burnup and 20 year cooling and the gamma ratio is from the 35 GWd/MTU burnup and 10 year cooling.



K-896(36)  
6-28-93

Fig. 5.4-1. Azimuthal midplane dose rate profile for GA-4 cask (mR/h)



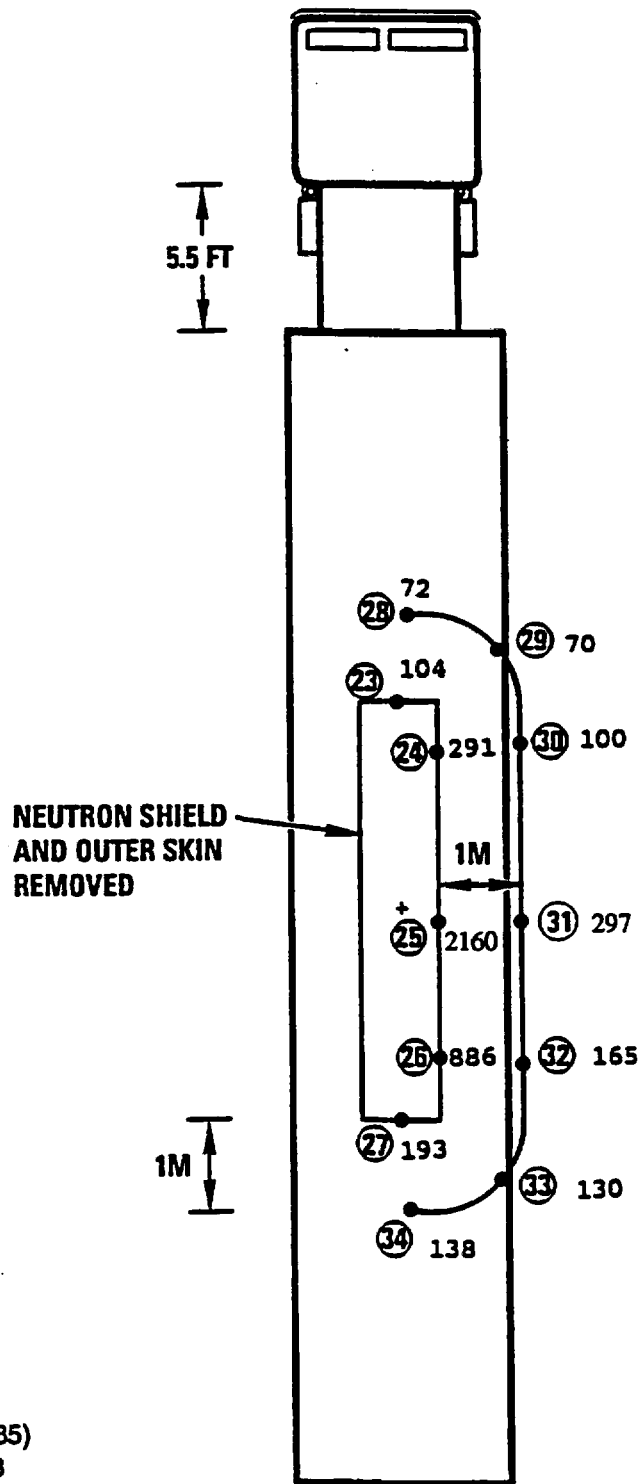
K-213(2)  
8-27-93

Fig. 5.4-2. Total dose rate (mR/h) around GA-4 cask for normal conditions

**TABLE 5.4-4**  
**GA-4 CASK DOSE RATES (mR/h) FOR NORMAL CONDITIONS**

Point	Location	Gammas	Neutrons	Total	10 CFR Part 71 Limit
1	Surface of cask	26	7	33	None
2		33	14	47	200
3		112	41	153	200
4		86	31	117	200
5		133	49	182	None
6	Surface of IL <sup>(a)</sup>	8	1	9	200
7		13	2	15	200
8		12	6	18	200
9		28	6	34	200
10		15	2	17	200
11		38	6	44	200
12	Back of cab	0.20	0.04	0.24	2
13	2 m from trailer	0.3	0.2	0.5	10
14		0.8	0.3	1.1	10
15		2.4	1.0	3.4	10
16		5.7	1.5	7.2	10
17		7.6	1.8	9.4	10
18		5.5	1.6	7.1	10
19		1.9	1.0	2.9	10
20		0.9	0.3	1.2	10
21		0.6	0.2	0.8	10
22		0.96	0.15	1.11	10

<sup>(a)</sup>IL = impact limiter.



K-896(35)  
8-27-93

Fig. 5.4-3. Total dose rate (mR/h) around GA-4 cask for hypothetical accident conditions

**TABLE 5.4-5  
GA-4 CASK DOSE RATES (mR/h)  
FOR HYPOTHETICAL ACCIDENT CONDITIONS**

Point	Location	Gammas	Neutrons	Total	10 CFR Part 71 Limit
23	Surface of cask	39	65	104	None
24		187	104	291	None
25		580	1580	2160	None
26		349	537	886	None
27		128	65	193	None
28	1 m from cask <sup>(a)</sup>	12	60	72	1000
29		10	60	70	1000
30		40	60	100	1000
31		103	194	297	1000
32		60	105	165	1000
33		25	105	130	1000
34		33	105	138	1000

<sup>(a)</sup>Relative to damaged cask with neutron shield and skin removed.

**TABLE 5.4-6  
CORRELATION DATA FOR ACCIDENT CONDITIONS**

Burnup/Age GWd/MTU/Yrs	Accident Condition			Peak Cask Surface Normal Transport			RATIO (1-meter/surface)	
	1-meter Dose Rate mr/h		Reference	Cask Surface Dose Rate mr/h		Reference	Neutron	Gamma
	Neutron	Gamma		Neutron	Gamma			
35/10	194	103	Table 5.1-1	41	112	Table 5.5-17	4.7	0.9
45/15	398	75	Table 5.1-1	84	86	Table 5.5-17	4.7	0.9
55/20	571	56	Table 5.1-1	120	67	Table 5.5-17	4.8	0.8
60/25	608	38	Table 5.1-1	128	49	Table 5.5-17	4.8	0.8
35/05	115	131	Table 5.1-1	26	237	Table 5.5-18	4.4	0.6
45/07	269	114	Table 5.1-1	61	210	Table 5.5-18	4.4	0.5
55/10	414	88	Table 5.1-1	94	166	Table 5.5-18	4.4	0.5
60/11	514	86	Table 5.1-1	116	164	Table 5.5-18	4.4	0.5

## 5.5 Appendices

### 5.5.1 Additional Burnup and Age Shielding Analysis

GA has performed analyses to verify the GA-4 cask's ability to ship higher-burnup and/or shorter-cooled fuel at reduced capacity without exceeding the 10 CFR Part 71 dose rate limits. The authorized contents given in Section 1.2.3 include the higher-burnup and shorter-cooled fuel. GA has performed shielding analyses that determine the minimum cooling time required for fuel with burnups of 35, 45, 55, and 60 GWd/MTU. These analyses were performed for the fully loaded cask (4 elements) and for a down-loaded configuration consisting of two fuel assemblies and two stainless steel shield inserts.

Figures 5.5-1 and 5.5-2 show the minimum cooling time required as a function of burnup for the four-element-or-fewer configuration (Section 1.2.3, fuel loading I or II) and for the two-element configuration (Section 1.2.3, fuel loading III). The shielding analysis considered both normal and hypothetical accident conditions to comply with 10 CFR Part 71. The analysis used GA-4 cask models that are identical to those presented in Section 5.3. For the fully loaded cases, the models of the spent fuel and the FSS were identical with those presented in Section 5.3, with the exception that the source terms were changed to correspond to the particular burnup and age of interest. The model of the FSS, fuel, and shield inserts for the two-element case is shown in Fig. 5.5-3. The shield inserts are square, one-inch-thick stainless steel tubes which fit into the two fuel cavities not occupied by the spent fuel assemblies. In order to meet the dose rate limits as specified in 10 CFR Part 71, the shield inserts must be placed in the fuel cavities on the diagonal with the trunnions.

The results of the analysis, shown earlier in Table 5.1-1, demonstrate that radiation levels outside the package, including its personnel barrier, are all within the regulatory dose rate limits for transportation.

**5.5.1.1 Source Specification.** The neutron and gamma source terms for the different burnup and age combinations were generated in the same manner as the 35 GWd/MTU and 10-year-cooled fuel presented in Section 5.2. Six separate SAS2 calculations were performed, one for each power level as shown in Figure 5.2-1, for each burnup of interest. The output for each SAS2 run contained the neutron and gamma source terms as a function of cooling time. Table 5.5-1 gives the basis for the source terms and input parameters for SAS2 as a function of burnup.

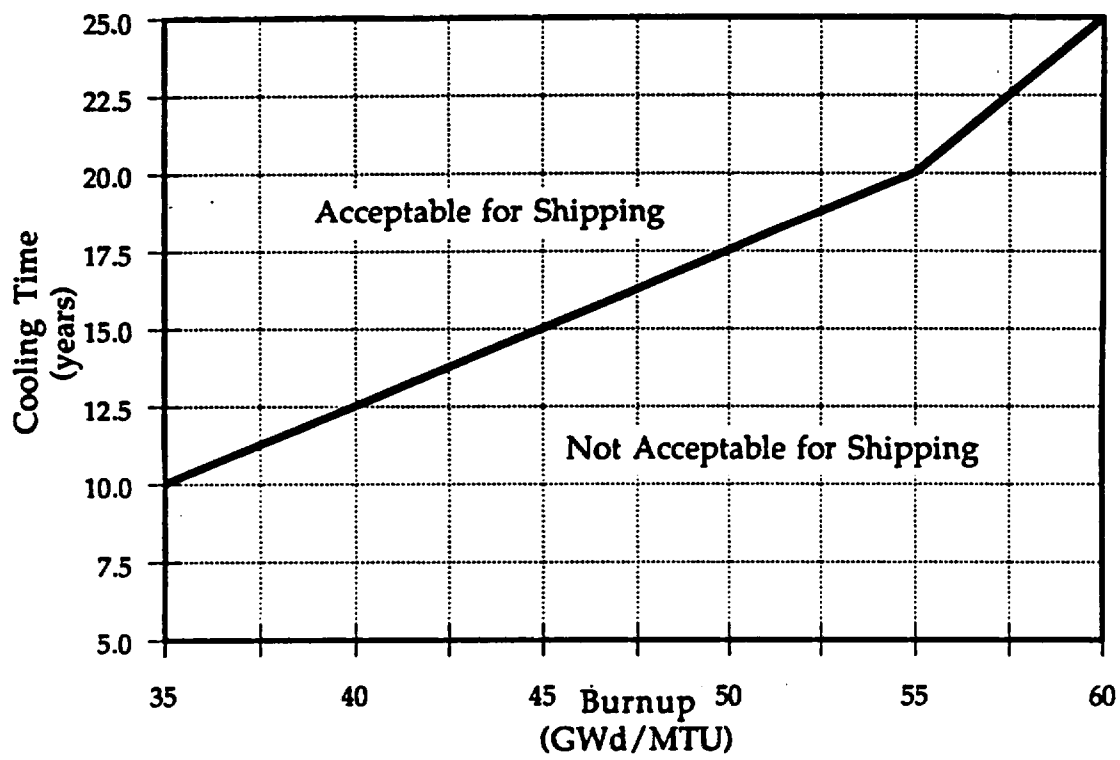


Fig. 5.5-1. Minimum cooling time for four or fewer fuel assemblies

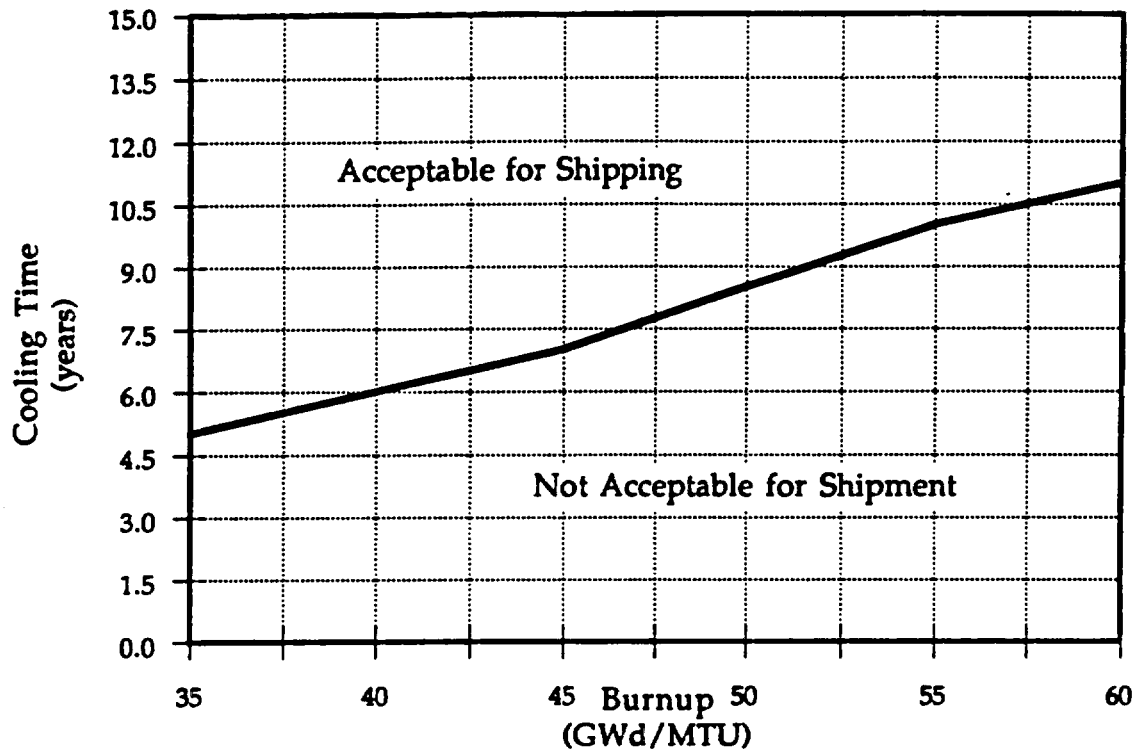
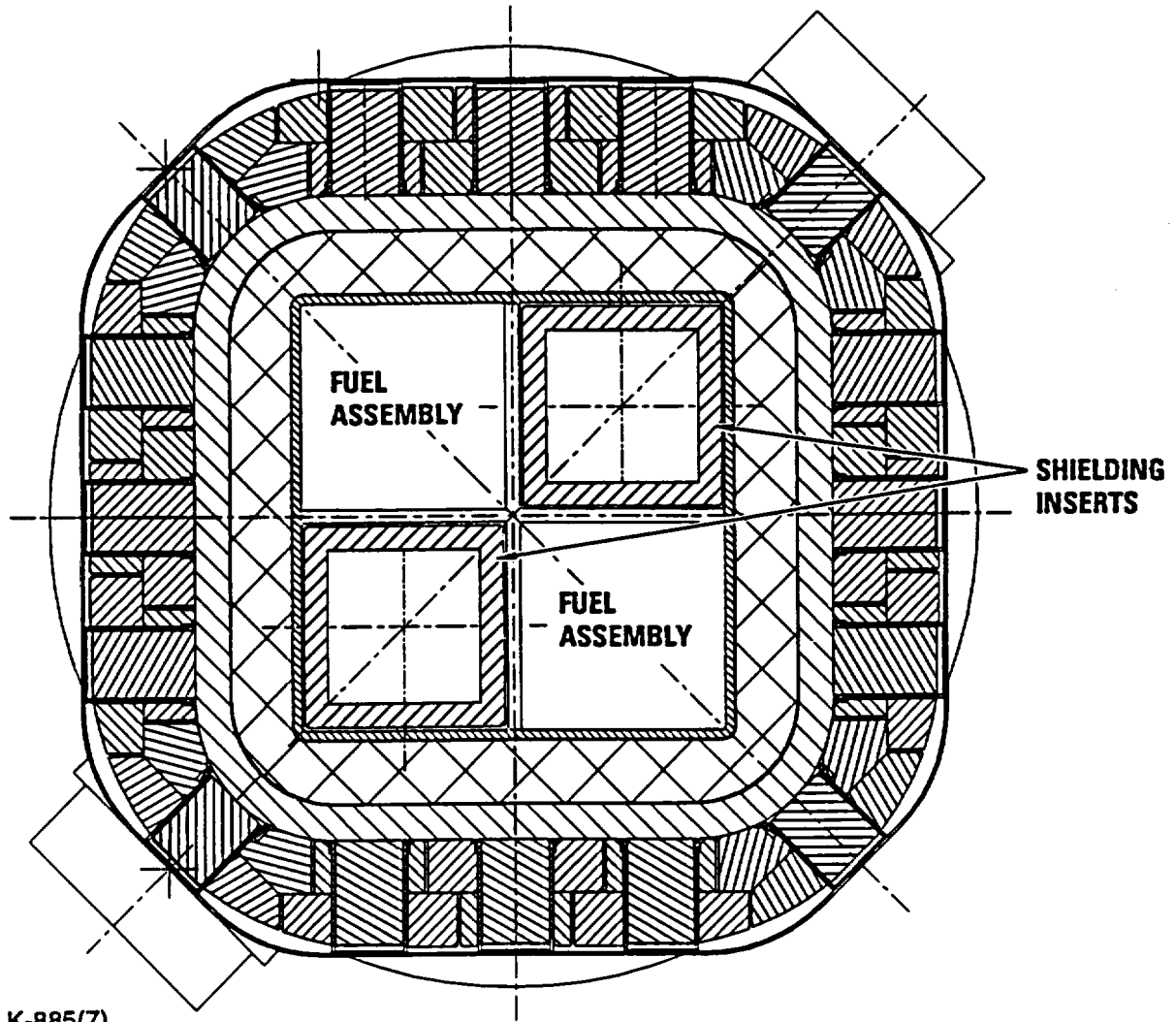


Fig. 5.5-2. Minimum cooling time for two fuel assemblies with two shield inserts



K-885(7)  
10-13-93

Fig. 5.5-3. Down-loaded GA-4 cask configuration with shield inserts

TABLE 5.5-1  
PWR FUEL ASSEMBLY AND EXPOSURE DATA FOR SAS2

Average burnup, GWd/MTU	35	45	55	60
Assembly type	W 15x15	W 15x15	W 15x15	W 15x15
Initial heavy metal loading, MTU	0.469	0.469	0.469	0.469
Initial U-235 enrichment, wt %	3.0	3.2	3.7	3.9
Number of fuel rods per assembly	204	204	204	204
Fuel temperature, K	1000	1000	1000	1000
Clad temperature, K	605	605	605	605
Moderator temperature, K	581	581	581	581
Moderator density, g/cm <sup>3</sup>	0.7113	0.7115.5 3	0.7113	0.7113
Number of cycles	3	3	3	3
Exposure time per cycle, days	313.5	444.4	444.4	444.4
Shutdown time per cycle, days	78.4	106	106	106
Soluble boron-10 concentration, atoms/b-cm:				
Cycle 1	4.388E -6	5.00E -6	8.00E -6	9.30E -6
Cycle 2	4.169E -6	4.75E -6	6.00E -6	7.00E -6
Cycle 3	4.037E -6	4.60E -6	4.40E -6	5.10E -6
Fuel rod				
Pellet diameter, in.	0.366	0.366	0.366	0.366
Gap, in.	0.0037	0.0037	0.0037	0.0037
Rod o.d., in	0.422	0.422	0.422	0.422
Fuel rod pitch, in.	0.563	0.563	0.563	0.563
Clad material	Zr	Zr	Zr	Zr
Active fuel length, in.	144	144	144	144
Burnup, GWd/MTU				
Relative power = 0.5	17.5	22.5	27.5	30.0
Relative power = 0.7	24.5	31.5	38.5	42.0
Relative power = 0.9	31.5	40.5	49.5	54.0
Relative power = 1.0	35.0	45.0	55.0	60.0
Relative power = 1.1	38.5	49.5	60.5	66.0
Relative power = 1.2	42.0	54.0	66.0	72.0
Light elements, kg per assembly				
O	62.6	62.6	62.6	62.6
Fe	4.6	4.6	4.6	4.6
Co	0.033	0.033	0.033	0.033
Ni	4.4	4.4	4.4	4.4
Zr	102	102	102	102
Nb	0.33	0.33	0.33	0.33
B	0.036	0.036	0.036	0.036

Tables 5.5-2 through 5.5-8 give the gamma source strengths for the fuel region of the PWR assemblies for each assembly average burnup level and cooling time studied used in the shielding analysis. In Section 5.2 the entire gamma source is given as output by SAS2. Only groups 10, 11, 12, and 13 contribute to the dose rate outside the cask. Tables 5.5-2 through 5.5-8 include only those groups that contribute to the dose rate outside the cask. Table 5.5-9 gives the end fitting and plenum gamma sources, and Tables 5.5-10 through 5.5-16 give the neutron source for each burnup and age combination. To save space, the tables in this appendix express numbers multiplied by exponents of 10 as the number followed by the exponent; e.g.,  $1.180 \times 10^{+13}$  is shown as 1.180+13.

TABLE 5.5-2 PWR FUEL GAMMA SOURCE DATA FOR 35 GWd/MTU AND 5-YEAR-COOLED							
		Gamma Source Strength (MeV/s per assembly)					
Group	Energy Range (MeV)	RP=0.5	RP=0.7	RP=0.9	RP=1.0	RP=1.1	RP=1.2
10	0.7 - 1.0	1.180+13	2.088+13	4.491+13	4.442+13	1.547+14	2.478+14
11	1.0 - 1.5	1.372+13	1.963+13	3.666+13	3.433+13	1.141+14	1.753+14
12	1.5 - 2.0	2.619+11	4.182+11	8.372+11	8.030+11	2.718+12	4.235+12
13	2.0 - 2.5	2.375+11	3.090+11	5.330+11	4.826+11	1.556+12	2.329+12

TABLE 5.5-3 PWR FUEL GAMMA SOURCE DATA FOR 45 GWd/MTU AND 7-YEAR-COOLED							
		Gamma Source Strength (MeV/s per assembly)					
Group	Energy Range (MeV)	RP=0.5	RP=0.7	RP=0.9	RP=1.0	RP=1.1	RP=1.2
10	0.7 - 1.0	1.002+13	1.761+13	3.733+13	3.658+13	1.261+14	1.997+14
11	1.0 - 1.5	1.306+13	1.899+13	3.562+13	3.330+13	1.103+14	1.686+14
12	1.5 - 2.0	2.364+11	3.909+11	7.847+11	7.484+11	2.510+12	3.870+12
13	2.0 - 2.5	4.724+10	6.245+10	1.091+11	9.932+10	3.217+11	4.832+11

TABLE 5.5-4 PWR FUEL GAMMA SOURCE DATA FOR 45 GWd/MTU AND 15-YEAR-COOLED							
		Gamma Source Strength (MeV/s per assembly)					
Group	Energy Range (MeV)	RP=0.5	RP=0.7	RP=0.9	RP=1.0	RP=1.1	RP=1.2
10	0.7 - 1.0	1.812+12	3.078+12	6.315+12	6.083+12	2.060+13	3.206+13
11	1.0 - 1.5	4.805+12	7.056+12	1.327+13	1.241+13	4.102+13	6.260+13
12	1.5 - 2.0	9.342+10	1.580+11	3.202+11	3.057+11	1.025+12	1.578+12
13	2.0 - 2.5	5.543+08	6.901+08	1.147+09	1.022+09	3.248+09	4.787+09

TABLE 5.5-5 PWR FUEL GAMMA SOURCE DATA FOR 55 GWd/MTU AND 10-YEAR-COOLED							
		Gamma Source Strength (MeV/s per assembly)					
Group	Energy Range (MeV)	RP=0.5	RP=0.7	RP=0.9	RP=1.0	RP=1.1	RP=1.2
10	0.7 - 1.0	6.220+12	1.075+13	2.244+13	2.176+13	7.415+13	1.159+14
11	1.0 - 1.5	1.056+13	1.550+13	2.911+13	2.708+13	8.746+13	1.361+14
12	1.5 - 2.0	1.860+11	3.133+11	6.256+11	5.913+11	1.963+12	2.994+12
13	2.0 - 2.5	5.263+09	7.117+09	1.262+12	1.158+10	3.777+10	5.708+10

TABLE 5.5-6 PWR FUEL GAMMA SOURCE DATA FOR 55 GWd/MTU AND 20-YEAR-COOLED							
		Gamma Source Strength (MeV/s per assembly)					
Group	Energy Range (MeV)	RP=0.5	RP=0.7	RP=0.9	RP=1.0	RP=1.1	RP=1.2
10	0.7 - 1.0	1.408+12	2.300+12	4.533+12	4.279+12	1.422+13	2.170+13
11	1.0 - 1.5	3.385+12	5.075+12	9.589+12	8.947+12	2.956+13	4.478+13
12	1.5 - 2.0	8.965+10	1.475+11	2.900+11	2.726+11	9.025+11	1.372+12
13	2.0 - 2.5	5.046+08	6.111+08	9.878+08	8.703+08	2.739+09	4.005+09

TABLE 5.5-7 PWR FUEL GAMMA SOURCE DATA FOR 60 GWd/MTU AND 11-YEAR-COOLED							
		Gamma Source Strength (MeV/s per assembly)					
Group	Energy Range (MeV)	RP=0.5	RP=0.7	RP=0.9	RP=1.0	RP=1.1	RP=1.2
10	0.7 - 1.0	5.989+12	1.027+13	2.108+13	2.030+13	6.871+13	1.068+14
11	1.0 - 1.5	1.032+13	1.521+13	2.848+13	2.650+13	8.720+13	1.324+14
12	1.5 - 2.0	1.979+11	3.299+11	6.494+11	6.102+11	2.013+12	3.049+12
13	2.0 - 2.5	3.813+09	5.074+09	8.908+09	8.122+09	2.634+10	3.961+10

TABLE 5.5-8 PWR FUEL GAMMA SOURCE DATA FOR 60 GWd/MTU AND 25-YEAR-COOLED							
		Gamma Source Strength (MeV/s per assembly)					
Group	Energy Range (MeV)	RP=0.5	RP=0.7	RP=0.9	RP=1.0	RP=1.1	RP=1.2
10	0.7 - 1.0	1.083+12	1.717+12	3.289+12	3.069+12	1.008+13	1.520+13
11	1.0 - 1.5	2.230+12	3.383+12	6.389+12	5.949+12	1.955+13	2.961+13
12	1.5 - 2.0	7.331+10	1.175+11	2.267+11	2.113+11	6.990+11	1.047+12
13	2.0 = 2.5	4.767+08	5.733+08	9.256+08	8.134+08	2.554+09	3.719+09

TABLE 5.5-9 PWR NON-FUEL REGION GAMMA SOURCE TERMS				
		Group 11 (1.0 - 1.5 MeV) Gamma Strength (MeV/s)		
Burnup (GWd/MTU)	Cooling Time (Years)	Bottom Tie Plate	Plenum	Top Tie Plate
35	5	6.664+11	1.217+12	1.824+12
45	7	6.074+11	1.110+12	1.663+12
45	15	2.121+11	3.875+11	5.807+11
55	10	4.763+11	8.701+11	1.304+12
55	20	1.279+11	2.336+11	3.500+11
60	11	4.499+11	8.219+11	1.232+12
60	25	7.138+10	1.304+11	1.954+11

**TABLE 5.5-10  
PWR FUEL NEUTRON SOURCE DATA FOR 35 GWd/MTU AND 5-YEAR-COOLED**

		Neutron Source Strength (n/s per assembly)					
Group	Energy Range (MeV)	RP=0.5	RP=0.7	RP=0.9	RP=1.0	RP=1.1	RP=1.2
1	6.43 - 15.0	1.213+04	5.155+04	2.143+05	2.769+05	1.220+06	2.405+06
2	3.00 - 6.43	1.383+05	5.881+05	2.444+06	3.159+06	1.391+07	2.743+07
3	1.85 - 3.00	1.538+05	6.536+05	2.717+06	3.511+06	1.547+07	3.049+07
4	1.40 - 1.85	8.634+04	3.670+05	1.525+06	1.971+06	8.684+06	1.712+07
5	0.90 - 1.40	1.167+05	4.959+05	2.061+06	2.664+06	1.173+07	2.313+07
6	0.40 - 0.90	1.271+05	5.402+05	2.245+06	2.902+06	1.278+07	2.520+07
7	0.10 - 0.40	2.485+04	1.056+05	4.390+05	5.674+05	2.499+06	4.927+06
8	0.0 - 0.1	0.000+00	0.000+00	0.000+00	0.000+00	0.000+00	0.000+00
	Total	6.592+05	2.802+06	1.165+07	1.505+07	6.630+07	1.307+08

**TABLE 5.5-11  
PWR FUEL NEUTRON SOURCE DATA FOR 45 GWd/MTU AND 7-YEAR-COOLED**

		Gamma Source Strength (n/s per assembly)					
Group	Energy Range (MeV)	RP=0.5	RP=0.7	RP=0.9	RP=1.0	RP=1.1	RP=1.2
1	6.43 - 15.0	3.082+04	1.311+05	5.244+05	6.654+05	2.845+06	5.474+06
2	3.00 - 6.43	3.516+05	1.496+06	5.982+06	7.550+06	3.245+07	6.244+07
3	1.85 - 3.00	3.908+05	1.663+06	6.649+06	8.323+06	3.607+07	6.940+07
4	1.40 - 1.85	2.194+05	9.335+05	3.733+06	4.708+06	2.025+07	3.897+07
5	0.90 - 1.40	2.965+05	1.261+06	5.044+06	6.388+06	2.737+07	5.266+07
6	0.40 - 0.90	3.229+05	1.374+06	5.494+06	6.971+06	2.981+07	5.736+07
7	0.10 - 0.40	6.315+04	2.687+05	1.074+06	1.363+06	5.829+06	1.122+07
8	0.0 - 0.1	0.000+00	0.000+00	0.000+00	0.000+00	0.000+00	0.000+00
	Total	1.675+06	7.127+06	2.850+07	3.597+7	1.546+08	2.975+08

**TABLE 5.5-12  
PWR FUEL NEUTRON SOURCE DATA FOR 45 GWd/MTU AND 15-YEAR-COOLED**

		Neutron Source Strength (n/s per assembly)					
Group	Energy Range (MeV)	RP=0.5	RP=0.7	RP=0.9	RP=1.0	RP=1.1	RP=1.2
1	6.43 - 15.0	2.389+04	9.809+04	3.884+05	4.889+05	2.096+06	4.017+06
2	3.00 - 6.43	2.725+05	1.119+06	4.431+06	5.557+06	2.391+07	4.583+07
3	1.85 - 3.00	3.029+05	1.244+06	4.925+06	6.198+06	2.657+07	5.094+07
4	1.40 - 1.85	1.701+05	6.983+05	2.766+06	3.481+06	1.492+07	2.016+07
5	0.90 - 1.40	2.298+05	9.436+05	3.737+06	4.703+06	2.016+07	3.864+07
6	0.40 - 0.90	2.503+05	1.028+06	4.070+06	5.122+06	2.196+07	4.209+07
7	0.10 - 0.40	4.894+04	2.010+05	7.959+05	1.002+06	4.294+06	8.231+06
8	0.0 - 0.1	0.000+00	0.000+00	0.000+00	0.000+00	0.000+00	0.000+00
	Total	1.298+06	5.331+06	2.111+07	2.657+07	1.139+08	2.183+08

TABLE 5.5-13 PWR FUEL NEUTRON SOURCE DATA FOR 55 GWd/MTU AND 10-YEAR-COOLED							
		Neutron Source Strength (n/s per assembly)					
Group	Energy Range (MeV)	RP=0.5	RP=0.7	RP=0.9	RP=1.0	RP=1.1	RP=1.2
1	6.43 - 15.0	5.088+04	2.136+05	8.331+05	1.037+06	4.393+06	8.332+06
2	3.00 - 6.43	5.804+05	2.437+06	9.504+06	1.183+07	5.011+07	9.505+07
3	1.85 - 3.00	6.451+05	2.708+06	1.056+07	1.314+07	5.570+07	1.056+08
4	1.40 - 1.85	3.622+05	1.521+06	5.931+06	7.381+06	3.127+07	5.932+07
5	0.90 - 1.40	4.894+05	2.055+06	8.014+06	9.973+06	4.226+07	8.015+07
6	0.40 - 0.90	5.331+05	2.238+06	8.730+06	1.086+07	4.603+07	8.731+07
7	0.10 - 0.40	1.042+05	4.376+05	1.707+06	2.124+06	9.001+06	1.707+07
8	0.0 - 0.1	0.000+00	0.000+00	0.000+00	0.000+00	0.000+00	0.000+00
	Total	2.765+06	1.161+07	4.528+07	5.635+07	2.388+08	4.529+08

**TABLE 5.5-14  
PWR FUEL NEUTRON SOURCE DATA FOR 55 GWd/MTU AND 20-YEAR-COOLED**

		Neutron Source Strength (n/s per assembly)					
Group	Energy Range (MeV)	RP=0.5	RP=0.7	RP=0.9	RP=1.0	RP=1.1	RP=1.2
1	6.43 - 15.0	3.664+04	1.488+05	5.753+05	7.144+05	3.019+06	5.660+06
2	3.00 - 6.43	4.180+05	1.697+06	6.563+06	8.150+06	3.444+07	6.456+07
3	1.85 - 3.00	4.646+05	1.886+06	7.295+06	9.059+06	3.828+07	7.176+07
4	1.40 - 1.85	2.609+05	1.059+06	4.096+06	5.087+06	2.150+07	4.029+07
5	0.90 - 1.40	3.525+05	1.431+06	5.534+06	6.873+06	2.904+07	5.444+07
6	0.40 - 0.90	3.840+05	1.559+06	6.028+06	7.486+06	3.164+07	5.930+07
7	0.10 - 0.40	7.508+04	3.048+05	1.179+06	1.464+06	6.186+06	1.160+07
8	0.0 - 0.1	0.000+00	0.000+00	0.000+00	0.000+00	0.000+00	0.000+00
	Total	1.992+06	8.087+06	3.127+07	3.883+07	1.641+08	3.076+08

**TABLE 5.5-15**  
**PWR FUEL NEUTRON SOURCE DATA FOR 60 GWd/MTU AND 11-YEAR-COOLED**

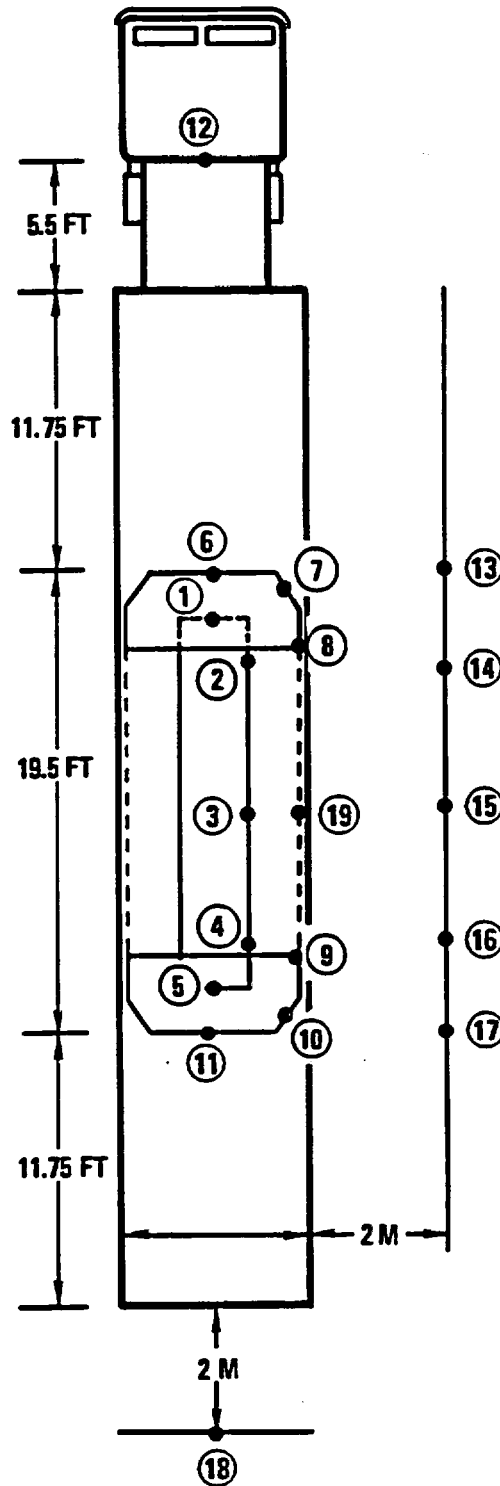
		Neutron Source Strength (n/s per assembly)					
Group	Energy Range (MeV)	RP=0.5	RP=0.7	RP=0.9	RP=1.0	RP=1.1	RP=1.2
1	6.43 - 15.0	6.601+04	2.740+05	1.052+06	1.299+06	5.459+06	1.028+07
2	3.00 - 6.43	7.530+05	3.126+06	1.200+07	1.481+07	6.228+07	1.172+08
3	1.85 - 3.00	8.369+05	3.475+06	1.334+07	1.647+07	6.922+07	1.303+08
4	1.40 - 1.85	4.699+05	1.951+06	7.490+06	9.245+06	3.887+07	7.316+07
5	0.90 - 1.40	6.349+05	2.636+06	1.012+07	1.249+07	5.251+07	9.885+07
6	0.40 - 0.90	6.916+05	2.871+06	1.102+07	1.361+07	5.720+07	1.077+08
7	0.10 - 0.40	1.352+05	5.615+05	2.155+06	2.661+06	1.119+07	2.106+07
8	0.0 - 0.1	0.000+00	0.000+00	0.000+00	0.000+00	0.000+00	0.000+00
	Total	3.588+06	1.489+07	5.718+07	7.058+07	2.967+08	5.586+08

TABLE 5.5-16 PWR FUEL NEUTRON SOURCE DATA FOR 60 GWd/MTU AND 25-YEAR-COOLED							
		Neutron Source Strength (n/s per assembly)					
Group	Energy Range (MeV)	RP=0.5	RP=0.7	RP=0.9	RP=1.0	RP=1.1	RP=1.2
1	6.43 - 15.0	4.133+04	1.657+05	6.256+05	7.701+05	3.226+06	6.038+06
2	3.00 - 6.43	4.715+05	1.879+06	7.137+06	8.785+06	3.680+07	6.888+07
3	1.85 - 3.00	5.240+05	2.088+06	7.932+06	9.764+06	4.090+07	7.656+07
4	1.40 - 1.85	2.942+05	1.172+06	4.454+06	5.483+06	2.297+07	4.299+07
5	0.90 - 1.40	3.976+05	1.584+06	6.018+06	7.408+06	3.103+07	5.808+07
6	0.40 - 0.90	4.331+05	1.716+06	6.555+06	8.069+06	3.380+07	6.327+07
7	0.10 - 0.40	8.468+04	3.374+05	1.282+06	1.578+06	6.610+06	1.237+07
8	0.0 - 0.1	0.000+00	0.000+00	0.000+00	0.000+00	0.000+00	0.000+00
	Total	2.246+06	8.951+06	3.400+07	4.186+07	1.753+08	3.282+08

**5.5.1.2 Model Specification.** The shielding models used for the fully loaded cases are identical to those described in Section 5.3. The models for the two-element case with shield inserts differ only in that two of the fuel assemblies are replaced with the one-inch-thick stainless steel shield inserts.

**5.5.1.3 Shielding Evaluation.** The shielding evaluations for the additional burnup and cooling time combinations are identical to those presented in Section 5.4. Figure 5.5-4 depicts the dose rate map for normal conditions of transport. Tables 5.5-17 and 5.5-18 give the neutron, gamma, and total dose rates for each burnup and age combination for the fully loaded and the two-element configurations.

Note that Fig. 5.5-4 shows the cask personnel barrier as a dotted line whereas Fig. 5.4-2 does not. This is because for some of the studied fuel burnup/age combinations, the dose rate on the cask surface (dose point #3) exceeds the package surface regulatory limit of 200 mR/h. If the cask surface meets the dose rate criterion, as it does in the base case presented in the main shielding section, the personnel barrier need not be modeled. If the surface exceeds 200 mR/h, however, analysis must be performed to verify that the dose rate on the personnel barrier does not exceed 200 mR/h. Therefore, we calculated the peak personnel barrier dose rate (dose point #19) in all of the high burnup shielding analyses. This dose rate never exceeds 100 mR/h for any of the studied cases.



K-213(2)(a)  
8-24-93

Fig. 5.5-4. GA-4 cask dose rate points for normal conditions of transport

**TABLE 5.5-17  
FULLY LOADED GA-4 CASK,  
DOSE RATES (mR/h) FOR NORMAL CONDITIONS**

Dose Point	Burnup = 35 GWd/MTU Age = 10 yr			Burnup = 45 GWd/MTU Age = 15 yr		
	Gamma	Neutron	Total	Gamma	Neutron	Total
1	26	7	33	17	14	31
2	33	14	47	25	29	54
3	112	41	153	86	84	170
4	86	31	117	66	64	130
5	133	49	182	97	100	197
6	8	1	9	5	2	7
7	13	2	15	8	4	12
8	12	6	18	9	12	21
9	28	6	34	21	12	33
10	15	2	17	10	4	14
11	38	6	44	27	12	39
12	0.2	0	0.2	0.1	0.1	0.2
13	1.3	1	2.3	1	2	3
14	4	1.1	5.1	3	2.4	5.4
15	7.6	1.8	9.4	5.7	3.8	9.5
16	5.5	1.6	7.1	4.2	3.4	7.6
17	1.9	1	2.9	1.5	2	3.5
18	0.9	0.2	1.1	0.7	0.3	1
19	59	14	73	45	28	73
Dose Point	Burnup = 55 GWd/MTU Age = 20 yr			Burnup = 60 GWd/MTU Age = 25 yr		
	Gamma	Neutron	Total	Gamma	Neutron	Total
1	12	20	32	8	22	30
2	18	45	63	13	48	61
3	67	120	187	49	128	177
4	52	92	144	38	98	136
5	74	144	218	54	153	207
6	3	3	6	2	3	5
7	5	6	11	3	6	9
8	7	17	24	5	18	23
9	16	17	33	12	18	30
10	7	6	13	5	6	11
11	20	17	37	14	18	32
12	0.1	0.1	0.2	0.1	0.1	0.2
13	0.8	2.9	3.7	0.6	3.1	3.7
14	2.3	3.4	5.7	1.7	3.6	5.3
15	4.4	5.4	9.8	3.1	5.8	8.9
16	3.2	4.9	8.1	2.3	5.2	7.5
17	1.2	2.9	4.1	0.9	3.1	4
18	0.5	0.5	1	0.3	0.5	0.8
19	35	41	76	26	43	69

**TABLE 5.5-18  
TWO-ELEMENT GA-4 CASK WITH SHIELD INSERTS,  
DOSE RATES (mR/h) FOR NORMAL CONDITIONS**

Dose Point	Burnup = 35 GWd/MTU Age = 5 yr			Burnup = 45 GWd/MTU Age = 7 yr		
	Gamma	Neutron	Total	Gamma	Neutron	Total
1	26	4	30	23	11	34
2	68	9	77	59	20	79
3	237	26	263	210	61	271
4	175	21	196	156	49	205
5	163	27	190	146	64	210
6	8	1	9	7	1	8
7	11	1	12	10	3	13
8	13	3	16	11	8	19
9	35	3	38	30	8	38
10	15	1	16	14	3	17
11	43	4	47	38	9	47
12	0.2	0	0.2	0.2	0.1	0.3
13	1.7	0.5	2.2	1.4	1.3	2.7
14	4.9	0.6	5.5	4.2	1.4	5.6
15	8.8	0.8	9.6	7.7	1.8	9.5
16	6.5	0.7	7.2	5.7	1.5	7.2
17	2.6	0.5	3.1	2.2	1.2	3.4
18	1.1	0.1	1.2	1	0.2	1.2
19	77	8	85	67	18	86
Dose Point	Burnup = 55 GWd/MTU Age = 10 yr			Burnup = 60 GWd/MTU Age = 11 yr		
	Gamma	Neutron	Total	Gamma	Neutron	Total
1	19	16	35	18	21	39
2	47	32	79	47	39	86
3	166	94	260	164	116	280
4	124	76	200	123	94	217
5	107	114	221	106	142	248
6	6	2	8	5	3	8
7	8	4	12	7	6	13
8	9	12	21	9	14	23
9	24	11	35	24	14	38
10	11	4	15	10	6	16
11	30	14	44	30	17	47
12	0.2	0.1	0.3	0.2	0.1	0.3
13	1.2	1.9	3.1	1.2	2.4	3.6
14	3.3	2.2	5.5	3.3	2.7	6
15	6.1	2.8	8.9	6	3.5	9.5
16	4.5	2.3	6.8	4.4	2.9	7.3
17	1.8	1.9	3.7	1.8	2.3	4.1
18	0.7	0.4	1.1	0.7	0.5	1.2
19	53	28	81	52	35	87

**5.5.2 References for Sections 5.2 through 5.5**

- 5.2-1 "SCALE-4.1: A Modular Code System for Performing Standardized Computer Analysis for Licensing Evaluation," CCC-545, Oak Ridge National Laboratory, February 1990.
- 5.2-2 "Topical Safety Analysis Report for the Westinghouse MC-10 Cask for an Independent Spent Fuel Storage Installation (Dry Storage)," December 1984.
- 5.2-3 "Revised Uranium-Plutonium Cycle PWR and BWR Models For the ORIGEN Computer Code," ORNL/TM-6051, September 1978.
- 5.4-1 Su, S., et al., "PATH Gamma Shielding Code User's Manual," GA-A16772 (Rev 1.), General Atomics, May 1987.
- 5.4-2 O'Dell, R. Douglas, et al., "User's Manual for ONEDANT: A Code Package for One-Dimensional, Diffusion-Accelerated, Neutral Particle Transport," LA-9184-M, Los Alamos National Laboratory, February 1982.
- 5.4-3 Alcouffe, R. E., "User's Guide for TWODANT — A Code Package for Two-Dimensional, Diffusion-Accelerated, Neutral-Particle Transport," LA-100049-M, Rev. 1.4, April 27, 1987.
- 5.4-4 Briesmeister, J. F. (editor), "MCNP — A General Monte Carlo Code for Neutron and Photon Transport," LA-7396-M, Rev. 2, September 1986.
- 5.4-5 "CASK-81 22 Neutrons, 18 Gamma-Ray Group, P<sub>3</sub> Cross Sections for Shipping Cask Analysis," DLC-23, Oak Ridge National Laboratory, June 1987.
- 5.4-6 "Neutron and Gamma-Ray Flux-to-Dose Rate Factors," ANSI/ANS 6.1.1-1977 (N666), March 1977.
- 5.5-1 "Characteristics of Spent Fuel, High-Level Waste, and Other Radioactive Wastes Which May Require Long-Term Isolation," DOE/RW-0184, December 1987.